

NASA
Technical Paper 1864

AVRADCOM
Technical Report 81-B-3



Experimental Investigation of a 10-Percent-Thick Helicopter Rotor Airfoil Section Designed With a Viscous Transonic Analysis Code

Kevin W. Noonan

JULY 1981

NASA



NASA
Technical Paper 1864

AVRADCOM
Technical Report 81-B-3

Experimental Investigation of a 10-Percent-Thick Helicopter Rotor Airfoil Section Designed With a Viscous Transonic Analysis Code

Kevin W. Noonan
*Structures Laboratory
AVRADCOM Research and Technology Laboratories
Langley Research Center
Hampton, Virginia*

NASA
National Aeronautics
and Space Administration

**Scientific and Technical
Information Branch**

1981

SUMMARY

An investigation has been conducted in the Langley 6- by 28-Inch Transonic Tunnel to determine the two-dimensional aerodynamic characteristics of a 10-percent-thick helicopter rotor airfoil at Mach numbers from 0.33 to 0.87 and respective Reynolds numbers from 4.9×10^6 to 9.8×10^6 . This airfoil, designated the RC-10(N)-1, was also investigated at Reynolds numbers from 3.0×10^6 to 7.3×10^6 at respective Mach numbers of 0.33 to 0.83 for comparison with the SC 1095 (with tab) airfoil. The RC-10(N)-1 airfoil was designed by the use of a viscous transonic analysis code.

The results of the investigation indicate that the RC-10(N)-1 airfoil met all the design goals. At a Reynolds number of about 9.4×10^6 , the drag divergence Mach number at zero normal-force coefficient was 0.815 with a corresponding pitching-moment coefficient of zero. The drag divergence Mach number at a normal-force coefficient of 0.9 and a Reynolds number of about 8.0×10^6 was 0.61. The drag divergence Mach number of this new airfoil was higher than that of the SC 1095 airfoil at normal-force coefficients above 0.3. Measurements in the same wind tunnel at comparable Reynolds numbers indicated that the maximum normal-force coefficient of the RC-10(N)-1 airfoil was higher than that of the NACA 0012 airfoil for Mach numbers above about 0.35 and was about the same as that of the SC 1095 airfoil for Mach numbers up to 0.5.

INTRODUCTION

Helicopter rotor airfoil design and evaluation have been part of an on-going effort by the U.S. Army and NASA to improve the main rotor performance of helicopters. One approach to this difficult airfoil design problem is the crestline method described in reference 1. This method is useful in predicting the drag divergence characteristics of airfoils at lift coefficients from near zero up to the first occurrence of separation. However, pitching-moment coefficients at transonic speeds and drag coefficients cannot be evaluated with this method. The crestline approach was developed prior to the development of an inexpensive viscous, transonic analysis code for supercritical airfoils. (See refs. 2 to 4.) This code offered the additional capability of calculating pitching-moment coefficients and drag coefficients at transonic speeds. An airfoil designated the RC-10(N)-1 has been designed with the use of this transonic analysis code in an attempt to provide improved drag divergence characteristics relative to other helicopter rotor airfoils.

An experimental investigation has been conducted to determine the aerodynamic characteristics of the RC-10(N)-1 airfoil and to evaluate the applicability of the analysis code to the helicopter rotor airfoil design problem. The airfoil was tested in the Langley 6- by 28-Inch Transonic Tunnel at Mach numbers from 0.33 to 0.87 and at respective Reynolds numbers (based on chord) from 3.0×10^6 to 9.8×10^6 . The majority of the testing was done with a smooth model surface; fixed transition data were measured at selected Mach numbers to

adequately represent the trends. Normal-force and pitching-moment coefficients were determined from measurements of airfoil surface static pressures. Drag coefficients were determined from measurements of wake total and static pressures.

SYMBOLS

The units used for the physical quantities in this paper are given in both the International System of Units (SI) and U.S. Customary Units. The measurements and calculations were made in U.S. Customary Units.

c airfoil chord, cm (in.)

c_d section profile-drag coefficient, $\sum_{\text{Wake}} c_d'(\Delta h/c)$

c_d' point-drag coefficient,

$$2\left(\frac{p}{p_\infty}\right)^{6/7} \left[\frac{(p_t/p)^{2/7} - 1}{(p_{t,\infty}/p_\infty)^{2/7} - 1} \right]^{1/2} \left\{ \left(\frac{p_t}{p_{t,\infty}}\right)^{1/7} - \left[\frac{(p_t/p_\infty)^{2/7} - 1}{(p_{t,\infty}/p_\infty)^{2/7} - 1} \right]^{1/2} \right\}$$

$c_{d_{M_{dd}}}$ section profile-drag coefficient at drag divergence Mach number

c_m section pitching-moment coefficient about quarter-chord,

$$\sum_{\text{U.S.}} \left[C_p \left(0.25 - \frac{x}{c} \right) \left(\frac{\Delta x}{c} \right) + C_p \left(\frac{z}{c} \right) \left(\frac{\Delta z}{c} \right) \right] + \sum_{\text{L.S.}} \left[C_p \left(0.25 - \frac{x}{c} \right) \left(\frac{\Delta x}{c} \right) + C_p \left(\frac{z}{c} \right) \left(\frac{\Delta z}{c} \right) \right]$$

c_n section normal-force coefficient, $\sum_{\text{U.S.}} C_p(\Delta x/c) + \sum_{\text{L.S.}} C_p(\Delta x/c)$

C_p static-pressure coefficient, $\frac{p_l - p_\infty}{q_\infty}$

h height of wake-survey probe tubes from given reference plane, cm (in.)

M Mach number

M_{dd}	Mach number for drag divergence, $\frac{dc_d}{dM} = 0.1$
p	static pressure, Pa (psi)
q	dynamic pressure, $\frac{1}{2} \rho V^2$, Pa (psi)
R	Reynolds number based on airfoil chord and free-stream conditions
t	airfoil thickness, cm (in.)
V	velocity, m/sec (ft/sec)
x	airfoil abscissa, cm (in.)
z	airfoil ordinate, cm (in.)
z_C	ordinate of airfoil mean line, cm (in.)
α	angle of attack, angle between airfoil chord line and airstream direction, deg
α_C	angle of attack corrected for lift-interference effects, deg
ρ	density kg/m^3 (slugs/ft ³)

Subscripts:

l	local
max	maximum
min	minimum
sep	separation
sonic	Mach number equal to 1
t	total
∞	free stream

Abbreviations:

L.S.	lower surface
U.S.	upper surface

APPARATUS AND METHODS

Airfoil Design

The desired characteristics of an airfoil to be used on a helicopter main rotor have been mentioned in references 1, 5, 6, 7, and 8 and other unpublished documents. In general, these characteristics are (1) a high drag divergence Mach number over a range of lift coefficients from small negative values to high positive values for reduced power in forward flight, (2) a high maximum lift coefficient at Mach numbers from 0.40 to 0.60 for maneuverability and reduced power in forward flight, (3) a high lift-drag ratio at Mach numbers from 0.40 to 0.65 and at lift coefficients from 0.5 to 0.7 for hover efficiency, and (4) a pitching-moment coefficient with an absolute value less than 0.02 at all usable Mach-number—lift-coefficient conditions to minimize the pitch link loads and to increase the rotor blade structural life. The specific design goals set for this new helicopter rotor airfoil were

- (1) $M_{dd} \geq 0.80$ at $c_n = 0.0$ with $c_m \approx 0.00$
- (2) $M_{dd} > 0.56$ at $c_n = 0.9$
- (3) $c_{n,max} \geq 1.20$ at $M = 0.4$
- (4) $(t/c)_{max} = 0.10$

The design goals were described in terms of normal-force coefficients rather than lift coefficients in order to avoid the dependency on angle of attack which must be corrected for the usual interference effects. Rotor airfoils have been developed which have a drag divergence Mach number at zero normal-force coefficient in excess of 0.80 such as the FX-69-H-098 (ref. 9) and the 10-64C (ref. 10) airfoils, but both of these airfoils have corresponding pitching-moment coefficients greater than $|0.02|$ at Mach numbers of about 0.80 and higher. Therefore, the first design goal represents an improvement by extending the low pitching-moment range up to a Mach number of at least 0.80. The second design goal was based on the fact that the FX-69-H-098 airfoil had a measured drag divergence Mach number at a normal-force coefficient of 0.9 equal to 0.56 (at $R \approx 7.0 \times 10^6$) and this value was high in relation to other airfoils of similar thickness. (See ref. 9.) The design goal for $c_{n,max}$ was believed to be a value which could reasonable be achieved considering the two drag divergence design goals and the $c_{n,max}$ performance of existing airfoils with high drag divergence Mach numbers. A specific design goal was not set for the lift-drag ratios at Mach numbers from 0.40 to 0.65 because it was believed that values higher than most other airfoils would be a by-product of achieving the two drag divergence design goals. The maximum thickness of this new airfoil design was restricted to 10 percent chord for two reasons. Data were available in the literature for a number of airfoils with a maximum thickness of about 10 percent chord for comparison purposes and it was believed that the experimental results for a 10-percent-thick section could be extrapolated with confidence to other thickness ratios normally used on helicopter rotors (0.08 to 0.12) by using reference 10 as a guide to the increments.

This new airfoil was designated the RC-10(N)-1 in order to be consistent with the nomenclature used for new airfoil designs in previous papers. The first two letters of the designation indicate the type of airfoil, in this case rotorcraft. The two digits following the first hyphen represent the maximum thickness in percent chord. The following letter represents the designer of the airfoil and the final number indicates the generation of the design.

The design approach involved combining an arbitrary camber line and thickness distribution to result in an airfoil shape which was subsequently evaluated with a transonic analysis code. (See refs. 2 to 4.) An iteration process of modifying the airfoil shape by changing the camber line and/or thickness distribution and of evaluating the new airfoil was used to converge on the design goals. The maximum thickness of the initial thickness distribution was located at the 40-percent-chord station based on drag divergence trends reported in reference 1. This approach allowed direct control of the maximum thickness and the pitching-moment coefficients. Helicopter rotor airfoils have generally been evaluated on the basis of smooth model data since (1) the boundary-layer-transition location on the airfoil in flight is unknown, (2) the application of grit to cause transition on small-chord wind-tunnel models is difficult to repeat from model to model thus causing doubts about the drag coefficients, and (3) some significant amount of laminar flow (>5 percent chord) might now be attained on an airfoil section in flight with the advent of composite construction rotor blades with aerodynamically smooth surfaces. However, the analysis code available did not have a laminar boundary-layer computation so a natural transition option was not possible. Therefore, each airfoil in the design iteration was evaluated with the code with transition fixed at 5 percent chord on the upper and lower surface in order to have conservative results. Since the analysis code did not have the capability to handle regions of separated flow, only calculations with an indicated boundary-layer separation point aft of about 95 percent chord were considered reliable and an indication of the maximum normal-force coefficient of an airfoil could not be obtained with this code. Without any consistent and accurate method to predict the maximum normal-force coefficient at a Mach number of 0.4, the design approach taken was to try to obtain an airfoil which would have a normal-force coefficient of 1.2 at this Mach number with no separation as indicated by the analysis code. Correlation of the analysis code results with experimental data on existing airfoils had indicated that the prediction of the separation point was conservative.

Analysis Code

The code (refs. 2, 3, and 4), which was first developed for off-design analysis of supercritical airfoils, calculates weak solutions of equations of motion that can include one or more isentropic shocks (in the mathematical sense). The full potential equation, including a semiempirical turbulent boundary-layer correction, is solved by a rotated finite-difference scheme in a more-or-less arbitrary curvilinear-coordinate system. The inputs to the analysis code include the airfoil geometry (coordinates), the free-stream Mach number, the lift coefficient (or angle of attack), the Reynolds number, and the boundary-layer transition points on the upper and lower surface. The selection of some of the input parameters, which have no physical significance only a mathematical one, was made on the basis of correlations of the analysis code results

with experimental force data of existing airfoils measured in the Langley 6-by 28-Inch Transonic Tunnel. The correlation indicated that use of the default (or preset) values for the number of mesh intervals ($M \times N$), the boundary-layer relaxation parameter (RDEL), and the convergence tolerance (ST) resulted in the best agreement with the experimental data. The correlation further indicated that the maximum number of flow cycles of 20 for the course grid and 10 for the fine grid was sufficient. The parameter XSEP was set to -0.93 so that the calculated lower surface boundary-layer-displacement thickness would increase monotonically near the airfoil trailing edge (the default value of 0.93 allows the development of a lower surface boundary-layer-displacement thickness which is characteristic of supercritical airfoils). During the design iteration, it was found that the parameter LL, the index of location on the airfoil where the sweep through the upper and lower surfaces begins for the finite-difference scheme, should be set to 73 for analyzing airfoils at lift coefficients above 1.0 at a Mach number of 0.40.

Model

The airfoil profile, thickness distribution, and camber line are shown in figure 1. The maximum thickness is 10 percent chord and is located at the 37.5-percent-chord station. The maximum camber is 2 percent chord and is located at the 25-percent-chord station; the camber line is reflexed aft of about the 95-percent-chord station. The design coordinates for this airfoil are given in table I and those for an 8-percent-thick and a 12-percent-thick derivative of the RC-10(N)-1 airfoil are given in tables II and III, respectively.

The airfoil was machined from a heat-treated stainless-steel block and has a span of 15.27 cm (6.010 in.) and a chord of 15.24 cm (6.000 in.). The model has 23 orifices located in one chordwise row on each surface; the upper and lower surface orifice rows are positioned 12.6 percent span on opposite sides of the midspan (table IV). Slots were milled in the airfoil surface and tubes were placed in the slots and then covered with epoxy. The final airfoil contour has a surface finish of 0.813 μm (0.000032 in.). The orifices were then drilled from the metal side of the model to the embedded tubes so there are no surface irregularities near the orifice row. The orifices have a diameter of 0.0508 cm (0.020 in.) and were drilled perpendicular to the local surface contour.

Wind Tunnel

Tunnel description.- The Langley 6- by 28-Inch Transonic Tunnel (ref. 11) is a blowdown wind tunnel with a slotted floor and ceiling and is generally operated at stagnation pressures from about 207 to 621 kPa (30 to 90 psia) and at Mach numbers from 0.35 to 0.90. The selection of the 0.05-open-slot geometry is described in detail in reference 12. Mach number is controlled by hydraulically actuated choker doors located downstream of the test section. The airfoil model spans the 15.27-cm (6.01-in.) width of the tunnel (fig. 2) and is rigidly attached by mounting tangs to two circular end plates which are driven by a hydraulic actuator to position the airfoil at the desired angle of attack. A test run usually consists of an angle-of-attack sweep at a constant Mach number and Reynolds number.

Two-dimensionality of flow.- The results of a previous investigation of rotorcraft airfoils in the Langley 6- by 28-Inch Transonic Tunnel (ref. 9) have shown that the indicated maximum normal-force coefficient is reduced by tunnel-wall boundary-layer influences. This reduction is characteristic of two-dimensional wind tunnels without proper sidewall boundary-layer control and occurs because the tunnel-wall boundary layer is thicker than that of the airfoil; therefore, initial separation begins at the tunnel wall.

Although it is not possible to determine precisely the affected Mach number range or the loss in maximum normal-force coefficient of the airfoils reported herein, a comparison of the NACA 0012 data measured in this facility with 0.05 open slots with unpublished data from two other facilities has been useful in indicating the magnitude of these losses. The maximum normal-force coefficients measured in the Langley Low-Turbulence Pressure Tunnel and the United Technologies Research Center 8-Foot Subsonic/Transonic Wind Tunnel at similar Reynolds numbers and at a Mach number of 0.36 are higher than that from the Langley 6- by 28-Inch Transonic Tunnel by about 0.15. The difference between the data from the Langley 6- by 28-Inch Transonic Tunnel and the United Technologies data decreased to 0.05 at a Mach number of about 0.53. Incremental values for other airfoils may vary slightly because of specific configuration influences.

An investigation conducted in the Office National d'Études et de Recherches Aérospatiale (ONERA) R1 Ch wind tunnel (ref. 13) has shown that the tunnel sidewall boundary layer can affect the normal-force coefficients at all angles of attack (that is, with either attached or separated boundary layers). In this investigation, the sidewall boundary-layer thickness was varied by applying sidewall suction upstream of the model while the Mach number and Reynolds number were held constant. Generally, an increase in sidewall boundary-layer thickness resulted in a decrease in the normal-force coefficient at a given angle of attack; the trend reversed at Mach numbers greater than 0.85 with a supercritical airfoil.

Apparatus

Wake-survey probe.- A traversing wake-survey probe is cantilevered from one tunnel sidewall to measure the profile drag of the airfoils. The vertical sweep rate of the probe, which was selected after experimental determination of acceptable lag time in the pressure measurements, was about 2.54 cm/sec (1.00 in/sec).

The probe was located 1.67 chords (based on the 15.24-cm (6.00-in.) chord model) downstream of the airfoil trailing edge and has a maximum vertical travel of about ± 27.9 cm (± 11.0 in.) from the tunnel center line (fig. 2). Data are acquired with four total-pressure tubes, which are made of stainless-steel tubing, with a 1.53-mm (0.060-in.) outside diameter and a 1.02-mm (0.040-in.) inside diameter; the tubes are spaced 0.953 cm (0.375 in.) apart laterally as shown in figure 3.

Instrumentation.- All measurements made during the test program were obtained with the use of a high-speed, computer-controlled digital data acquisition system and were recorded by a high-speed tape-recording unit (ref. 11).

All free-stream conditions were determined from stagnation and static pressures. All airfoil surface pressures and all wake pressures were measured with precision capacitive potentiometer pressure transducers. The electrical outputs from each of these transducers were connected to individual autoranging signal conditioners which have seven available ranges. The output signals from the four signal conditioners measuring the wake pressures were filtered with 20-Hz low-pass filters before input to the data acquisition system; the range of frequencies to be passed was experimentally determined during a previous investigation. The geometric angle of attack was determined from the output of a digital shaft encoder attached to a pinion engaging a rack on one model support end plate.

Tests and Methods

Test runs were made with a smooth model surface at a stagnation pressure of 414 kPa (60 psia) at Mach numbers from 0.33 to 0.87 to obtain Reynolds numbers typical of full-scale main rotors. Smooth model testing was also conducted at stagnation pressures from 262 to 310 kPa (38 to 45 psia) at Mach numbers from 0.33 to 0.83, respectively, to obtain Reynolds numbers similar to those obtained on the SC 1095 airfoil (ref. 14) so that a direct comparison of these two airfoils could be made. Some test runs were made with a roughness strip applied to both the upper and lower surfaces of the model; the leading edge of the 1.27-mm (0.050-in.) wide roughness strip was located at the 5-percent-chord station on both surfaces. The roughness was sized according to reference 15 and consisted of No. 220 carborundum grit. The grit was thinly spread to cover about 5 to 10 percent of the strip surface area and was attached to the model with lacquer. The smooth model data (Test 52) and the data with roughness applied (Test 73) were measured during two separate entries into the same wind tunnel. Smooth model data were also measured at selected test conditions during the second tunnel entry in order to check the repeatability of the smooth data. At the lower test Mach numbers, geometric angles of attack ranged from -4° to 13° with 2° increments between the lower angles and 1° increments between the angles approaching the stall angle; this range was decreased at the higher test Mach numbers.

Section normal-force and pitching-moment coefficients were calculated from the airfoil surface pressures by a trapezoidal integration of the pressure coefficients. The pressure coefficient at the most rearward orifice on each surface was applied from that station to the airfoil trailing edge in the integration. Each of the pressure coefficients represents the average of five measurements obtained in a 1.0-sec interval. A form of the equation described in reference 16 was used to calculate the point-drag coefficients from the measured wake pressures, and a trapezoidal integration of the point-drag coefficients was used to calculate the drag coefficient. The static pressures used in the wake drag calculation were measured with tunnel sidewall orifices located at the same longitudinal tunnel station as the tips of the tubes on the wake-survey probe. All drag coefficients presented in this paper represent the mean of the measurements made with four total-pressure tubes on the wake-survey probe in one sweep through a wake.

The corrections for lift interference, which have been applied to the angles of attack, were obtained from references 12 and 17. The basic equations for the correction (ref. 17) are

$$\alpha_c = \alpha + \Delta\alpha$$

where

$$\Delta\alpha = \frac{-c_n}{8} \left(\frac{c}{36.195} \right) \left(\frac{1}{k+1} \right) \left(\frac{180}{\pi} \right)$$

$$k = \frac{a}{h} K$$

a is the slot spacing, and h is the semiheight of the tunnel. The slotted-wall boundary-condition coefficient k for the present tunnel configuration is $0.4211K$. A value of 3.5 was selected for the slotted-wall performance coefficient K , based on the data and discussion presented in reference 12. This substitution results in a correction given by the equation

$$\Delta\alpha = -c_n c (0.0800)$$

where c is in centimeters, α is in degrees, and the constant is in degrees per centimeter.

PRESENTATION OF RESULTS

The results of the investigation have been reduced to coefficient form and are presented as follows:

<u>Basic characteristics</u>	Figure
Aerodynamic characteristics of RC-10(N)-1 airfoil	4
Effect of roughness on aerodynamic characteristics of RC-10(N)-1 airfoil	5
Comparison of smooth model data from two separate tunnel entries	6
Variation of maximum section normal-force coefficient with Mach number of RC-10(N)-1 and NACA 0012 airfoils	7
Variation of maximum section normal-force—drag ratio with Mach number	8
Variation of section normal-force coefficient with drag divergence Mach number	9
Effect of Reynolds number on variation of section drag coefficient with Mach number	10

Comparisons of RC-10(N)-1 and SC 1095 airfoils

Comparison of aerodynamic characteristics of RC-10(N)-1 and SC 1095 airfoils 11
Comparison of drag divergence characteristics and maximum section normal-force coefficients of RC-10(N)-1 and SC 1095 airfoils 12
Comparison of section drag coefficient at drag divergence Mach number of RC-10(N)-1 and SC 1095 airfoils 13
Comparison of variation of section drag coefficient with Mach number of RC-10(N)-1 and SC 1095 airfoils 14

Theoretical characteristics and comparisons of theory and experiment

Comparison of experimental and theoretical drag divergence characteristics and section normal-force coefficients; experimental data are for smooth model 15
Variation of theoretical section drag coefficient with Mach number; transition fixed 16
Comparison of experimental and theoretical section pitching-moment coefficients; experimental data are for smooth model 17
Comparison of experimental and theoretical section drag coefficients; transition fixed 18
Drag divergence characteristics of RC-XX(N)-1 airfoil family; experimental data are for smooth model 19

Pressure distributions and separation

Effect of angle of attack on chordwise pressure distribution 20
Effect of Mach number on angle of attack at which boundary-layer separation first occurs and on separation point 21
Effect of Mach number on chordwise pressure distribution 22
Comparison of experimental and theoretical chordwise pressure distributions 23

DISCUSSION OF RESULTS

Normal Force

The normal-force coefficients measured with a smooth model surface at two Reynolds numbers are presented in figure 4(a), and those measured with roughness strips applied are presented in figure 5(a). The maximum normal-force coefficients determined from these two figures are presented as a function of Mach number in figure 7 along with unpublished data for an NACA 0012 airfoil measured in the same facility with the same slot configuration. The maximum normal-force coefficient for the smooth RC-10(N)-1 airfoil at the higher Reynolds numbers decreases with increasing Mach number up to a Mach number of about 0.53 where the trend reverses; the corresponding $C_{n,max}$ values range from 1.10 at $M = 0.33$ to 1.0 at $M = 0.53$. This trend is the result of separation due to supercritical flow influences occurring at a lower angle of attack with increasing Mach number up to a Mach number of about 0.53 (figs. 20 and 21). The

maximum normal-force coefficient increases with an increase in Mach number from 0.53 to 0.58 because of a favorable expansion of the supersonic zone on the upper surface of the airfoil which provides more suction from about 6 to 21 percent chord at a corrected angle of attack of 8° at the higher Mach number (fig. 22(a)). At comparable Reynolds numbers, the $c_{n,max}$ values of the smooth RC-10(N)-1 airfoil are higher than those for the NACA 0012 airfoil at all Mach numbers above about 0.35. The maximum normal-force coefficient design goal of 1.2 at a Mach number of 0.4 is achieved by the RC-10(N)-1 airfoil when the measured value of $c_{n,max}$ is incremented by the same value required to match the maximum normal-force coefficient of the NACA 0012 airfoil measured in the Langley 6- by 28-Inch Transonic Tunnel at a Mach number of 0.36 to those measured in two other facilities. (See section "Wind Tunnel.") Lowering the Reynolds number did not change the $c_{n,max}$ trend with Mach number of the RC-10(N)-1 airfoil but it did have the usual effect of reducing the $c_{n,max}$ values.

The addition of roughness strips to the model surface to insure boundary layer transition had no effect on either the $c_{n,max}$ trend with Mach number or the magnitude of the $c_{n,max}$ values for Mach numbers up to about 0.53. The pressure distributions for the smooth model presented in figures 20(a) to (e) suggest that natural boundary-layer transition on the upper surface would occur in front of or near the 5-percent-chord station at geometric angles of attack equal to or greater than 8° because of the pressure recovery in that region. Therefore, the expected effect of a grit strip located at 5 percent chord on the upper surface would simply be a thickening of an already turbulent boundary layer at these high angles of attack; this would have a minimal effect on $c_{n,max}$. It should be noted that the data with roughness applied are compared to the smooth model data measured during the same tunnel entry in figure 7 (also figs. 5, 8, and 9) in order to minimize the typical small differences that occur because of separate tunnel entries. (See fig. 6.) The differences in normal-force coefficient shown in figure 6(a) are about 0.02 in the linear range of the curves and about 0.03 in the nonlinear part of the curves where separated flow is usually present on an airfoil and repeatability of data is difficult even during the same tunnel entry.

The smooth RC-10(N)-1 airfoil exhibits a gradual stall at all Mach numbers up to 0.58 at both sets of Reynolds numbers (fig. 4(a)); the addition of roughness did not change the stall characteristics. (See fig. 5(a).) The pressure distributions presented in figures 20(a) to (e) indicate that the stall is of the trailing-edge type by the characteristic loss of pressure recovery (more negative C_p) near the upper surface trailing edge at angles of attack near $c_{n,max}$.

The maximum local Mach number corresponding to the first occurrence of boundary-layer separation varied from 1.14 to 1.59 for free-stream Mach numbers of 0.33 and 0.58, respectively, and that corresponding to the maximum normal-force coefficient was about the same or higher than the values just mentioned. These values of the maximum local Mach number may not be precisely the true maximum values occurring on the airfoil particularly at free-stream Mach numbers up to 0.43, since only one to three orifices are available to measure the local pressures in the supersonic zone and because of tunnel-wall boundary-layer influences. However, it is interesting to note that the maximum local Mach

numbers corresponding to the first occurrence of boundary-layer separation at free-stream Mach numbers up to 0.43 are considerably lower for the RC-10(N)-1 airfoil (1.14 to 1.45) than for the 10-64C airfoil (1.80) (ref. 10); this suggests that the maximum local Mach number is not a very accurate parameter for predicting separation during an airfoil design process. The maximum local Mach number (or minimum pressure coefficient) at the stall has been used successfully to predict $c_{n,max}$ (ref. 7) suggesting that the new airfoils for which the prediction worked were similar to airfoils previously tested and used as a data base for developing the prediction technique.

The maximum normal-force coefficients of the RC-10(N)-1 and the SC 1095 (with tab) airfoils have been determined from figure 11 and are compared in figure 12. The SC 1095 airfoil was chosen for comparison because it is used on the main rotor of two new helicopters, the UH-60A (UTTAS) and the S-76 (refs. 18 and 19), it was tested in the same wind tunnel (ref. 14) as the RC-10(N)-1 airfoil, and it has close to the same maximum thickness ratio (9.1 percent chord) as the RC-10(N)-1 airfoil. The maximum normal-force coefficients of the RC-10(N)-1 airfoil are about the same as those of the SC 1095 airfoil for Mach numbers up to 0.50.

Pitching Moment

The pitching-moment coefficient about the aerodynamic center (c_m at $c_n = 0$) for the smooth model (fig. 4(b)) at the higher Reynolds numbers varies from about 0.007 at subcritical flow conditions ($M \leq 0.68$) to -0.025 at supercritical flow conditions ($M = 0.87$). This trend of the pitching-moment coefficient about the aerodynamic center to become more nose-down with increasing Mach number is caused by the development and expansion of a supercritical flow region near the leading edge of the airfoil on the lower surface with increasing Mach number and also a rearward shift of the upper surface shock position with increasing Mach number. (See fig. 22(b).) The pitching-moment coefficient about the aerodynamic center is about zero at the higher Reynolds numbers for Mach numbers from 0.77 to 0.82; thus, the design goal is met. Neither a decrease in Reynolds number (fig. 4(b)) nor the addition of roughness strips to the model (fig. 5(b)) had any effect on the pitching-moment coefficients.

At Mach numbers as high as 0.68, the pitching-moment coefficients are positive for positive normal-force coefficients up to the maximum indicating a center of pressure forward of the quarter-chord and the slopes of the curves indicate that the center of pressure moves rearward with increasing normal-force coefficient except for normal-force coefficients near the maximum at some Mach numbers where a positive slope indicates a forward movement of the center of pressure. This positive slope is the result of an expansion of the supersonic zone near the leading edge on the upper surface with increasing normal-force coefficient. (See fig. 20(g), for example.) The center of pressure is aft of the quarter-chord only for the higher normal-force coefficients at Mach numbers of 0.73 and 0.77 and is aft of the quarter-chord for most positive normal-force coefficients at Mach numbers of 0.80 and higher. The aerodynamic center (based on positive normal-force coefficients up to 0.6) is rearward of the quarter-chord for Mach numbers up to 0.83 and is coincident with the quarter-chord point at a Mach number of 0.87.

The pitching-moment coefficients of the RC-10(N)-1 airfoil are compared with those of the SC 1095 airfoil (ref. 14) in figure 11(b). Both airfoils have near-zero pitching-moment coefficients for a wide range of normal-force coefficients at Mach numbers up to 0.78. The pitching-moment coefficient about the aerodynamic center (c_m at $c_n = 0$) of the RC-10(N)-1 airfoil is the same as that of the SC 1095 airfoil at Mach numbers up to 0.78 and is more negative than that of the SC 1095 airfoil by about 0.01 at a Mach number of 0.83.

Drag

Minimum drag.- At Mach numbers up to 0.73, the minimum drag coefficient for the smooth model at the higher Reynolds numbers (fig. 4(c)) is about 0.0065 and the minimum drag coefficient occurs at a normal-force coefficient of about 0.1. At Mach numbers above 0.73, the minimum drag coefficient increases with increasing Mach number and the minimum drag coefficient occurs at progressively lower normal-force coefficients with increasing Mach number; the values of $c_{d,min}$ range from 0.0070 to 0.0235 at Mach numbers of 0.77 and 0.87, respectively. This trend of $c_{d,min}$ with Mach number is caused by the development of supercritical flow with its associated wave drag. Lowering the Reynolds number had no effect on the minimum drag coefficient for Mach numbers up to 0.77 and it increased $c_{d,min}$ by a small amount for Mach numbers greater than 0.77. The addition of roughness strips increased the minimum drag coefficients by about 0.0010 for Mach numbers up to 0.80 and by about 0.0015 for the higher Mach numbers. (See fig. 5(c).)

The drag coefficients of the RC-10(N)-1 airfoil are compared with those of the SC 1095 airfoil in figure 11(c). At Mach numbers up to 0.49, minimum drag coefficients of the RC-10(N)-1 airfoil are about 0.0015 lower than those of the SC 1095 airfoil. However, the SC 1095 airfoil data were obtained by testing at stagnation pressures above 517 kPa (75 psia), approximately twice those used to obtain the RC-10(N)-1 airfoil data, where the tunnel turbulence level is believed to cause higher drag coefficients (ref. 14) than those which would be measured in free air. At Mach numbers of 0.73 and 0.78, the minimum drag coefficients of the RC-10(N)-1 airfoil are lower than those of the SC 1095 airfoil and they occur at higher normal-force coefficients than those of the SC 1095 airfoil. The minimum drag coefficient of the RC-10(N)-1 airfoil is about 0.0020 lower than that of the other airfoil at a Mach number of 0.83 but it also occurs at a lower normal-force coefficient than that of the other airfoil.

Maximum normal-force—drag ratio.- The maximum normal-force—drag ratios for the smooth model at two Reynolds numbers have been determined from figure 4(c) and the ratios for the model with and without roughness applied have been determined from figure 5(c) and these are presented as a function of Mach number in figure 8. The smooth model values at the higher Reynolds numbers decrease from 97 at a Mach number of 0.33 to 92 at a Mach number of 0.63 and above this Mach number the values decrease sharply with increasing Mach number. Reducing the Reynolds number lowered the ratios a small amount at Mach numbers less than 0.73, as expected, but it had no effect on the ratios at higher Mach numbers. The addition of roughness reduced the maximum normal-force—drag ratios at Mach numbers up to about 0.68 but it had no effect on the ratios at Mach numbers of 0.78 and higher.

By drawing a tangency to the drag curves presented in figure 11(c), the values of $(c_n/c_d)_{\max}$ of the RC-10(N)-1 airfoil are shown to exceed those of the SC 1095 airfoil at all Mach numbers except 0.83; the difference is large at a Mach number of 0.73 where the value of the RC-10(N)-1 airfoil is about 55 and that of the SC 1095 airfoil is about 32. Since the drag coefficients of the RC-10(N)-1 airfoil at normal-force coefficients from 0.5 to 0.7 at Mach numbers from near 0.4 to near 0.7 are lower than the corresponding drag coefficients of the SC 1095 airfoil, the normal-force--drag ratios important to hover performance are higher for the RC-10(N)-1 airfoil. (See fig. 11(c).)

Drag divergence.— The smooth model drag coefficients (fig. 4(c)) and the drag coefficients with and without roughness applied to the model (fig. 5(c)) were cross plotted to obtain the drag divergence Mach numbers at a constant normal-force coefficient and these results are presented in figure 9. The drag divergence Mach number for the smooth model at the higher Reynolds numbers varies from 0.815 at zero normal-force coefficient to 0.61 at a normal-force coefficient of 0.9; thus, both drag divergence design goals (including the pitching-moment constraints) are met. (See fig. 4(b).) Decreasing the Reynolds number reduced the drag divergence Mach number by 0.01 at most at normal-force coefficients less than 0.2 and it did not affect the drag divergence Mach numbers at normal-force coefficients from 0.2 to 0.7. At normal-force coefficients of 0.6 and 0.7, the drag divergence Mach numbers at the lower Reynolds numbers were estimated by a comparison of the drag coefficients at the lower Reynolds numbers to the faired c_d -M curves at the higher Reynolds numbers (fig. 10) since the drag coefficients at the lower Reynolds numbers were not measured at small enough increments in Mach number for these normal-force coefficients (fig. 4(c)). It was not possible to estimate the drag divergence Mach numbers at normal-force coefficients above 0.7. The addition of roughness reduced the drag divergence Mach numbers at some normal-force coefficients with the maximum decrement being about 0.02.

The drag divergence characteristics of the RC-10(N)-1 airfoil are compared with those of the SC 1095 airfoil in figure 12. The RC-10(N)-1 airfoil has a higher drag divergence Mach number at normal-force coefficients above 0.3; at normal-force coefficients of 0.6 and 0.7, the increment in M_{dd} is about 0.1. At normal-force coefficients between about 0.3 and -0.05, the SC 1095 airfoil has a higher drag divergence Mach number, but these differences would be reduced if the maximum thickness ratio of the RC-10(N)-1 airfoil were reduced about 1 percent to match that of the SC 1095 airfoil (maximum thickness ratio of 9.1 percent). The theoretical values shown in figure 19 imply that the drag divergence Mach number at zero normal-force coefficient would increase by less than 0.01 as a result of decreasing the maximum thickness ratio of the RC-10(N)-1 airfoil to 9.1 percent chord. Although the SC 1095 airfoil does have a higher drag divergence Mach number at low normal-force coefficients, the drag coefficient of the SC 1095 airfoil at the drag divergence Mach number is also 0.0016 to 0.0048 higher than that of the RC-10(N)-1 airfoil. (See fig. 13.) In fact, the SC 1095 airfoil offers little advantage over the RC-10(N)-1 airfoil at a normal-force coefficient of 0.2 because the drag coefficient of the RC-10(N)-1 airfoil is less than that of the SC 1095 airfoil for Mach numbers up to 0.795, which is only 0.01 less than the drag divergence Mach number of the SC 1095 airfoil (fig. 14).

Comparison With Theory

Normal force.- The maximum normal-force coefficient of the smooth model at a Mach number of 0.4 is compared with normal-force coefficients predicted by theory in figure 15. The theoretical values were obtained by inputting a normal-force coefficient at a Mach number of 0.4 to the code and then letting the code solve for the angle of attack required to achieve (if possible) the desired normal-force coefficient. The theoretical values were calculated with transition fixed at 5 percent chord as previously explained. The experimental value of $C_{n,max}$ is lower than the calculated normal-force coefficients by about 0.12 to 0.22 when the predicted upper surface separation point is at 99 percent chord and 93 percent chord, respectively. The primary reason for these differences is believed to be the premature separation of the tunnel side-wall boundary layer which reduces the experimental value of $C_{n,max}$. A comparison of the experimental and theoretical pressure distributions at a Mach number of 0.39 indicates that the experimental upper surface pressures do not recover to positive values as large as those predicted by theory near the airfoil trailing edge. (See figs. 23(a) to (d).) The difference in experiment and theory near the trailing edge increases with increasing normal-force coefficient; thus, the presence of separated flow is implied in the experimental data. The decrease in slope of the normal-force curve at normal-force coefficients above about 0.95 at a Mach number of 0.39 is a further indication of the presence of separated flow in the experimental data (fig. 4(a)).

Pitching moment.- The smooth model pitching-moment coefficients at four Mach numbers are compared with those predicted by theory in figure 17. At the lowest Mach number, the differences in the two curves are no more than 0.01 for normal-force coefficients up to about 0.8 and then they increase with increasing normal-force coefficient. The differences in pitching-moment coefficient at the higher normal-force coefficients (>0.95) are caused by the presence of separated flow in the experimental data. The experimental and theoretical pitching-moment curves at the three higher Mach numbers differ by about 0.01 or less. At Mach numbers of 0.80 and 0.82, comparisons are not presented at higher normal-force coefficients because the theory indicated separation of the upper surface boundary layer near 60 percent chord for normal-force coefficients 0.1 greater than those shown. A comparison of the pressure distributions at a Mach number of 0.80 (figs. 23(g) and (h)) suggests that the theoretical pitching-moment coefficients are more negative because the shock position calculated by theory is about 5 percent chord farther aft than the experimental shock position.

Drag.- The minimum drag coefficients with roughness applied to the model agree well with those calculated by theory (fig. 18) for Mach numbers up to 0.82 but there is a 0.0020 difference in the experimental and calculated values at the highest Mach number. At the two lower Mach numbers, the two drag curves compare well for normal-force coefficients up to about 0.6. Since the normal-force curve at a Mach number of 0.39 is nonlinear at normal-force coefficients above about 0.80 (fig. 5(a)), the differences in the experimental and calculated drag curves at these normal-force coefficients may be due to the presence of separated flow in the experimental data. Analysis of the normal-force curve and the pressure distributions at a Mach number of 0.68 indicates that the differences in the drag curves at this Mach number at normal-force coefficients between 0.60 and 0.77 are not caused by separated flow in the experimental data.

Theoretical drag coefficients at Mach numbers of 0.80 and higher are presented only for low normal-force coefficients because the theory indicated separation near 60 percent chord for normal-force coefficients 0.05 higher than those shown.

The drag divergence Mach numbers predicted by theory at three normal-force coefficients are compared to the experimentally determined drag divergence curve in figure 15. The theoretical drag divergence Mach numbers were determined from faired curves through the calculated drag coefficients as shown in figure 16. The theoretical drag divergence Mach number at each of the three normal-force coefficients (0.0, 0.5, and 0.9) differs from the experimental value by no more than 0.01. Note in figure 16 that the calculated drag coefficients at normal-force coefficients of 0.0 and 0.5 can define only a single faired curve but those at a normal-force coefficient of 0.9 could have defined at least two curves; for example, if calculations had been made only at Mach numbers of 0.60, 0.64, and 0.65, a different curve with a drag divergence Mach number 0.03 higher would have resulted. Therefore, it is important during an airfoil analysis to choose small increments in Mach number as the anticipated drag divergence Mach number at high normal-force coefficients is approached otherwise a significant over-prediction of M_{dd} could result. A comparison of the theoretical and experimental pressure distributions at three conditions (M and c_n) close to the experimentally determined drag divergence curve of figure 15 indicates a small shift of the shock position in each case and a close agreement of the pressure rise through the shock at the two higher Mach numbers. (See figs. 23(e) to (g).)

CONCLUSIONS

An investigation has been conducted in the Langley 6- by 28-Inch Transonic Tunnel to determine the two-dimensional aerodynamic characteristics of a 10-percent-thick helicopter rotor airfoil at Mach numbers M from 0.33 to 0.87 and respective Reynolds numbers from 4.9×10^6 to 9.8×10^6 . This airfoil, designated the RC-10(N)-1, was also investigated at Reynolds numbers from 3.0×10^6 to 7.3×10^6 at respective Mach numbers of 0.33 to 0.83 for comparison with the SC 1095 (with tab) airfoil. The RC-10(N)-1 airfoil was designed by the use of a viscous transonic analysis code; comparisons of experiment and theory have been made. Analysis of the test data has resulted in the following conclusions:

1. Measurements in the same wind tunnel at comparable Reynolds numbers indicated that the maximum normal-force coefficient $c_{n,max}$ of the RC-10(N)-1 airfoil was higher than that of the NACA 0012 airfoil for Mach numbers above about 0.35 and was about the same as that of the SC 1095 airfoil for Mach numbers up to 0.50.
2. The maximum normal-force coefficient design goal of 1.2 at a Mach number of 0.4 was achieved by the RC-10(N)-1 airfoil when the measured value of $c_{n,max}$ was incremented by the same value required to match the maximum normal-force coefficient of the NACA 0012 airfoil measured in the Langley 6- by 28-Inch Transonic Tunnel at a Mach number of 0.36 to those measured in two other test facilities.

3. The pitching-moment coefficient about the aerodynamic center of the RC-10(N)-1 airfoil varied from about 0.007 at subcritical flow conditions ($M \leq 0.68$) to -0.025 at supercritical flow conditions ($M = 0.87$). The pitching-moment coefficient about the aerodynamic center was about zero for Mach numbers from 0.77 to 0.82; thus, the design objective was met.

4. The drag divergence Mach number at the higher Reynolds numbers varied from 0.815 at zero normal-force coefficient to 0.61 at a normal-force coefficient of 0.9; thus, both drag divergence design goals (including the pitching-moment constraints) were met.

5. At comparable Reynolds numbers, the drag divergence Mach number of the RC-10(N)-1 airfoil was higher than that of the SC 1095 airfoil at normal-force coefficients above 0.3. While the SC 1095 airfoil did have a higher drag divergence Mach number at low normal-force coefficients (-0.05 to 0.3), the drag coefficient of the SC 1095 airfoil at the drag divergence Mach number was also 0.0016 to 0.0048 higher than that of the RC-10(N)-1 airfoil.

6. The drag divergence Mach numbers predicted by theory at normal-force coefficients of 0.0, 0.5, and 0.9 differed from the experimental values by no more than 0.01. The pitching-moment coefficients predicted by theory differed from the experimental values by 0.01 or less.

Langley Research Center
National Aeronautics and Space Administration
Hampton, VA 23665
May 6, 1981

REFERENCES

1. Bingham, Gene J.: An Analytical Evaluation of Airfoil Sections for Helicopter Rotor Applications. NASA TN D-7796, 1975.
2. Bauer, Frances; Garabedian, Paul; Korn, David; and Jameson, Antony: Supercritical Wing Sections II. Volume 108 of Lecture Notes in Economics and Mathematical Systems, Springer-Verlag, 1975.
3. Garabedian, P. R.: Computation of Wave Drag for Transonic Flow. J. Anal. Math., vol. 30, 1976, pp. 164-171.
4. Garabedian, P. R.: Transonic Flow Theory of Airfoils and Wings. Advances in Engineering Science, Volume 4, NASA CP-2001, [1976], pp. 1349-1358.
5. Wortmann, F. X.; and Drees, Jan M.: Design of Airfoils for Rotors. CAL/AVLABS Symposium Proceedings: Aerodynamics of Rotary Wing and V/STOL Aircraft, Volume I - Rotor/Propeller Aerodynamics, Rotor Noise, June 1969.
6. Thibert, Jean-Jacques; and Gallot, Jacques: A New Airfoil Family for Rotor Blades. ONERA T.P. No. 1977-113, Sept. 1977.
7. Thibert, Jean-Jacques; and Gallot, Jacques: Advanced Research on Helicopter Blade Airfoils. ONERA T.P. No. 1979-120, Sept. 1979.
8. Dadone, Leo: Rotor Airfoil Optimization: An Understanding of the Physical Limits. Preprint No. 78-4, 34th Annual National Forum, American Helicopter Soc., Inc., May 1978.
9. Noonan, Kevin W.; and Bingham, Gene J.: Two-Dimensional Aerodynamic Characteristics of Several Rotorcraft Airfoils at Mach Numbers From 0.35 to 0.90. NASA TM X-73990, 1977.
10. Bingham, Gene J.; and Noonan, Kevin W.: Experimental Investigation of Three Helicopter Rotor Airfoils Designed Analytically. NASA TP-1396, AVRADCOM TR 79-11, 1979.
11. Ladson, Charles L.: Description and Calibration of the Langley 6- by 28-Inch Transonic Tunnel. NASA TN D-8070, 1975.
12. Barnwell, Richard W.: Design and Performance Evaluation of Slotted Walls for Two-Dimensional Wind Tunnels. NASA TM-78648, 1978.
13. Bernard-Guelle, René: Influence of Wind Tunnel Wall Boundary Layers on Two-Dimensional Transonic Tests. NASA TT F-17,255, 1976.
14. Noonan, Kevin W.; and Bingham, Gene J.: Aerodynamic Characteristics of Three Helicopter Rotor Airfoil Sections at Reynolds Numbers From Model Scale to Full Scale at Mach Numbers From 0.35 to 0.90. NASA TP-1701, AVRADCOM TR 80-B-5, 1980.

15. Braslow, Albert L.; and Knox, Eugene C.: Simplified Method for Determination of Critical Height of Distributed Roughness Particles for Boundary Layer Transition at Mach Numbers From 0 to 5. NACA TN 4363, 1958.
16. Baals, Donald D.; and Mourhess, Mary J.: Numerical Evaluation of the Wake-Survey Equations for Subsonic Flow Including the Effect of Energy Addition. NACA WR L-5, 1945. (Formerly NACA ARR L5H27.)
17. Davis, Don D., Jr.; and Moore, Dewey: Analytical Study of Blockage- and Lift-Interference Corrections for Slotted Tunnels Obtained by the Substitution of an Equivalent Homogeneous Boundary for the Discrete Slots. NACA RM L53E07b, 1953.
18. Arcidiacono, Peter; and Zincone, Robert: Titanium UTTAS Main Rotor Blade. Preprint No. 980, 31st Annual National Forum, American Helicopter Soc., Inc., May 1975.
19. Fradenburgh, Evan A.: Aerodynamic Design of the Sikorsky S-76 Helicopter. Preprint No. 78-06, 34th Annual National Forum, American Helicopter Soc., Inc., May 1978.

TABLE I.- DESIGN COORDINATES FOR RC-10(N)-1 AIRFOIL

[Stations and ordinates given in percent airfoil chord]

Upper surface		Lower surface	
Station	Ordinate	Station	Ordinate
0.000	0.634	0.000	0.634
.040	.883	.460	-.042
.298	1.346	.702	-.164
.909	1.926	1.591	-.438
2.289	2.733	2.710	-.652
4.765	3.671	5.235	-.994
7.329	4.361	7.671	-1.268
9.841	4.892	10.159	-1.524
12.359	5.332	12.640	-1.758
14.884	5.703	15.115	-1.970
17.413	6.014	17.586	-2.163
19.951	6.269	20.048	-2.337
22.484	6.473	22.515	-2.498
25.005	6.630	24.994	-2.645
30.043	6.827	29.955	-2.895
35.076	6.884	34.922	-3.079
37.592	6.864	37.405	-3.145
40.105	6.810	39.893	-3.190
42.617	6.723	42.381	-3.214
45.130	6.599	44.868	-3.214
47.639	6.439	47.359	-3.191
50.144	6.245	49.853	-3.145
52.649	6.019	52.348	-3.078
55.152	5.764	54.845	-2.991
57.653	5.482	57.344	-2.888
60.155	5.174	59.842	-2.772
62.659	4.842	62.337	-2.646
65.161	4.487	64.835	-2.515
67.664	4.114	67.332	-2.385
70.158	3.730	69.838	-2.262
72.641	3.344	72.355	-2.146
75.134	2.962	74.862	-2.036
77.615	2.595	77.381	-1.923
80.078	2.251	79.917	-1.794
82.549	1.925	82.446	-1.641
85.027	1.618	84.968	-1.460
87.511	1.329	87.483	-1.253
90.004	1.058	89.991	-1.031
92.500	.806	92.495	-.802
94.995	.576	94.999	-.569
97.491	.367	97.503	-.315
100.000	.179	100.000	.020

TABLE II.- DESIGN COORDINATES FOR RC-08(N)-1 AIRFOIL

[Stations and ordinates given in percent airfoil chord]

Upper surface		Lower surface	
Station	Ordinate	Station	Ordinate
0.000	0.541	0.000	0.541
.082	.837	.418	.056
.338	1.181	.662	-.031
.977	1.690	1.523	-.120
2.331	2.381	2.669	-.328
4.812	3.207	5.188	-.531
7.363	3.802	7.637	-.710
9.873	4.255	10.127	-.887
12.387	4.623	12.612	-1.056
14.907	4.936	15.092	-1.211
17.430	5.196	17.569	-1.354
19.961	5.408	20.038	-1.487
22.487	5.576	22.512	-1.611
25.004	5.703	24.995	-1.728
30.034	5.856	29.964	-1.931
35.061	5.890	34.937	-2.089
37.574	5.865	37.424	-2.149
40.084	5.813	39.914	-2.195
42.594	5.731	42.405	-2.226
45.104	5.620	44.894	-2.240
47.611	5.478	47.387	-2.236
50.115	5.308	49.882	-2.215
52.619	5.111	52.379	-2.177
55.122	4.890	54.876	-2.125
57.622	4.647	57.375	-2.060
60.124	4.381	59.873	-1.985
62.627	4.094	62.370	-1.905
65.129	3.788	64.868	-1.822
67.632	3.466	67.365	-1.742
70.127	3.133	69.870	-1.669
72.613	2.796	72.384	-1.604
75.107	2.464	74.889	-1.542
77.592	2.145	77.404	-1.477
80.062	1.847	79.934	-1.396
82.539	1.569	82.457	-1.290
85.022	1.311	84.975	-1.156
87.509	1.071	87.487	-.998
90.003	.849	89.992	-.824
92.500	.646	92.496	-.643
94.996	.462	94.999	-.456
97.493	.299	97.503	-.249
100.000	.164	100.000	.036

TABLE III.- DESIGN COORDINATES FOR RC-12(N)-1 AIRFOIL

[Stations and ordinates given in percent airfoil chord]

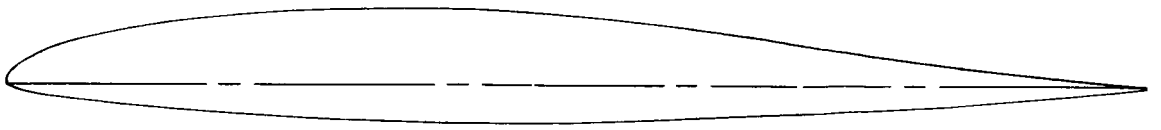
Upper surface		Lower surface	
Station	Ordinate	Station	Ordinate
0.000	0.801	0.000	0.801
.259	1.552	.002	.742
.842	2.186	.504	-.093
2.249	3.097	.745	-.255
4.720	4.134	1.661	-.653
7.296	4.921	2.755	-.960
9.811	5.534	5.284	-1.454
12.333	6.046	7.707	-1.825
14.862	6.477	10.192	-2.160
17.397	6.839	12.670	-2.460
19.943	7.137	15.140	-2.731
22.482	7.377	17.605	-2.975
25.007	7.565	20.059	-3.194
30.053	7.806	22.519	-3.392
35.093	7.888	24.994	-3.570
37.612	7.872	29.948	-3.866
40.127	7.818	34.907	-4.076
42.641	7.724	37.388	-4.146
45.157	7.588	39.873	-4.191
47.668	7.410	42.358	-4.210
50.174	7.192	44.842	-4.199
52.679	6.937	47.331	-4.158
55.183	6.647	49.824	-4.088
57.684	6.327	52.319	-3.990
60.187	5.976	54.815	-3.869
62.692	5.597	57.313	-3.728
65.194	5.194	59.810	-3.569
67.698	4.771	62.305	-3.397
70.190	4.336	64.802	-3.218
72.670	3.901	67.299	-3.039
75.161	3.469	69.806	-2.864
77.638	3.054	72.326	-2.698
80.094	2.661	74.835	-2.539
82.559	2.287	77.357	-2.377
85.033	1.930	79.901	-2.201
87.514	1.591	82.435	-1.999
90.005	1.269	84.962	-1.769
92.500	.969	87.480	-1.512
94.994	.692	89.989	-1.240
97.489	.437	92.494	-.963
100.000	.195	94.999	-.684
		97.504	-.385
		100.000	.005

TABLE IV.- LOCATIONS OF STATIC-PRESSURE ORIFICES

FOR RC-10(N)-1 AIRFOIL

[Locations given in percent airfoil chord]

Upper surface station	Lower surface station
0.00	0.00
1.19	1.20
2.44	2.46
4.96	4.95
7.47	7.44
9.93	9.95
14.94	14.96
19.94	19.97
24.94	24.97
29.94	29.97
34.84	34.96
39.89	39.96
44.86	44.90
49.91	49.91
54.91	54.90
59.86	59.90
64.91	64.87
69.92	69.92
74.93	74.90
79.91	79.92
84.92	84.92
89.90	89.94
94.93	94.92



RC-10(N)-1

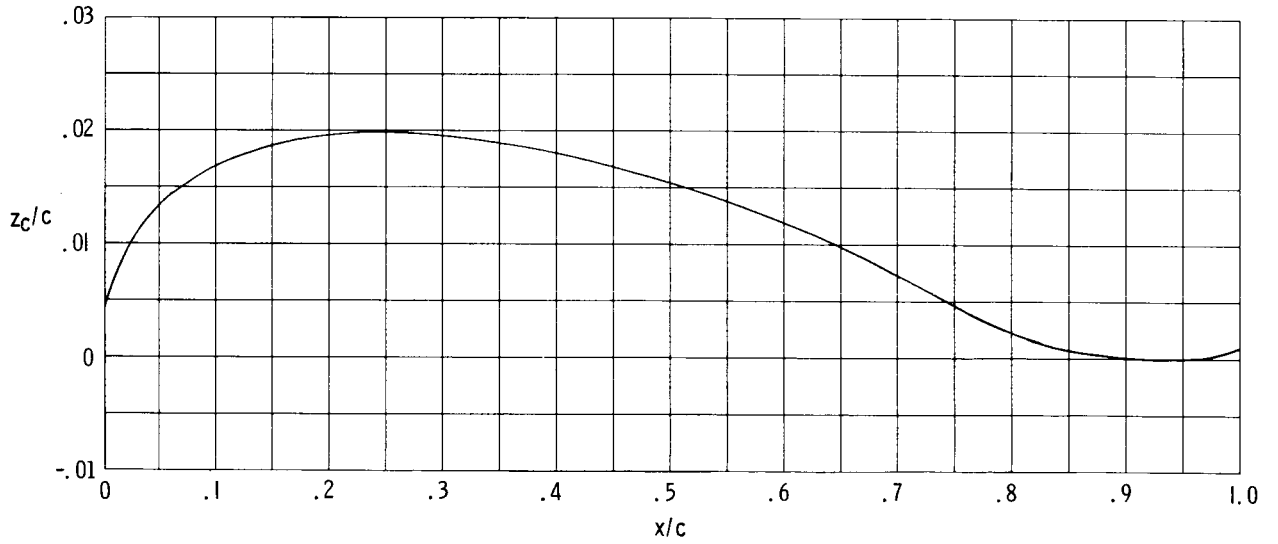
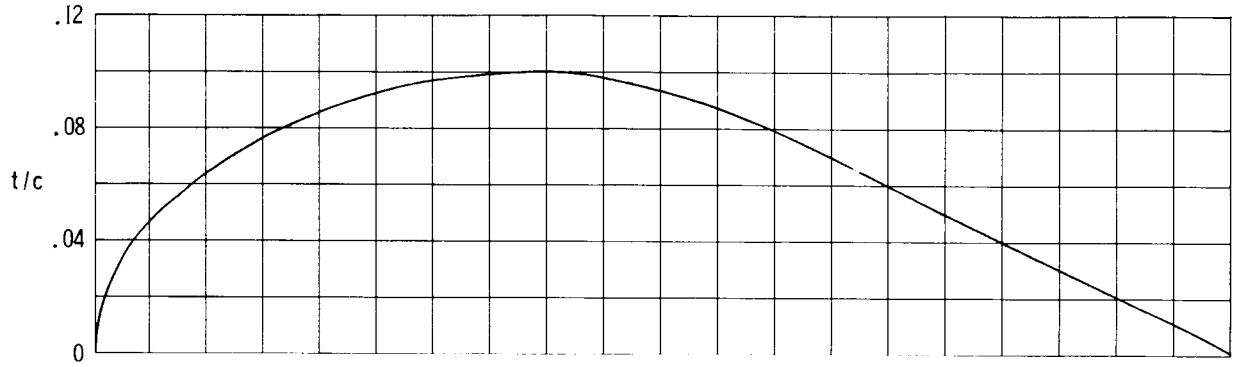


Figure 1.- Airfoil profile, thickness distribution, and camber line.

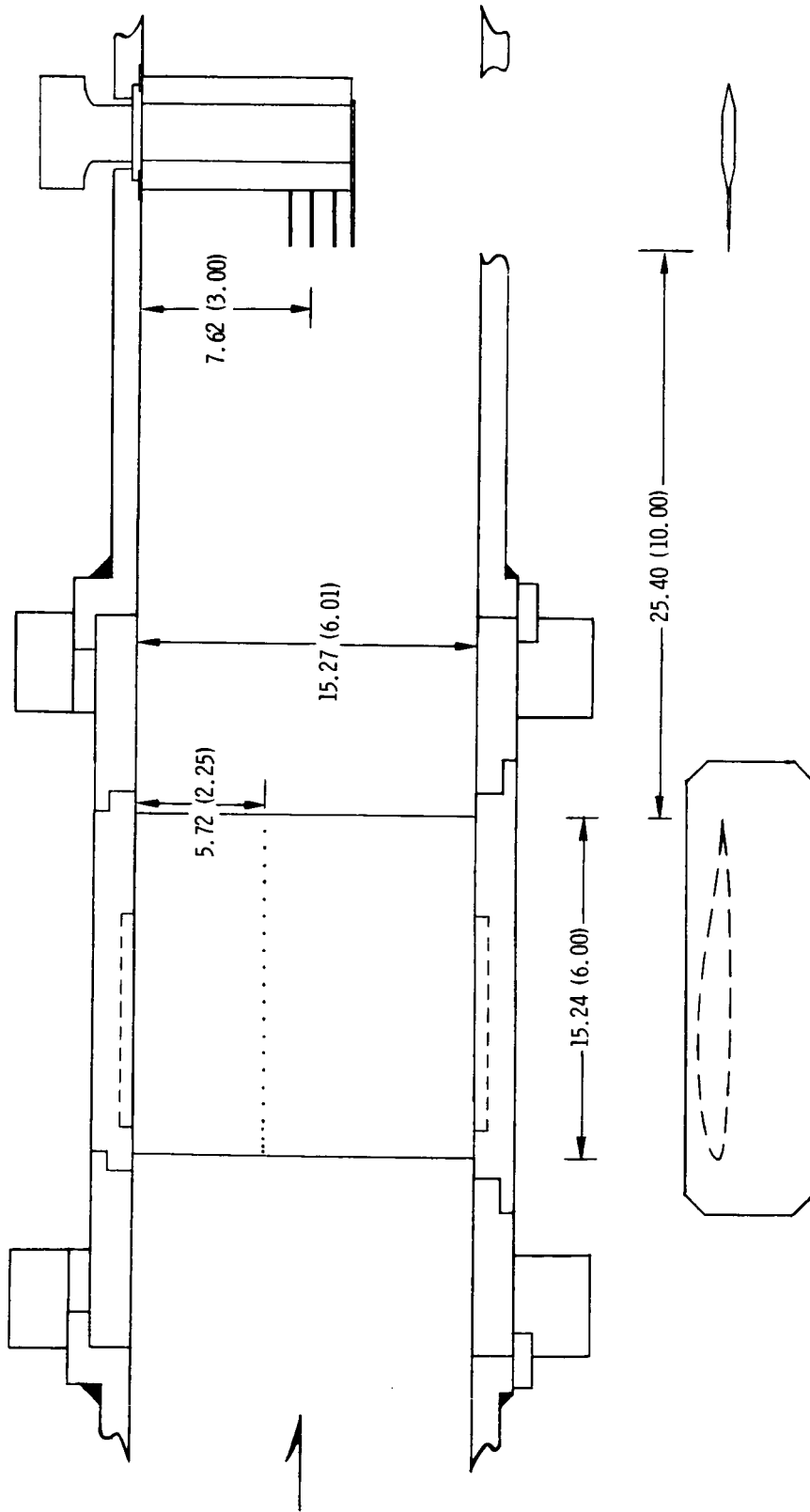


Figure 2.- Model and wake-survey probe installation in Langley 6- by 28-Inch Transonic Tunnel. All dimensions are in centimeters (inches).

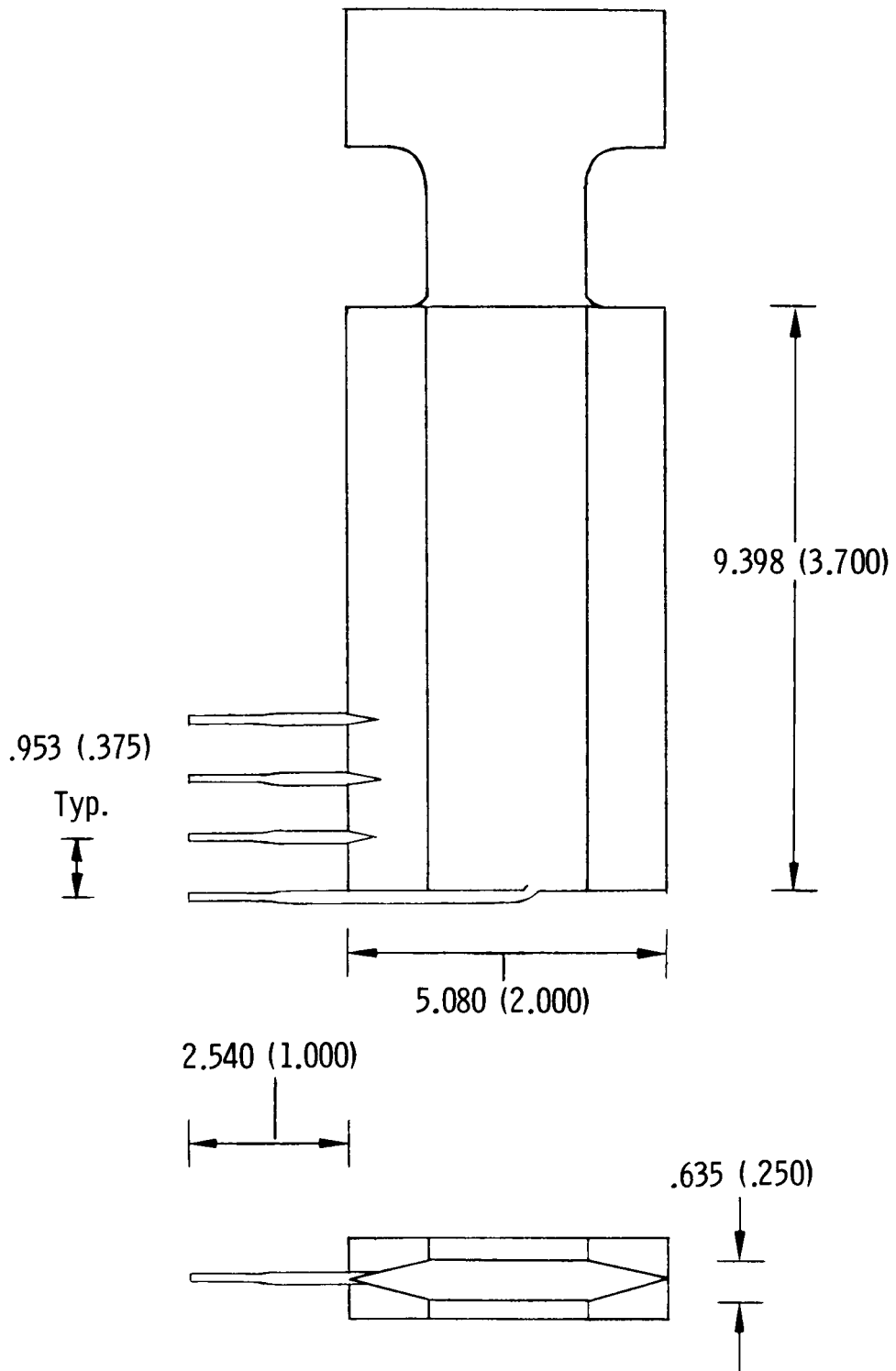
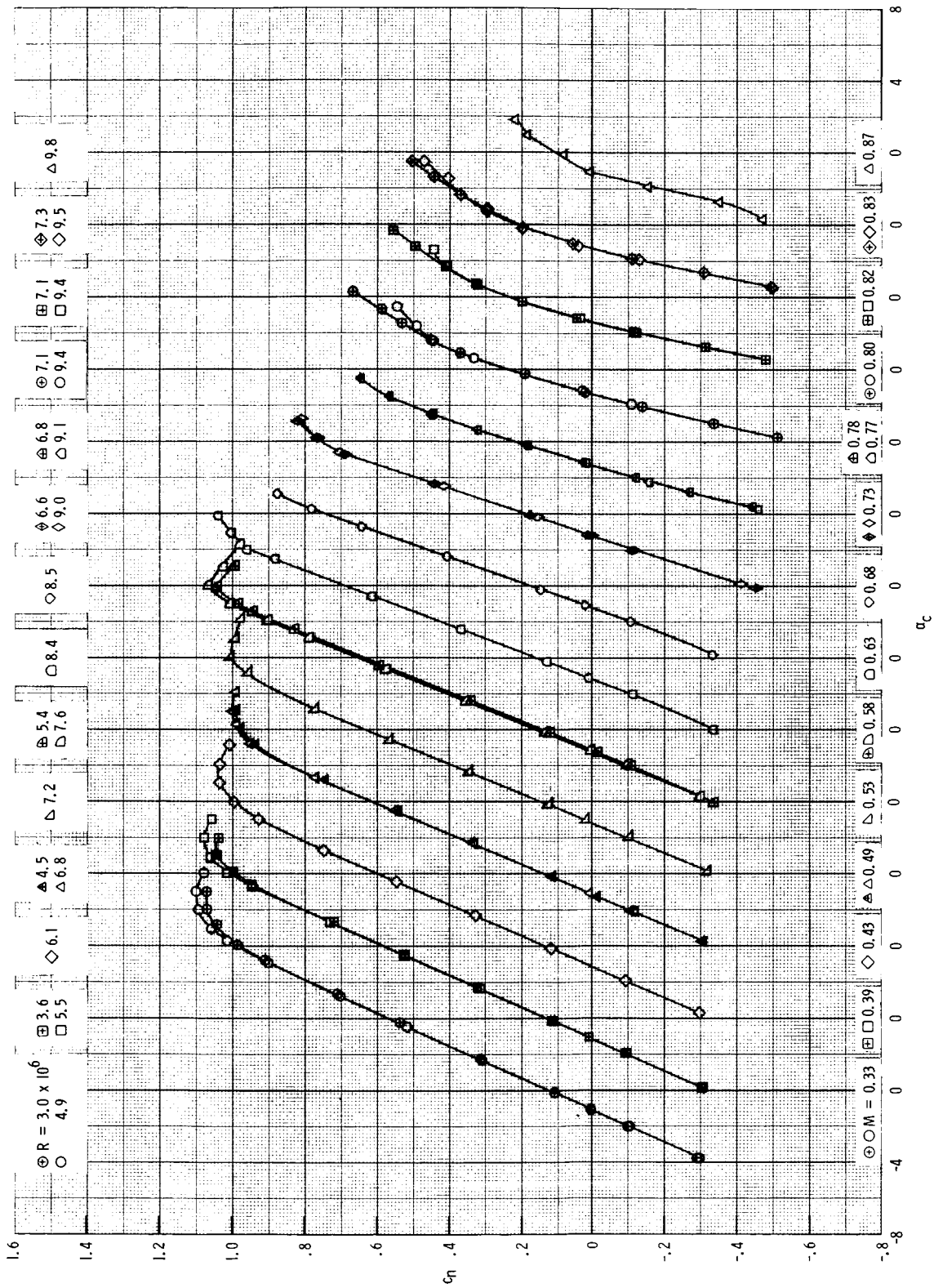
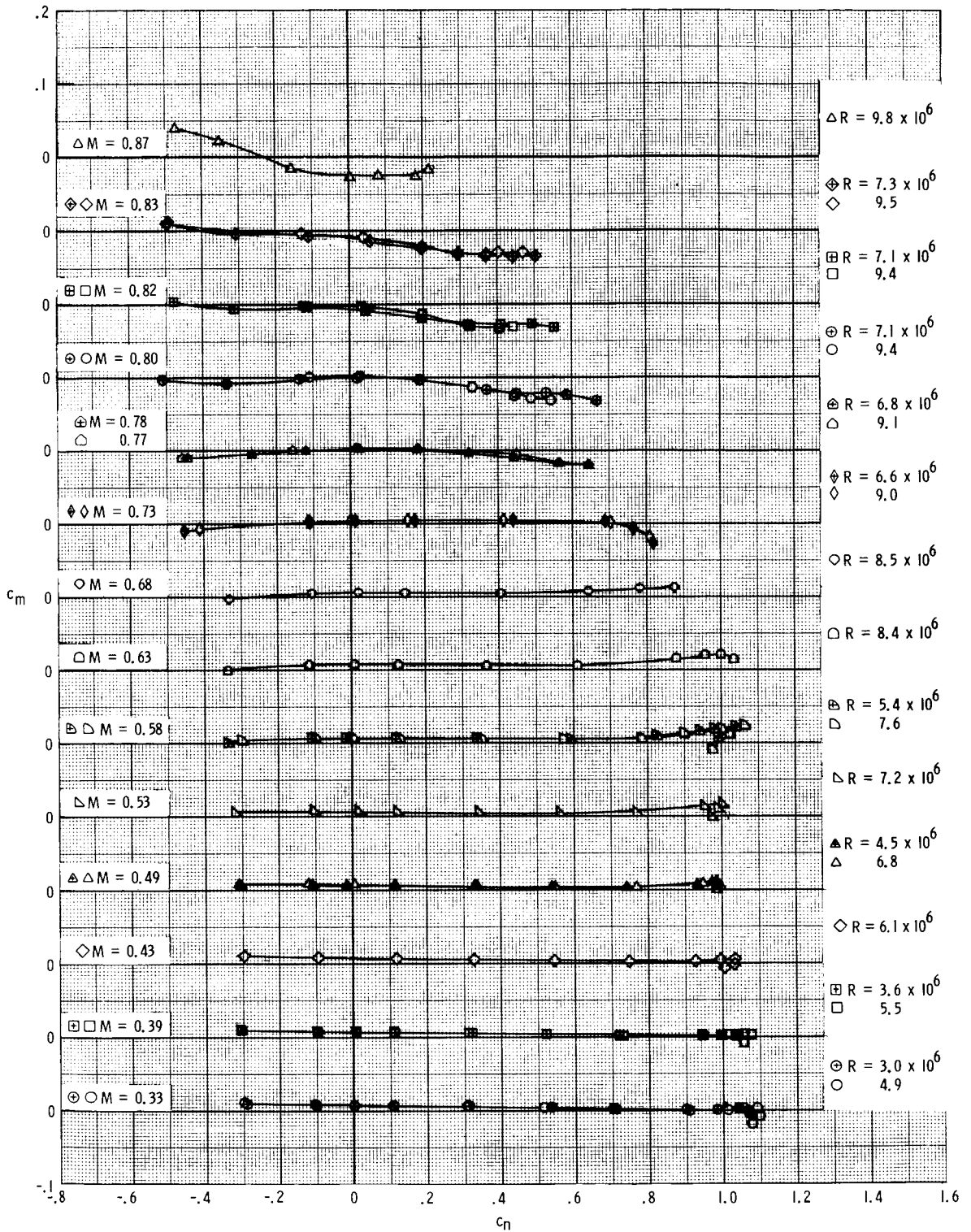


Figure 3.- Wake-survey probe used in Langley 6- by 28-Inch Transonic Tunnel. All dimensions are in centimeters (inches).



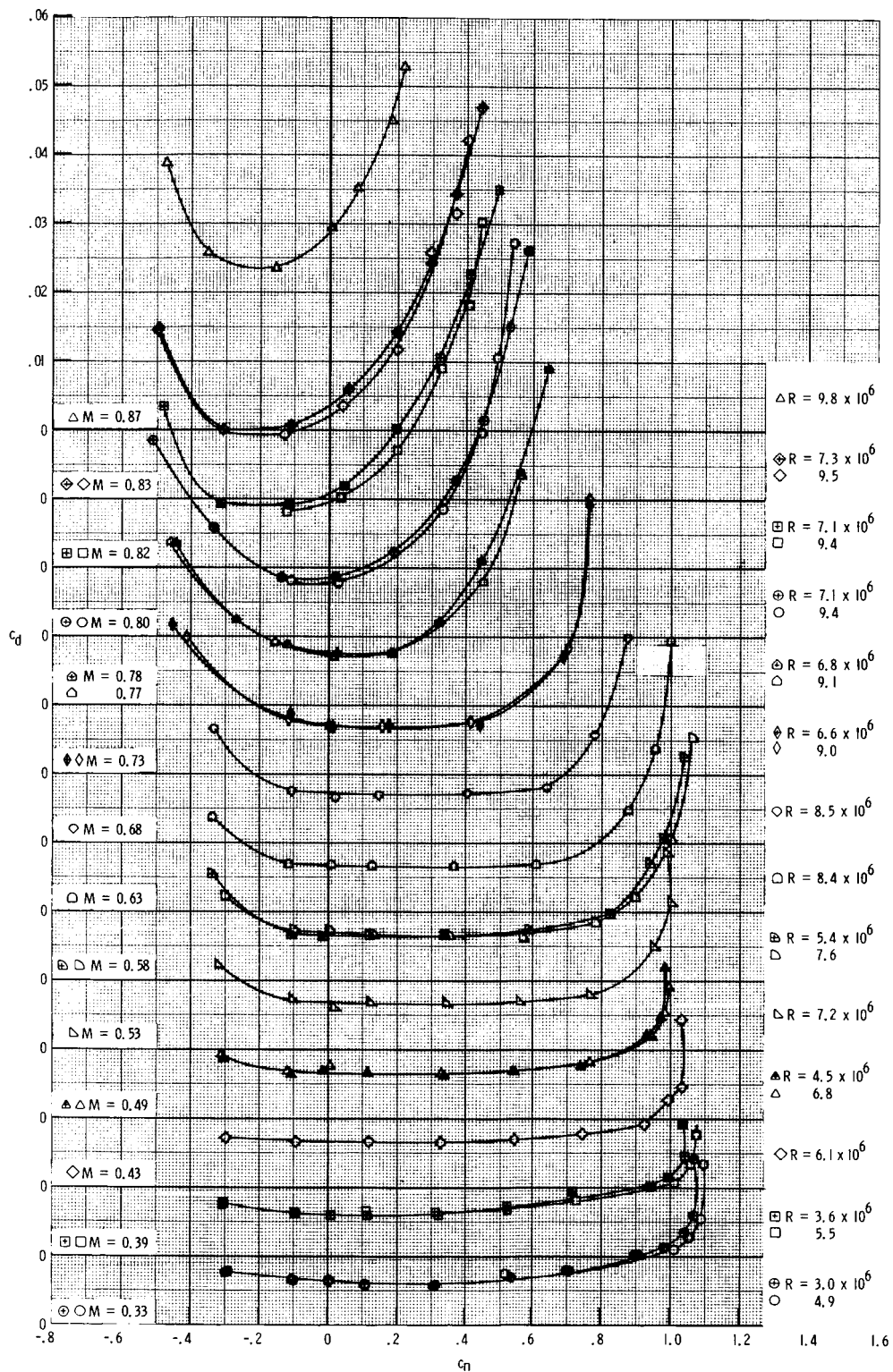
(a) Section normal-force coefficients.

Figure 4.- Aerodynamic characteristics of RC-10(N)-1 airfoil.



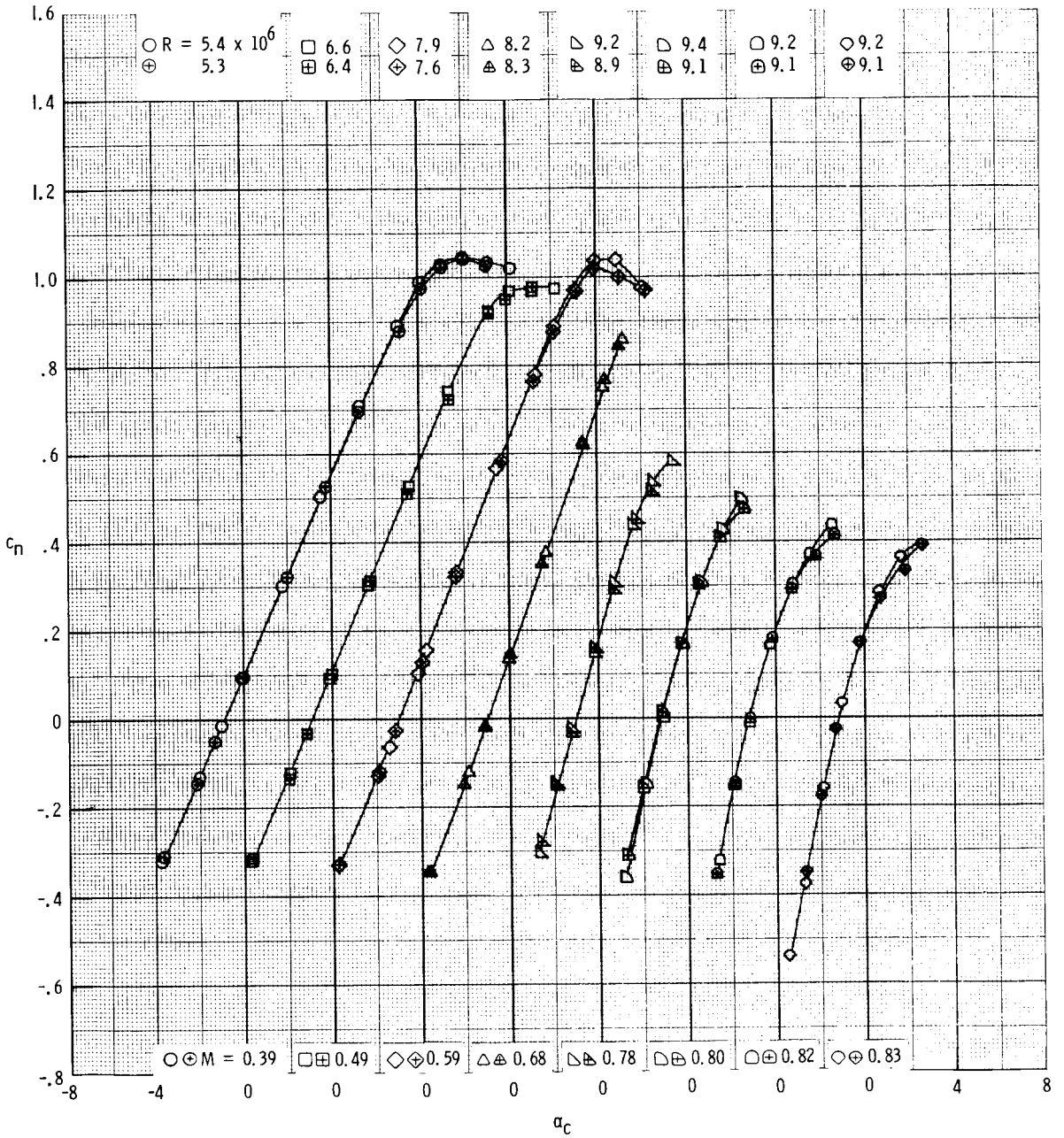
(b) Section pitching-moment coefficients.

Figure 4.- Continued.



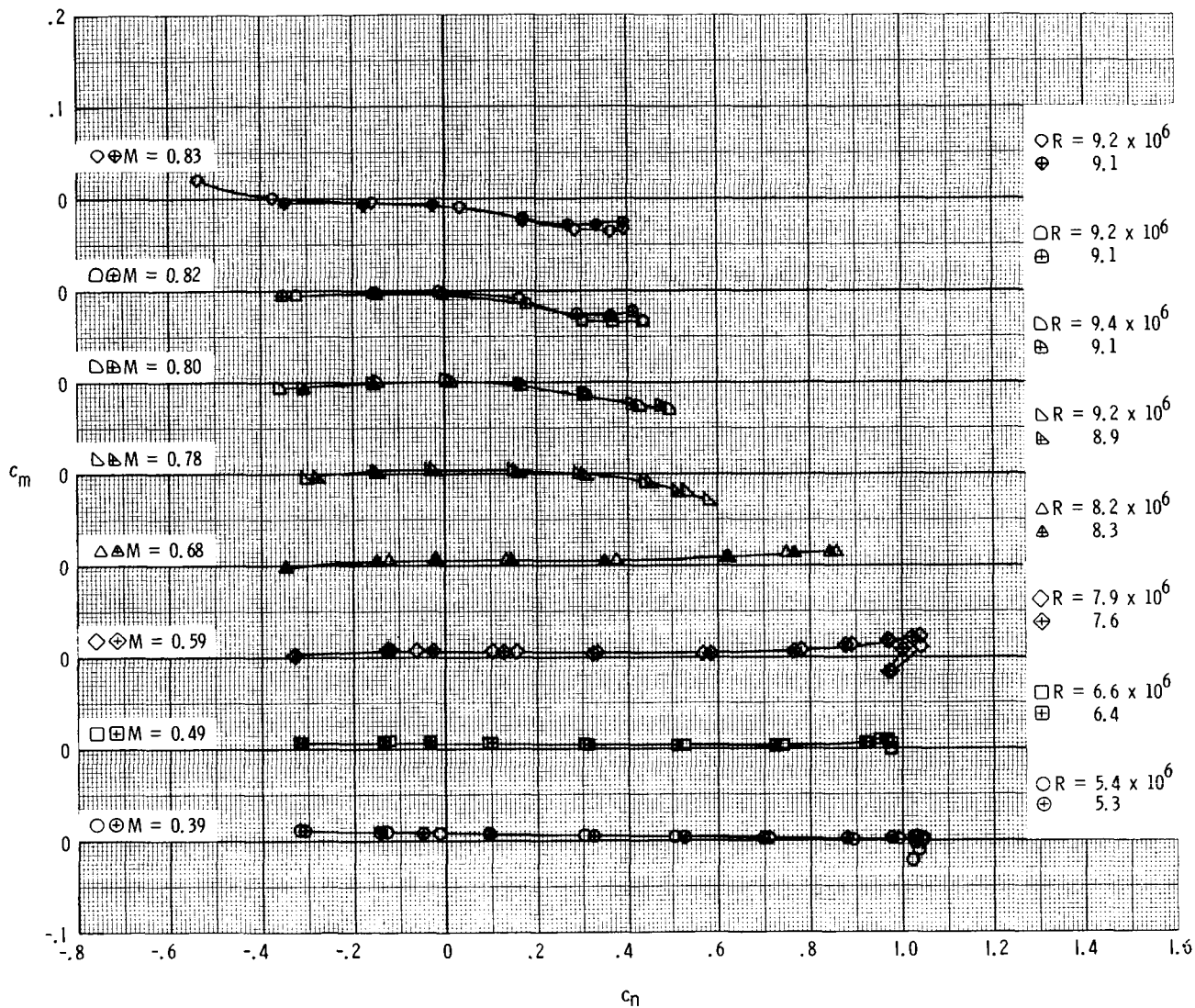
(c) Section drag coefficients.

Figure 4.- Concluded.



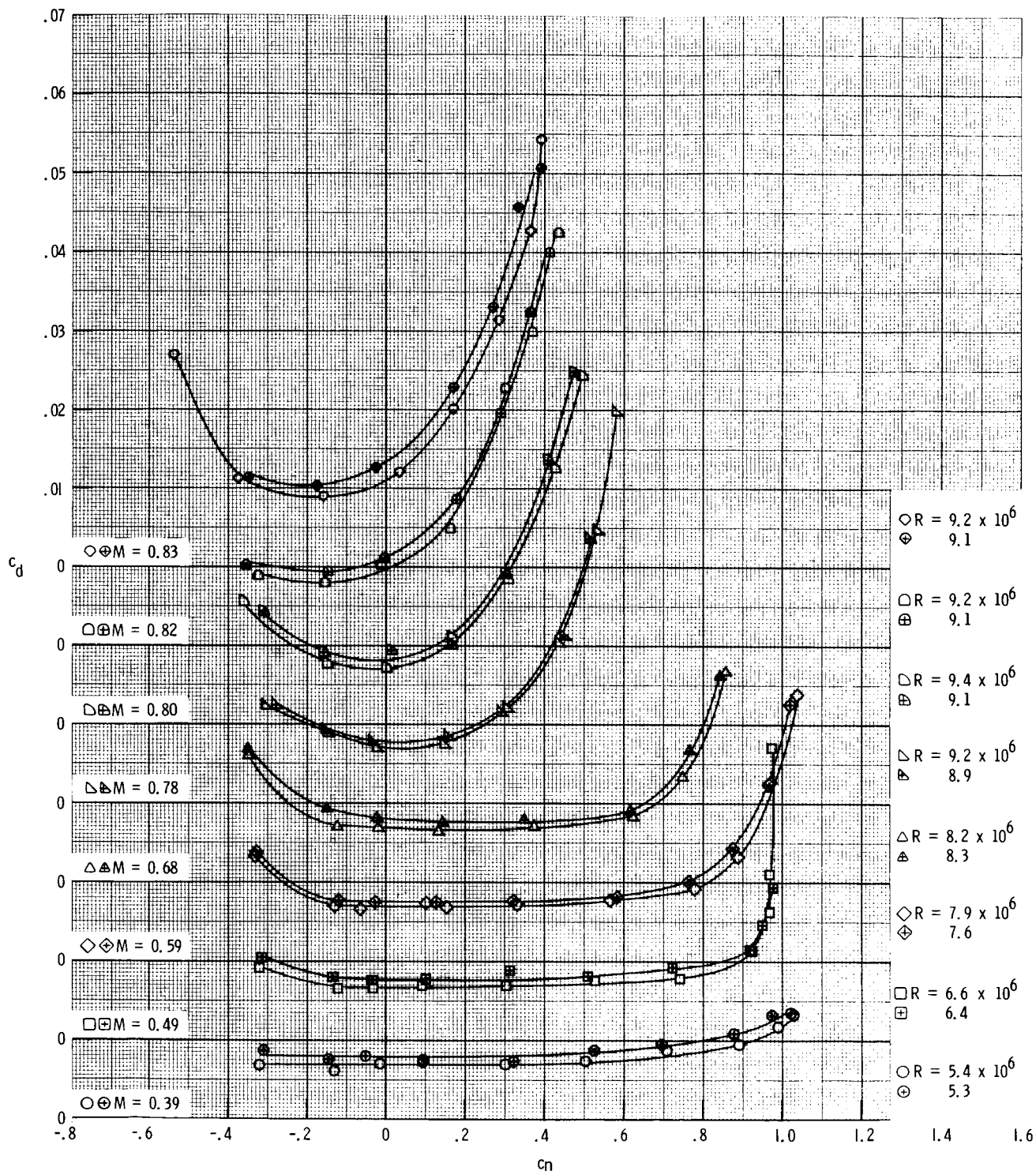
(a) Section normal-force coefficients.

Figure 5.- Effect of roughness on aerodynamic characteristics of RC-10(N)-1 airfoil. Open symbols indicate smooth model surface; centered symbols indicate transition fixed.



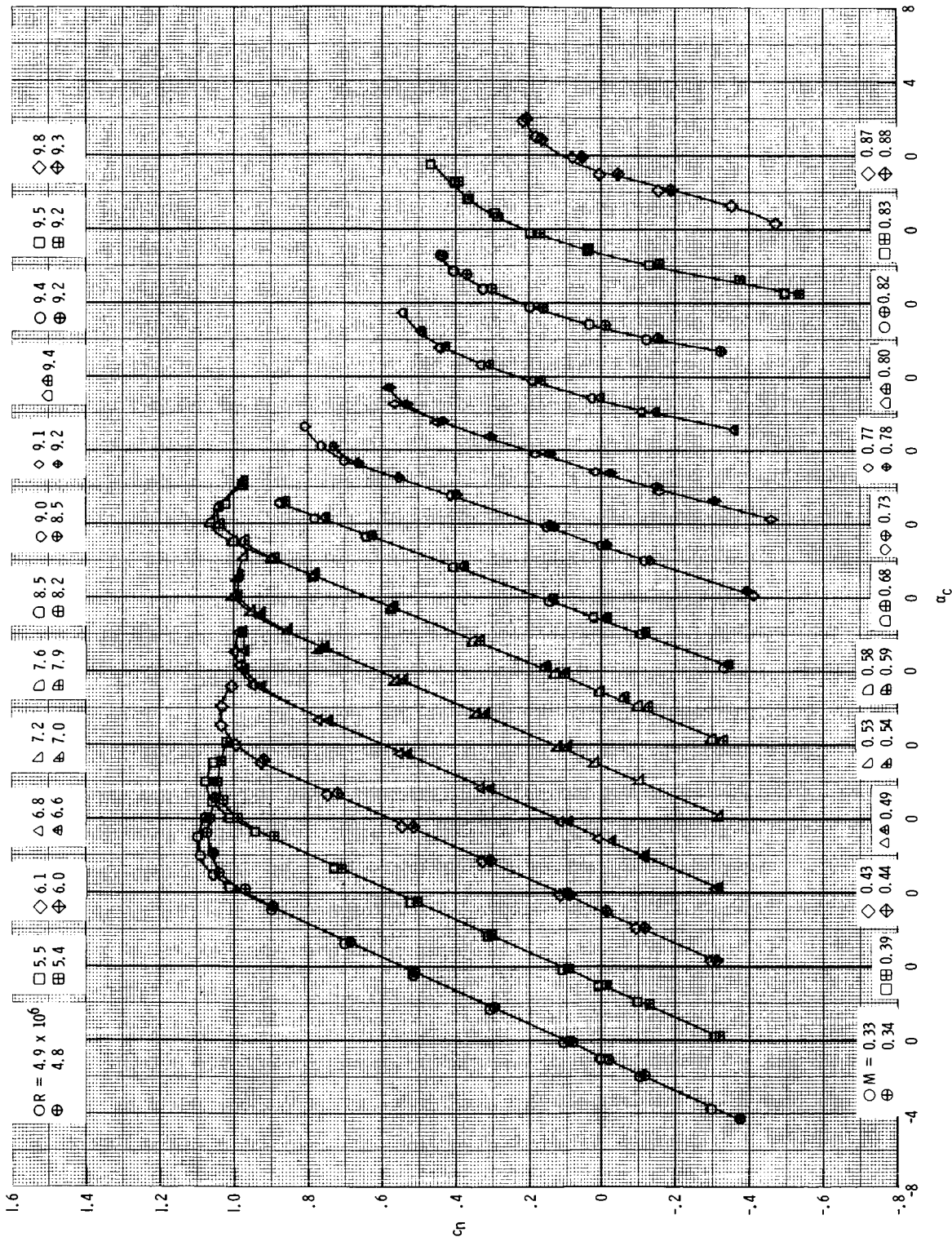
(b) Section pitching-moment coefficients.

Figure 5.- Continued.



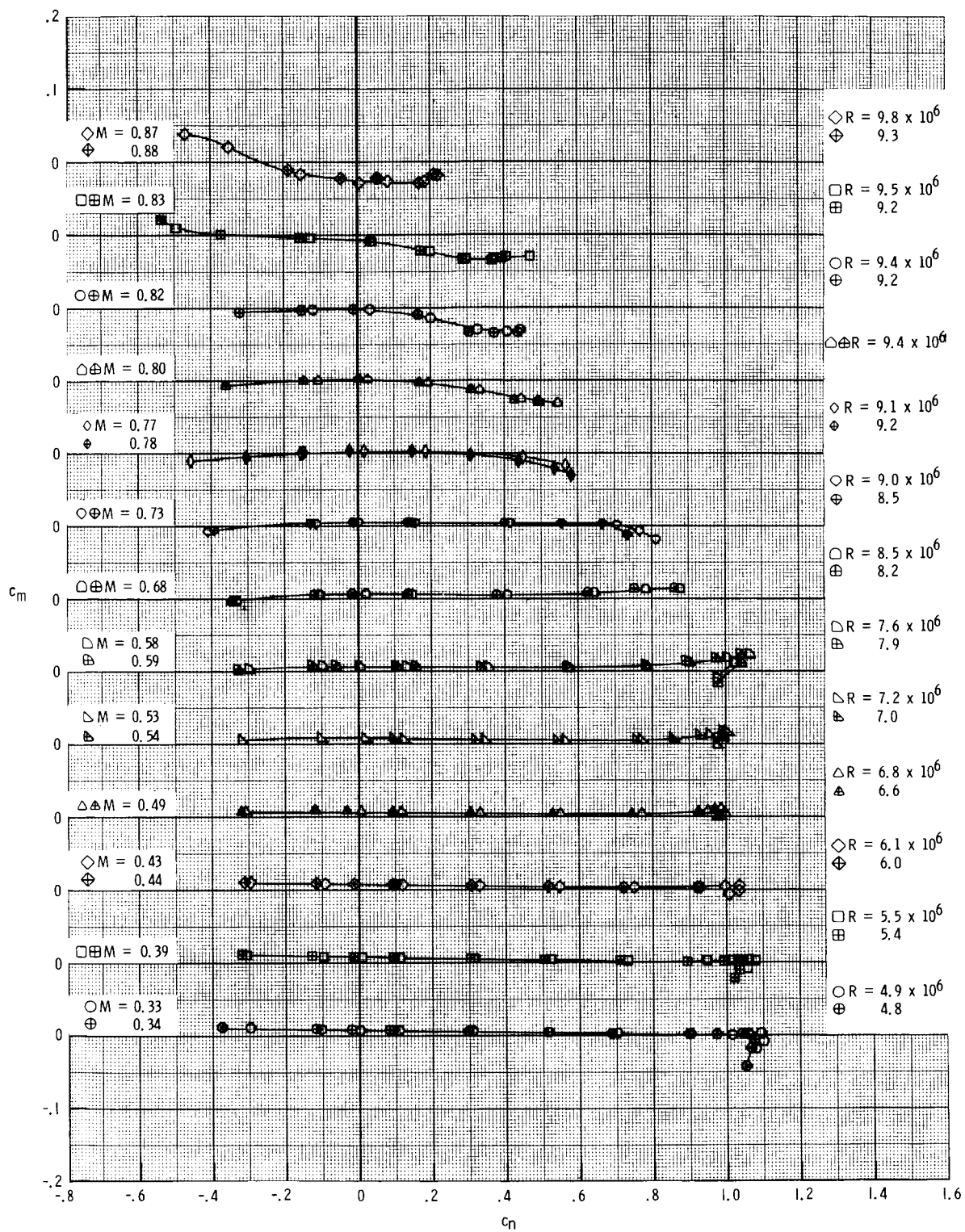
(c) Section drag coefficients.

Figure 5.- Concluded.



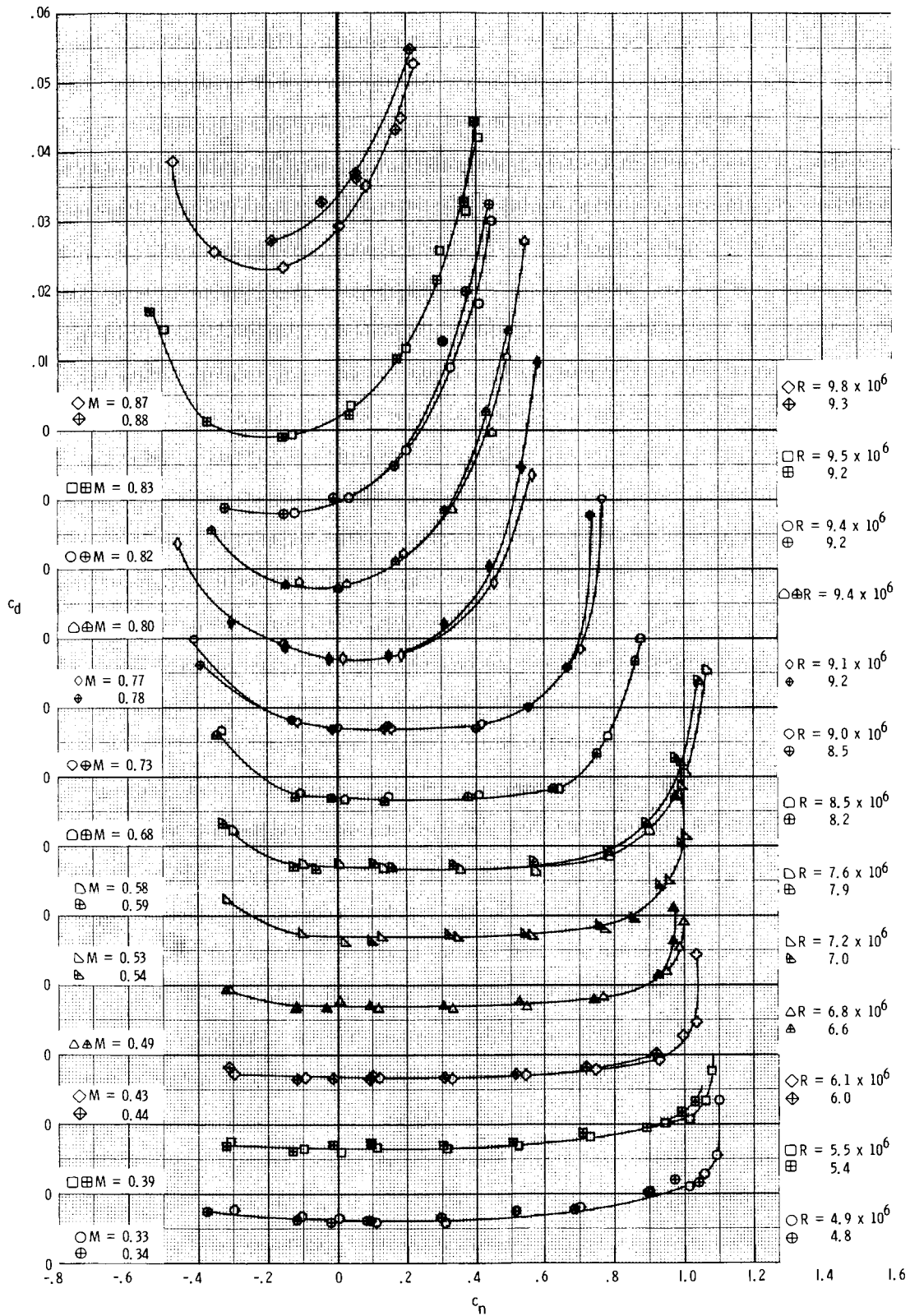
(a) Section normal-force coefficients.

Figure 6.- Comparison of smooth model data from two separate tunnel entries. Open symbols indicate Test 52 data; centered symbols indicate Test 73 data.



(b) Section pitching-moment coefficients.

Figure 6.- Continued.



(c) Section drag coefficients.

Figure 6.- Concluded.

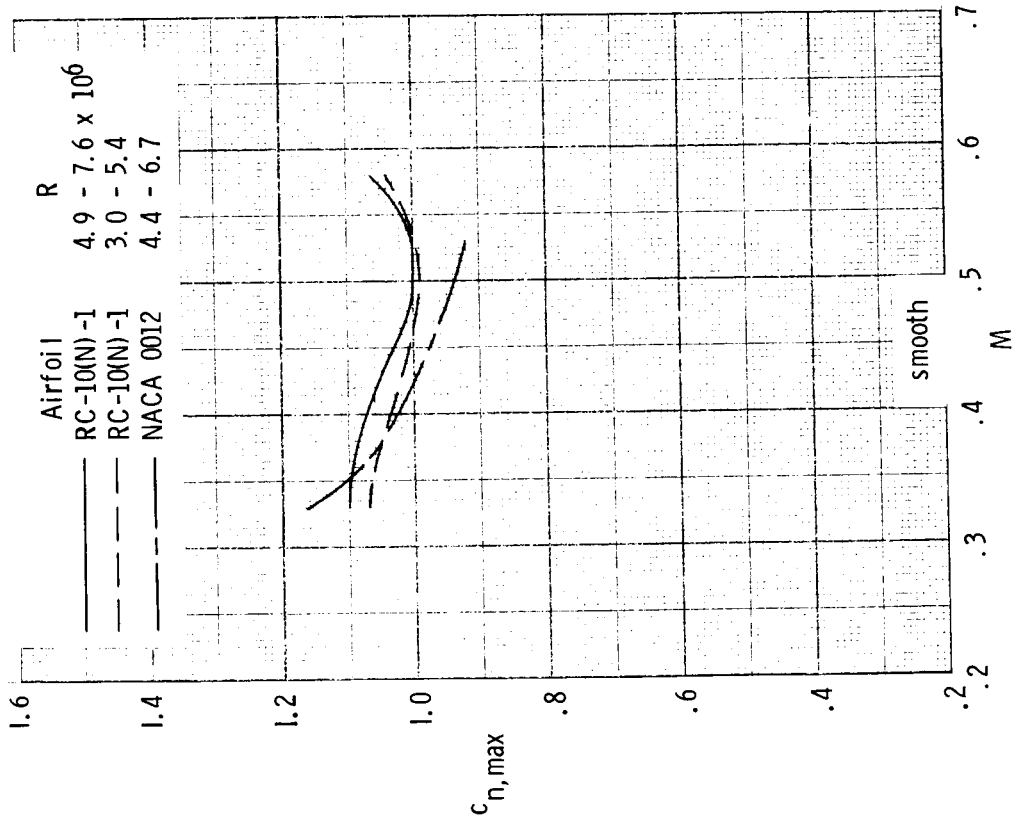
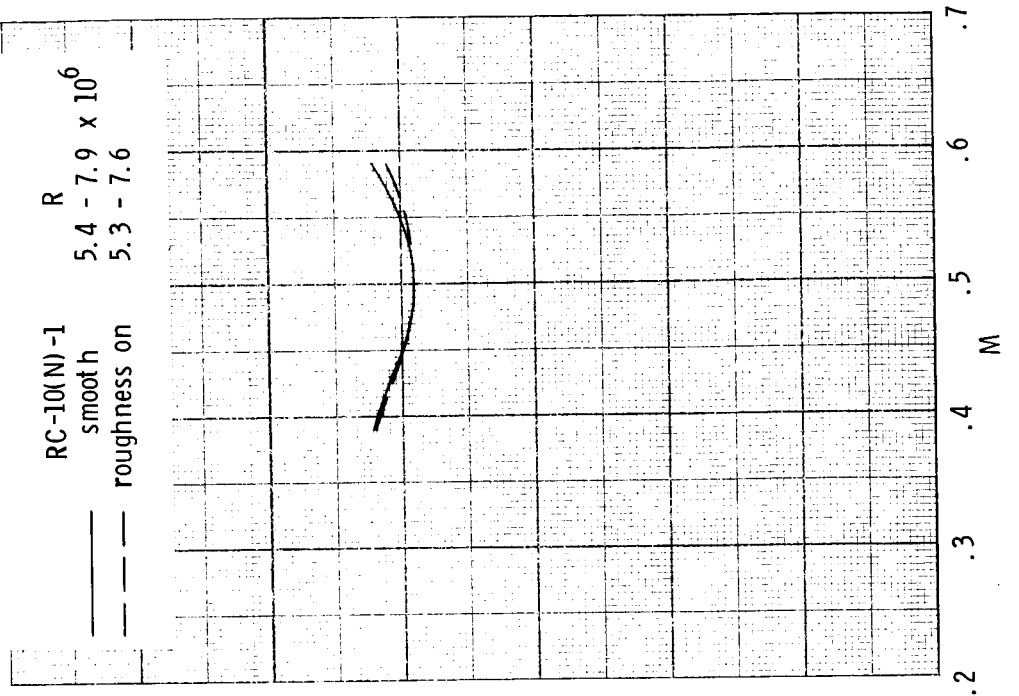


Figure 7.- Variation of maximum section normal-force coefficient with Mach number of RC-10(N)-1 and NACA 0012 airfoils.

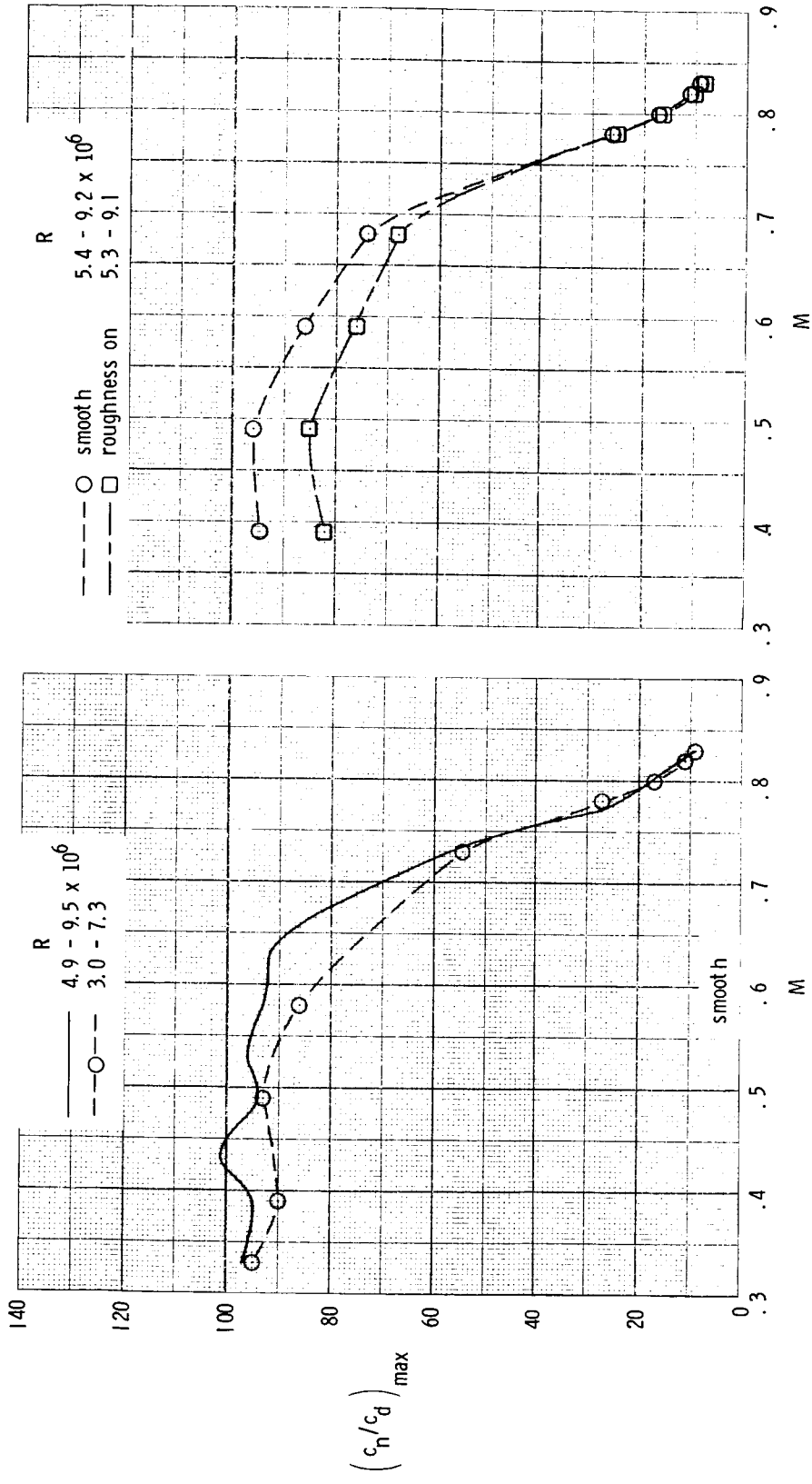


Figure 8.- Variation of maximum section normal-force-drag ratio with Mach number of RC-10(N)-1 airfoil.

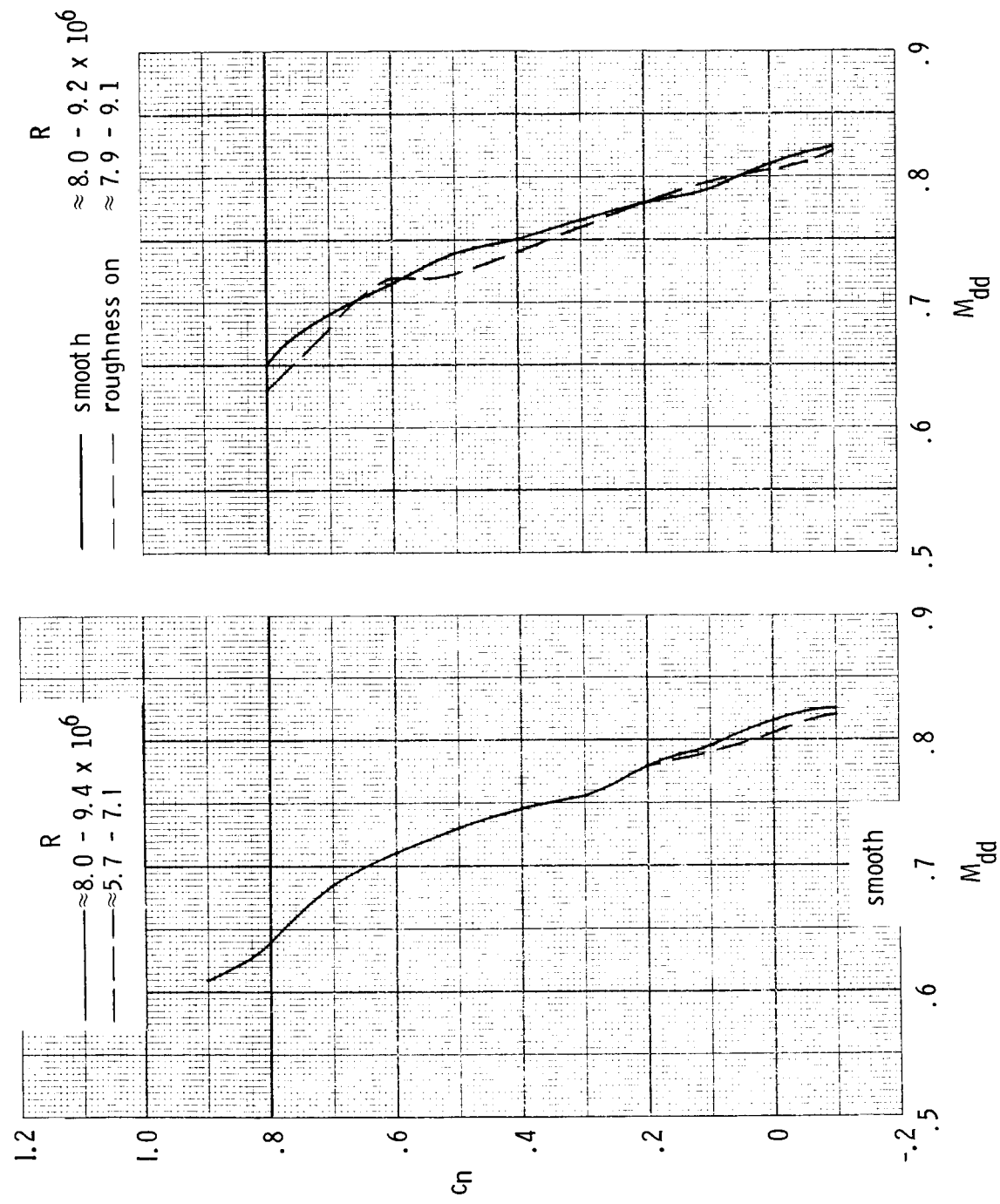


Figure 9.- Variation of section normal-force coefficient with drag divergence Mach number of RC-10(N)-1 airfoil.

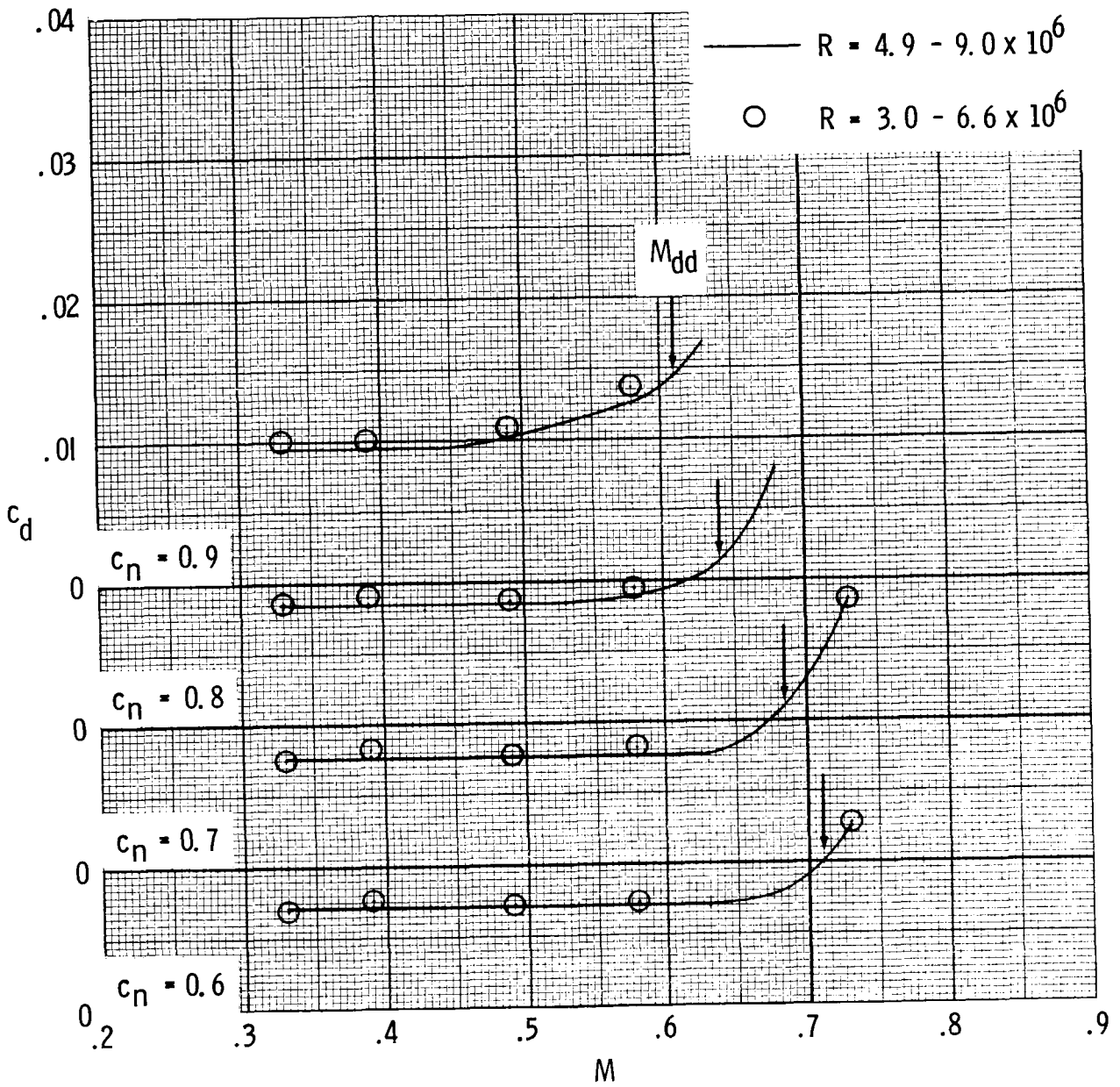
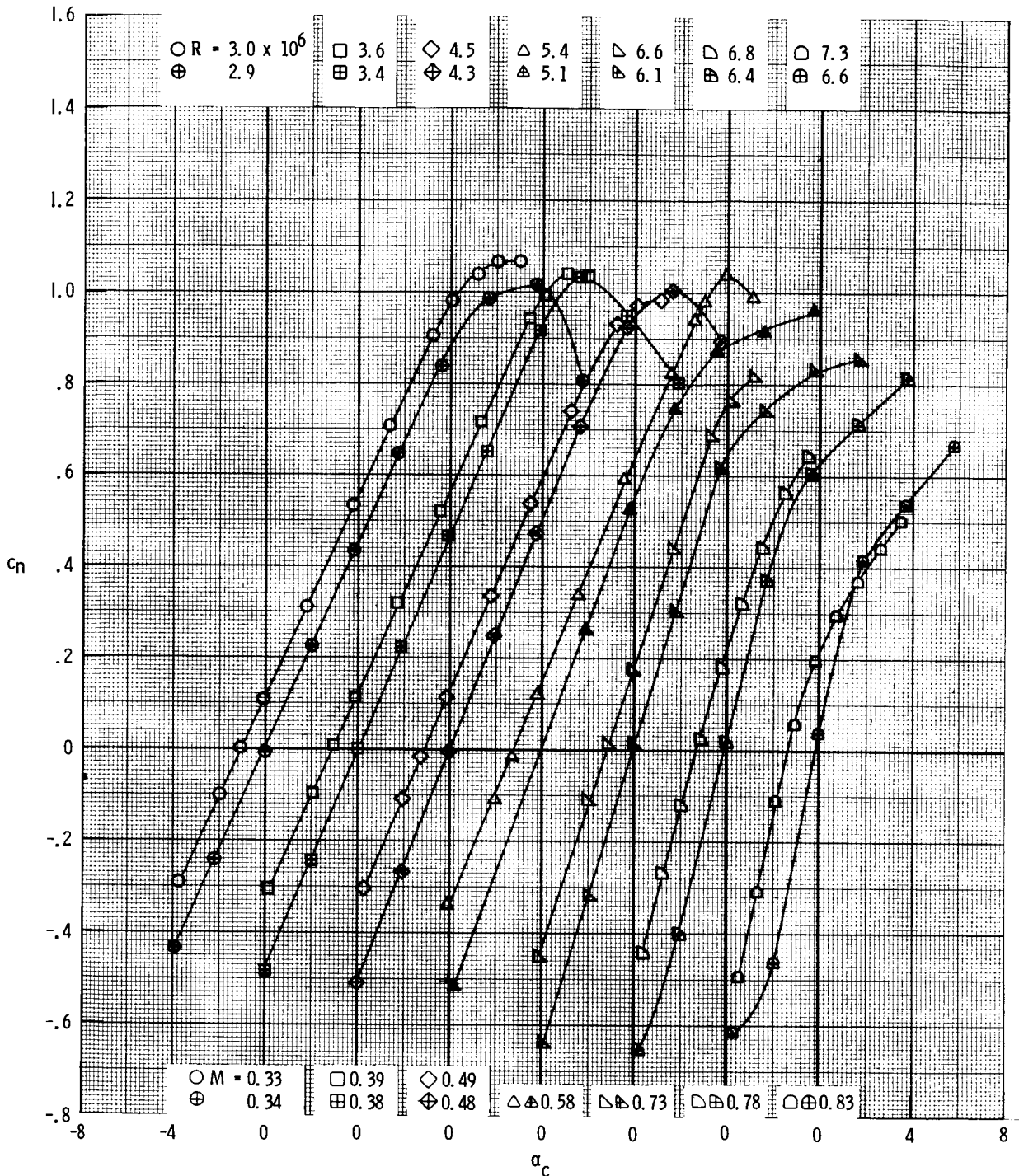
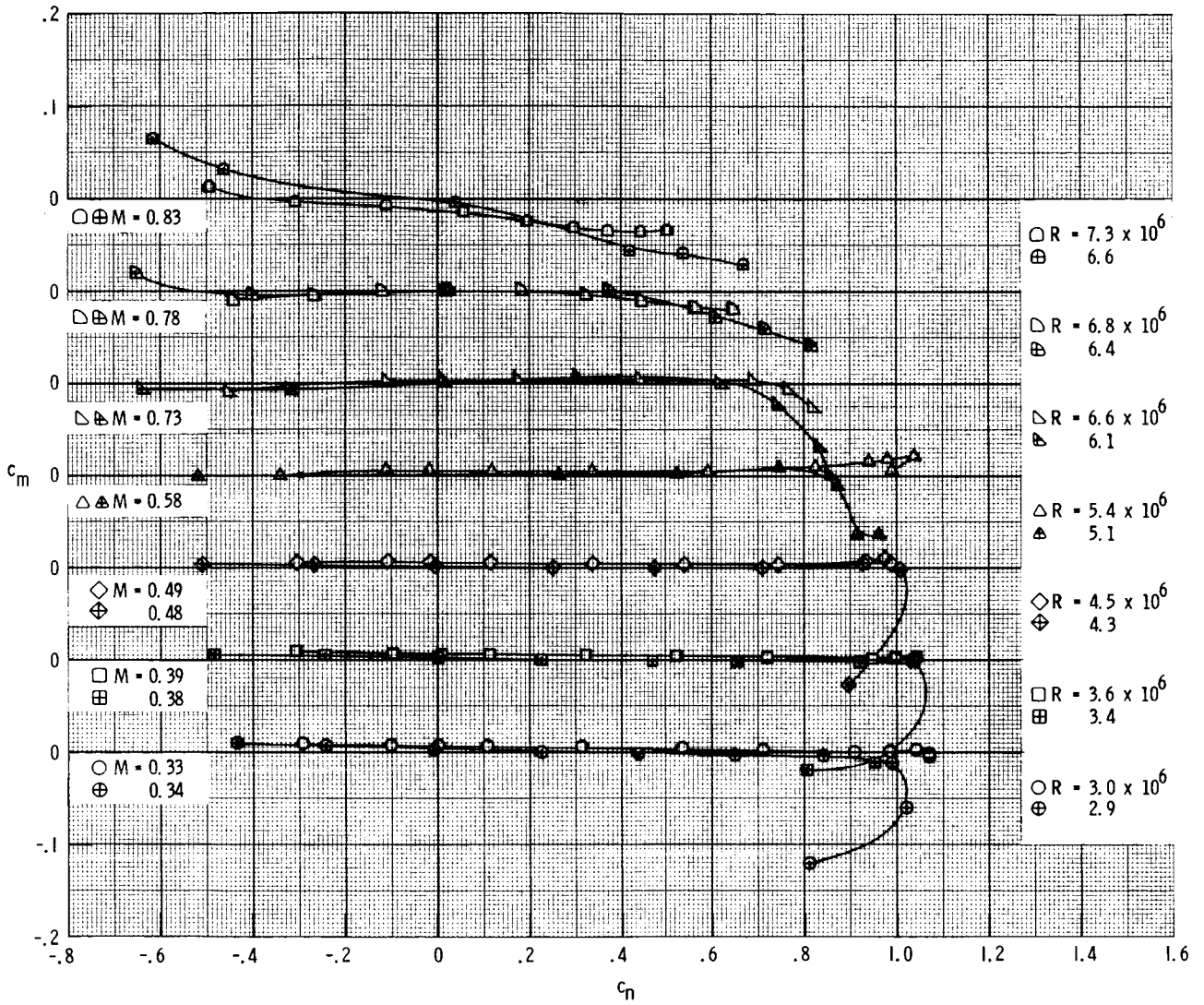


Figure 10.- Effect of Reynolds number on variation of section drag coefficient with Mach number of RC-10(N)-1 airfoil.



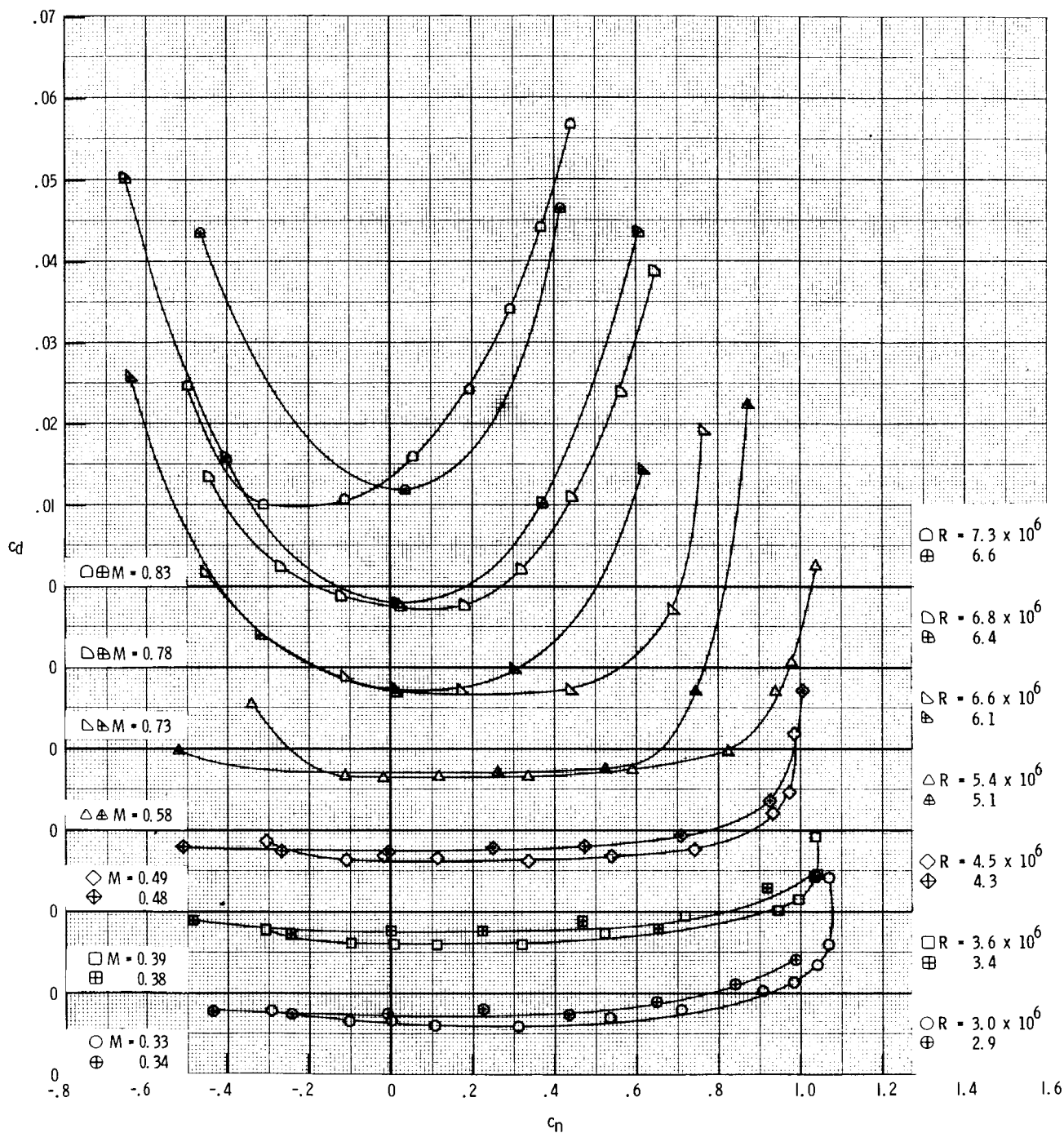
(a) Section normal-force coefficients.

Figure 11.- Comparison of aerodynamic characteristics of RC-10(N)-1 and SC 1095 airfoils. Open symbols indicate RC-10(N)-1 airfoil; centered symbols indicate SC 1095 airfoil.



(b) Section pitching-moment coefficients.

Figure 11.- Continued.



(c) Section drag coefficients.

Figure 11.- Concluded.

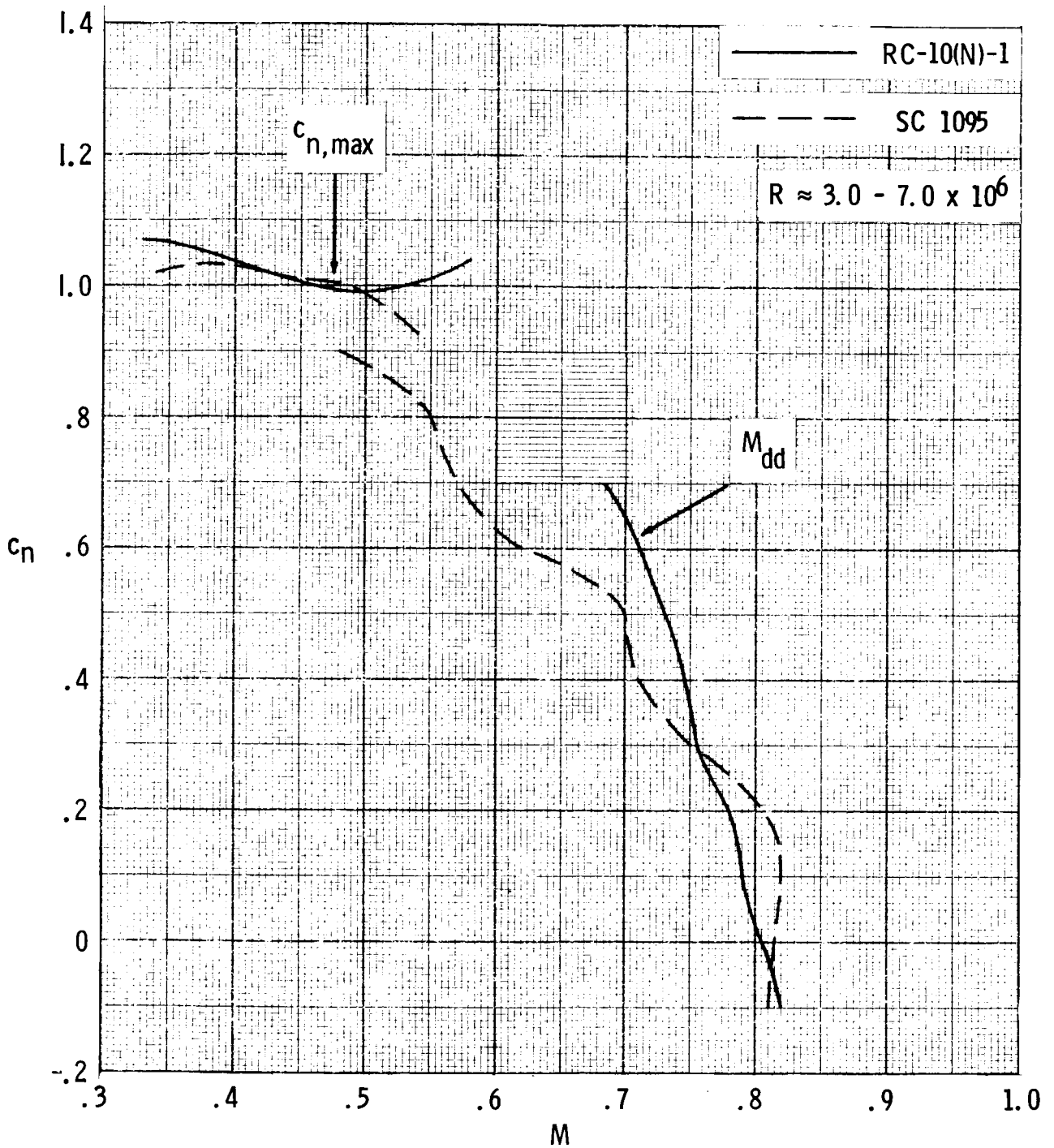


Figure 12.- Comparison of drag divergence characteristics and maximum section normal-force coefficients of RC-10(N)-1 and SC 1095 airfoils.

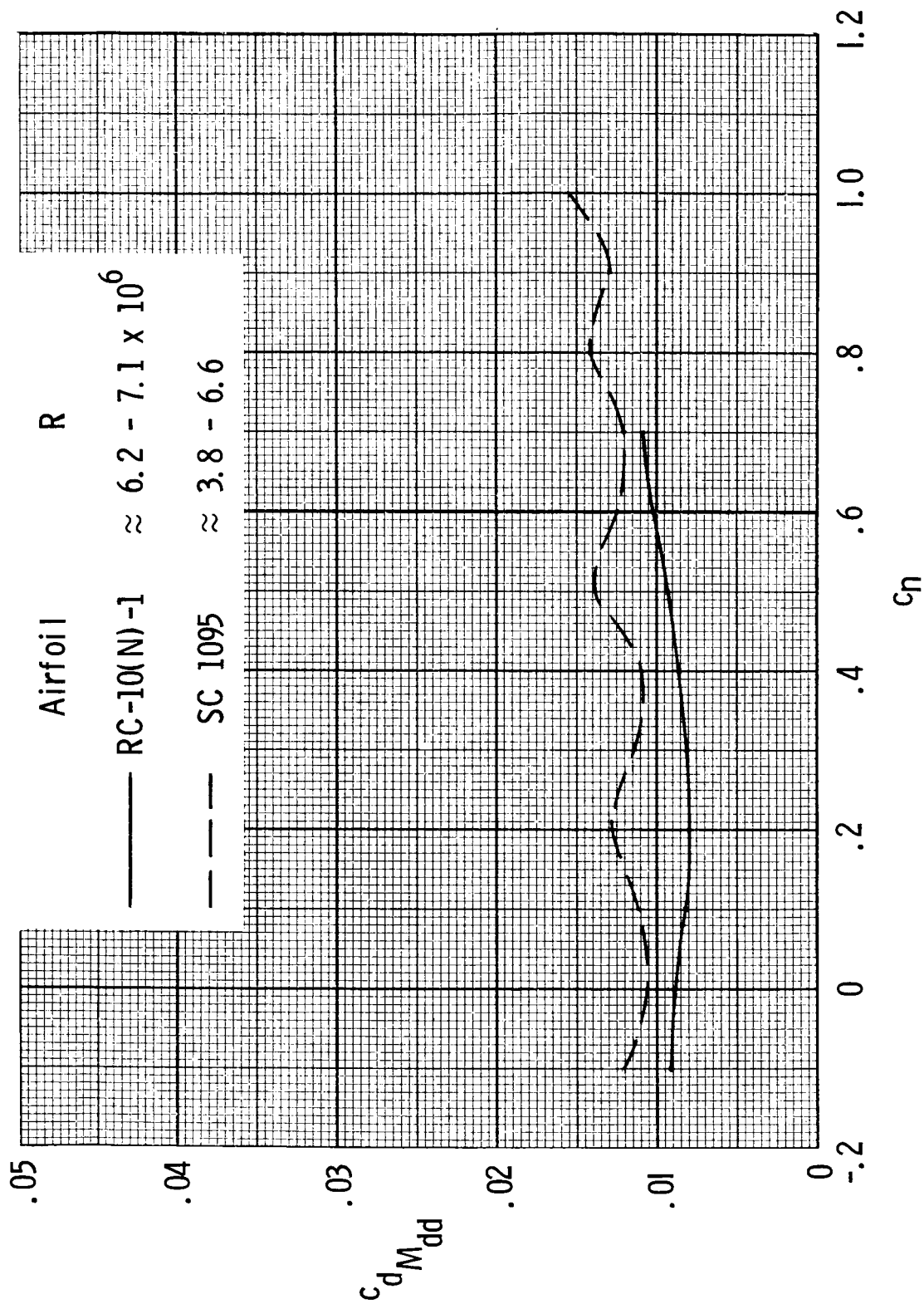


Figure 13.- Comparison of section drag coefficient at drag divergence Mach number of RC-10(N)-1 and SC 1095 airfoils.

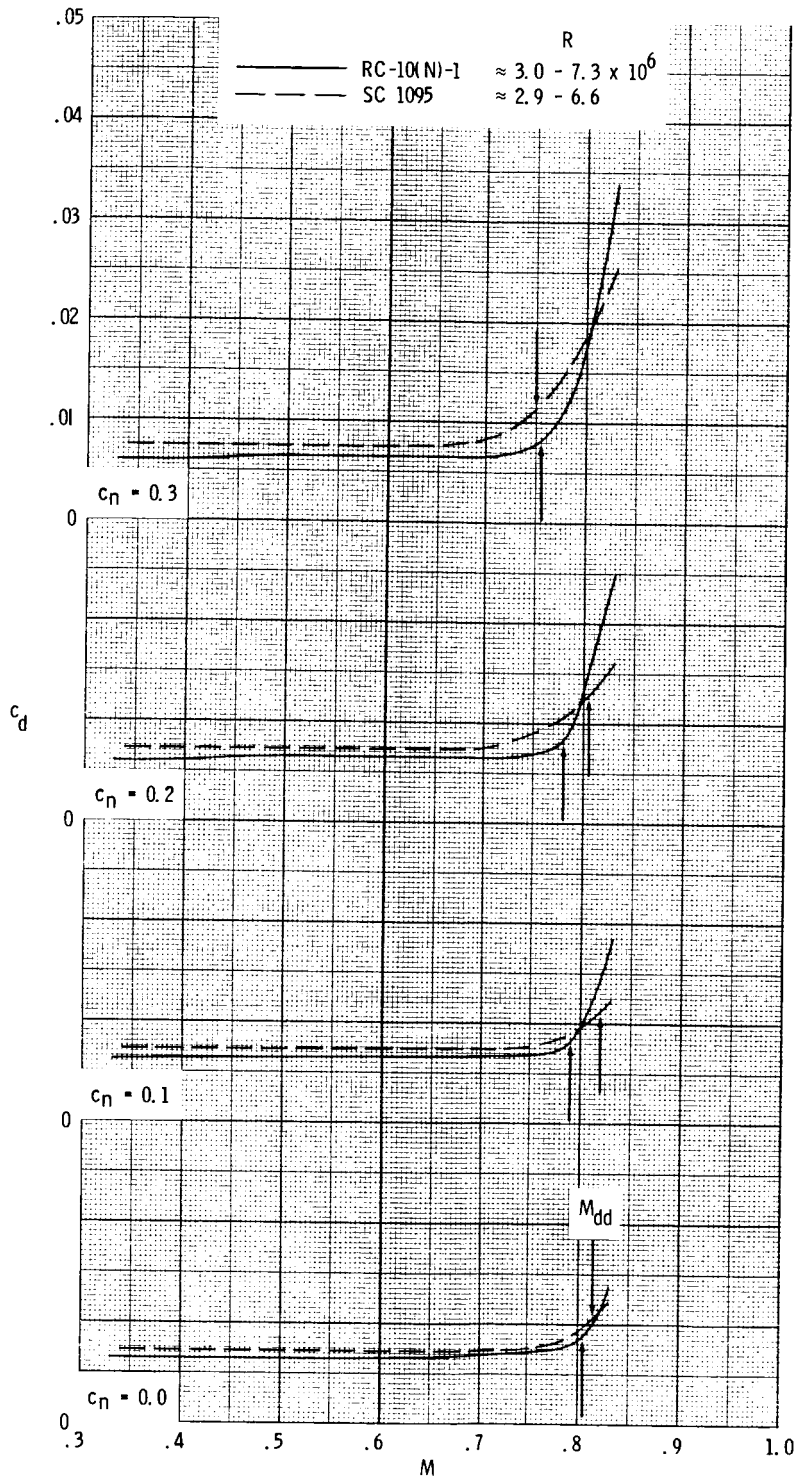


Figure 14.- Comparison of variation of section drag coefficient with Mach number of RC-10(N)-1 and SC 1095 airfoils.

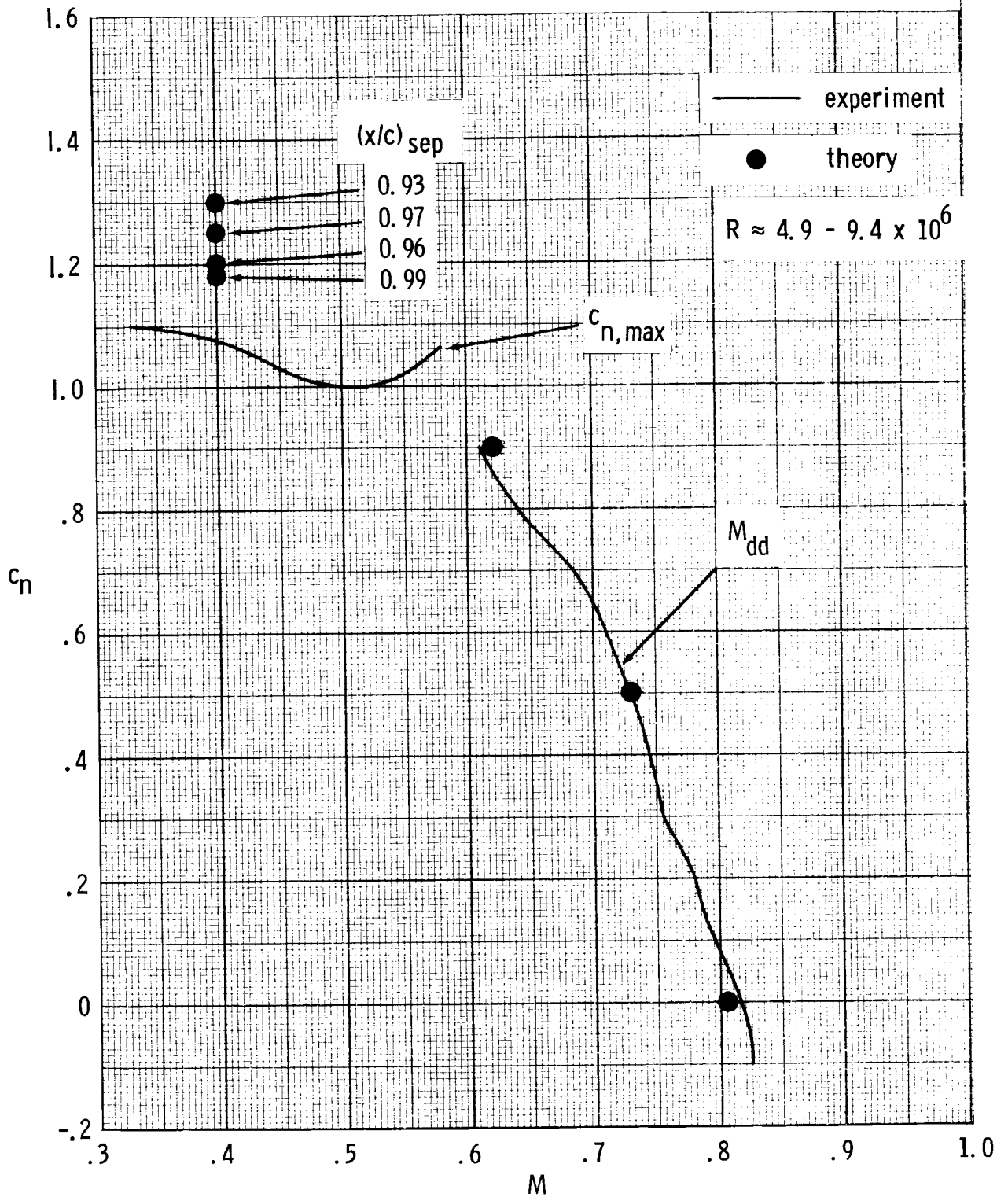


Figure 15.- Comparison of experimental and theoretical drag divergence characteristics and section normal-force coefficients of RC-10(N)-1 airfoil. Experimental data are for smooth model.

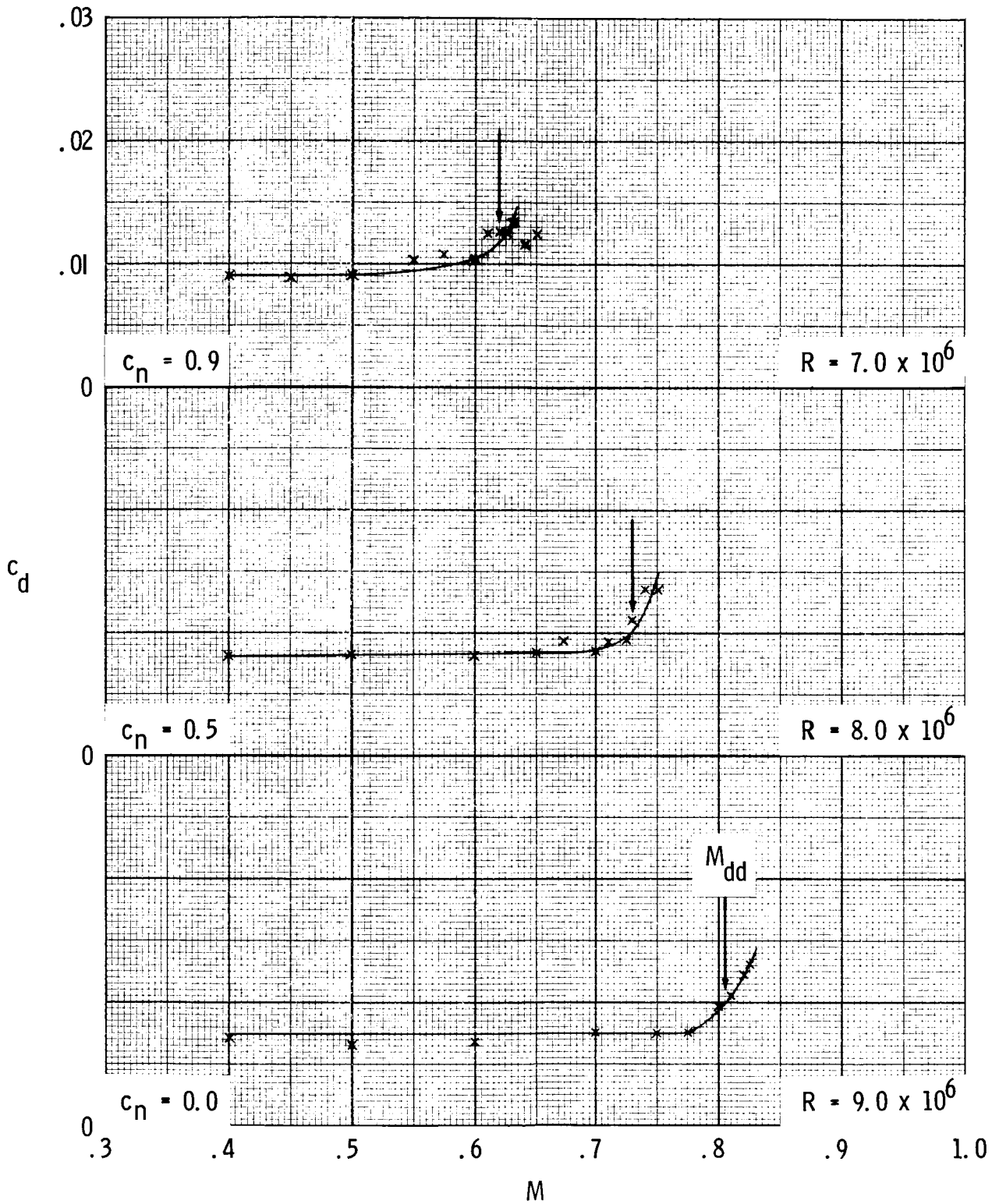


Figure 16.- Variation of theoretical section drag coefficient with Mach number of RC-10(N)-1 airfoil. Transition fixed.

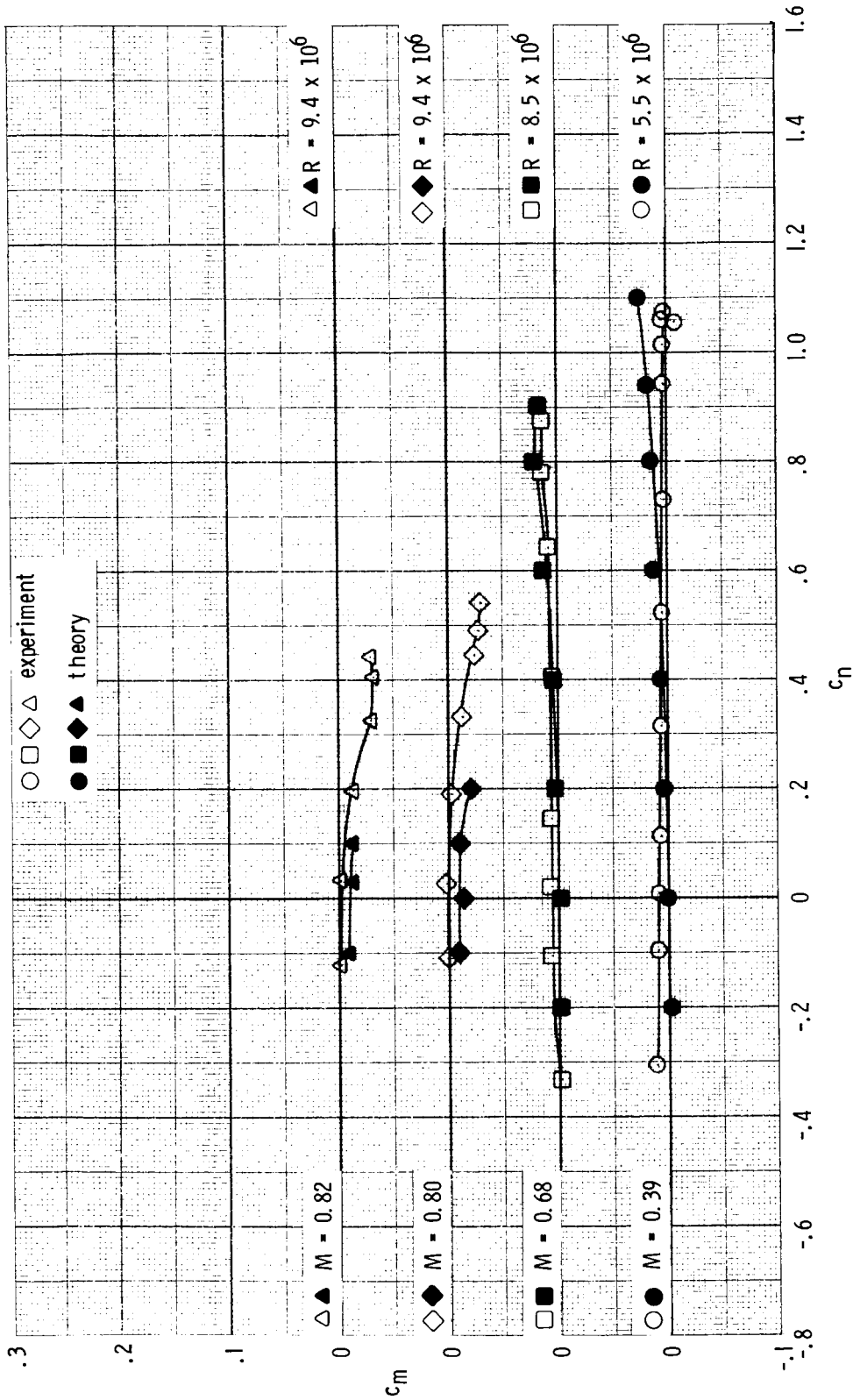


Figure 17.- Comparison of experimental and theoretical section pitching-moment coefficients of RC-10(N)-1 airfoil. Experimental data are for smooth model.

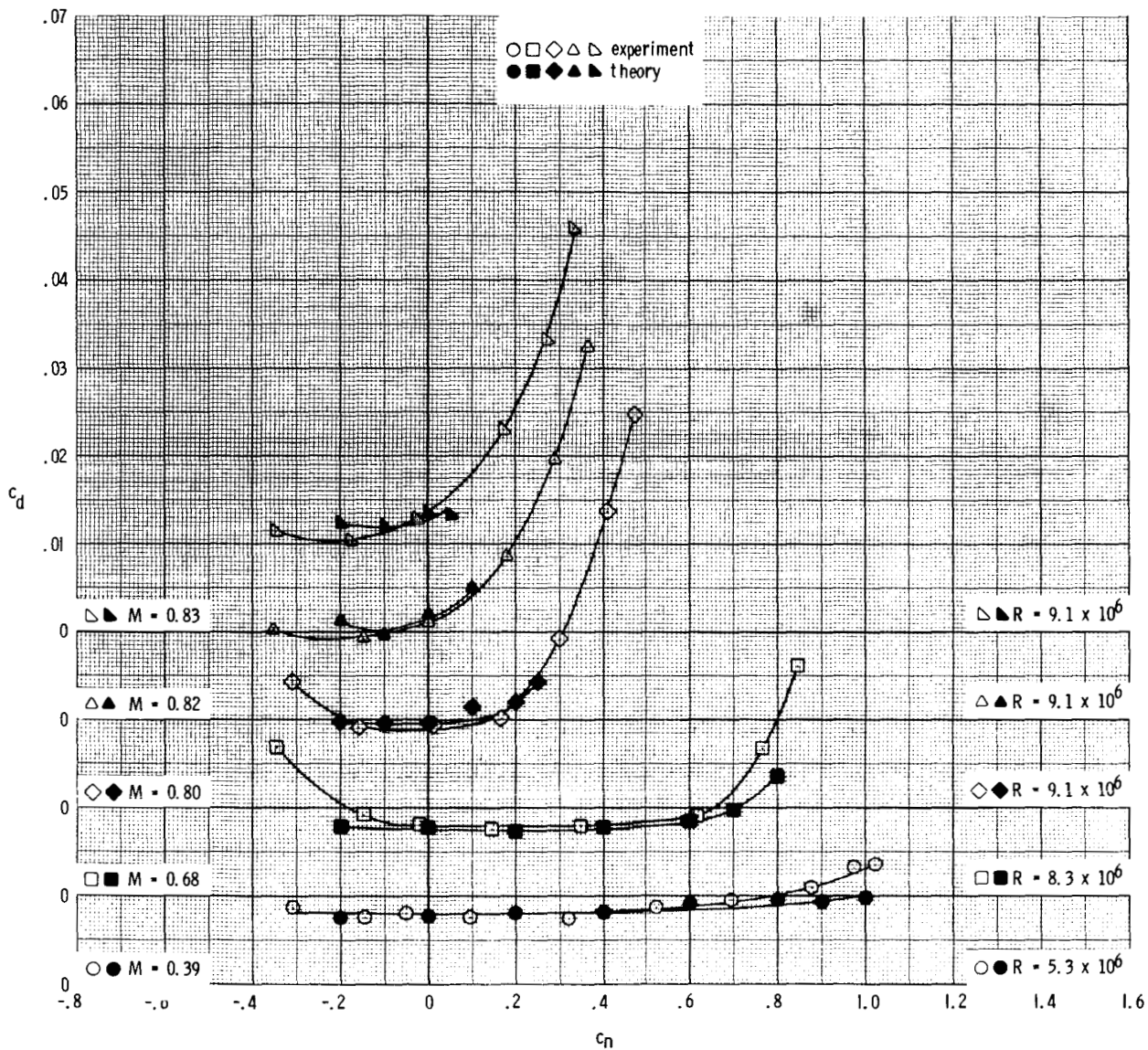


Figure 18.- Comparison of experimental and theoretical section drag coefficients of RC-10(N)-1 airfoil. Transition fixed.

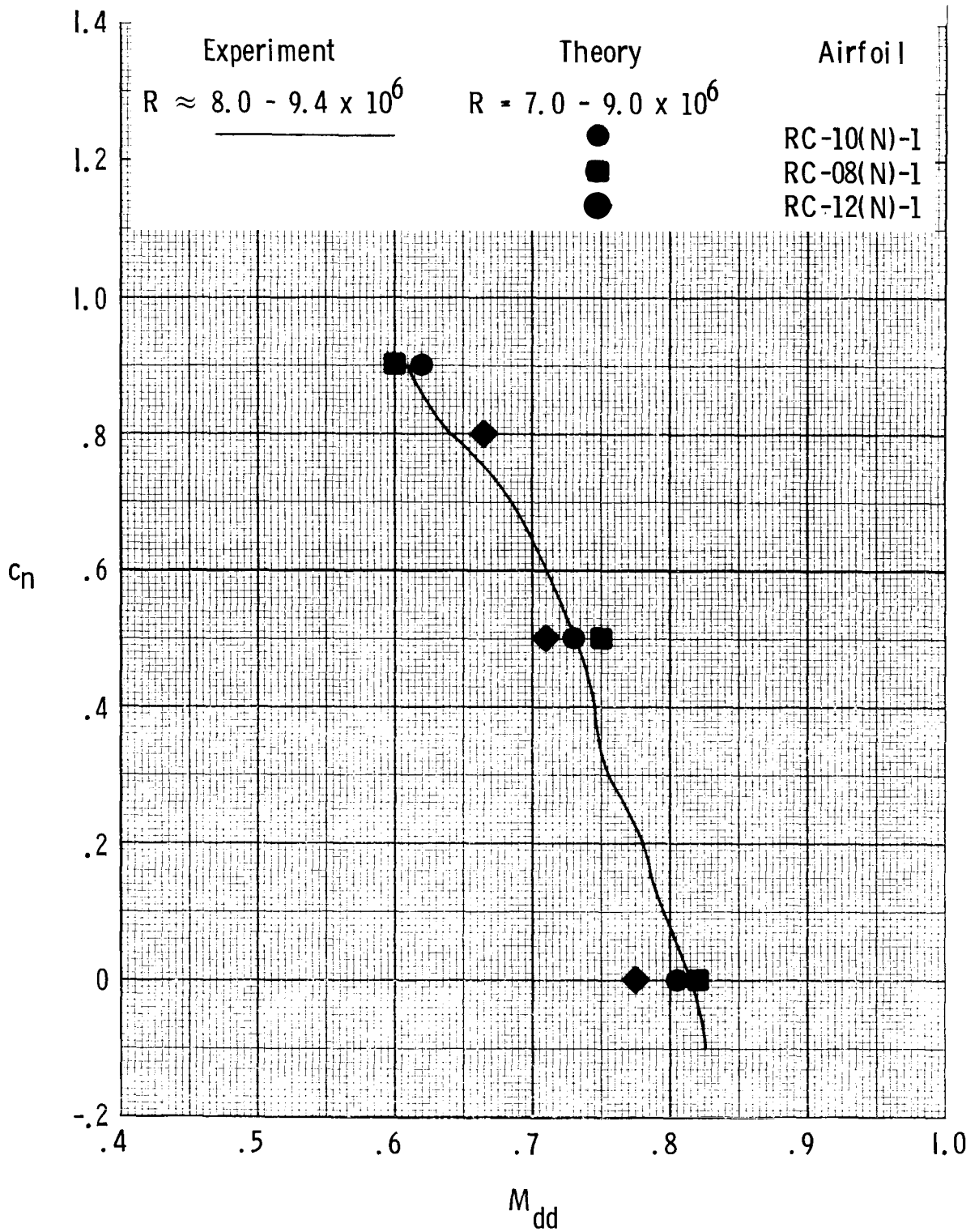
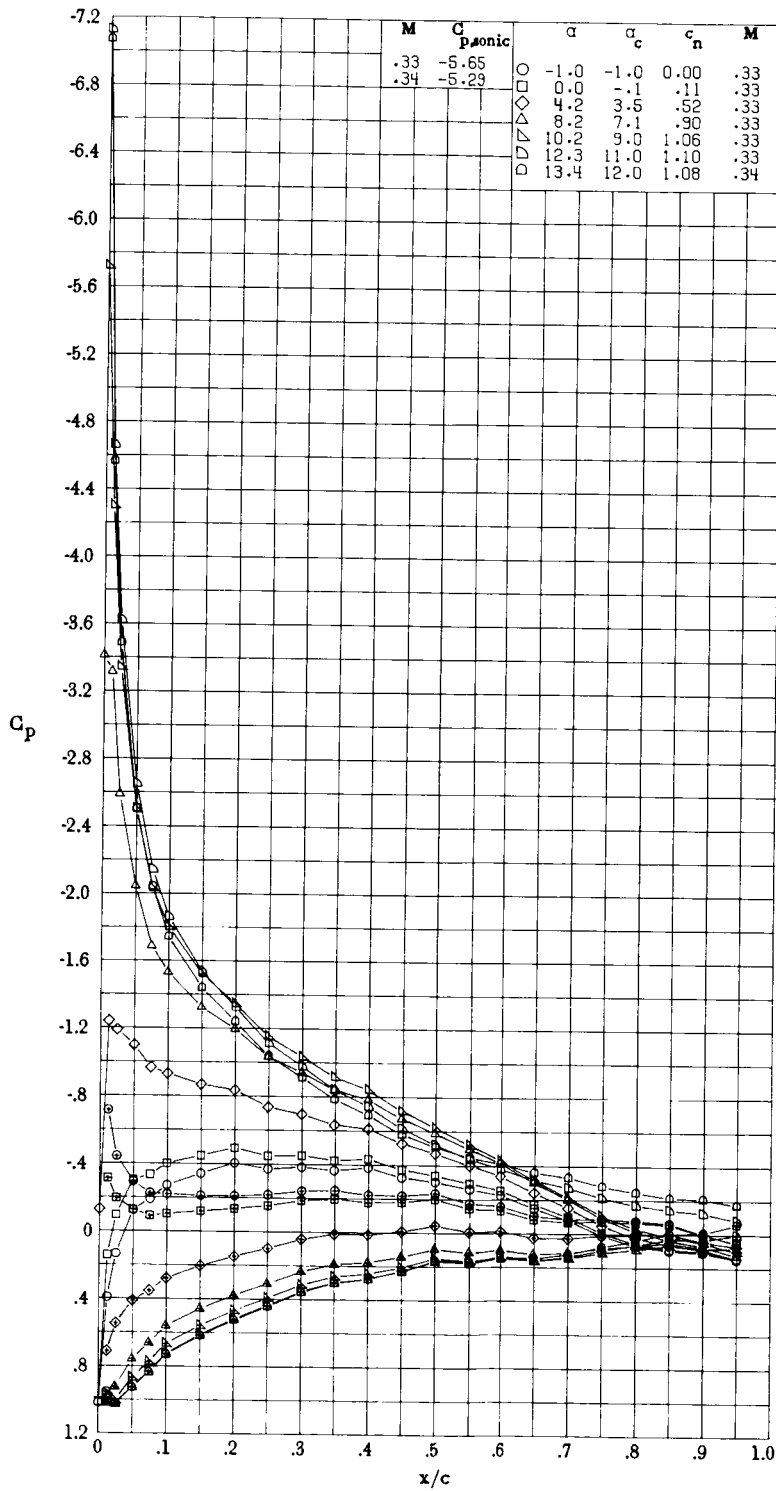
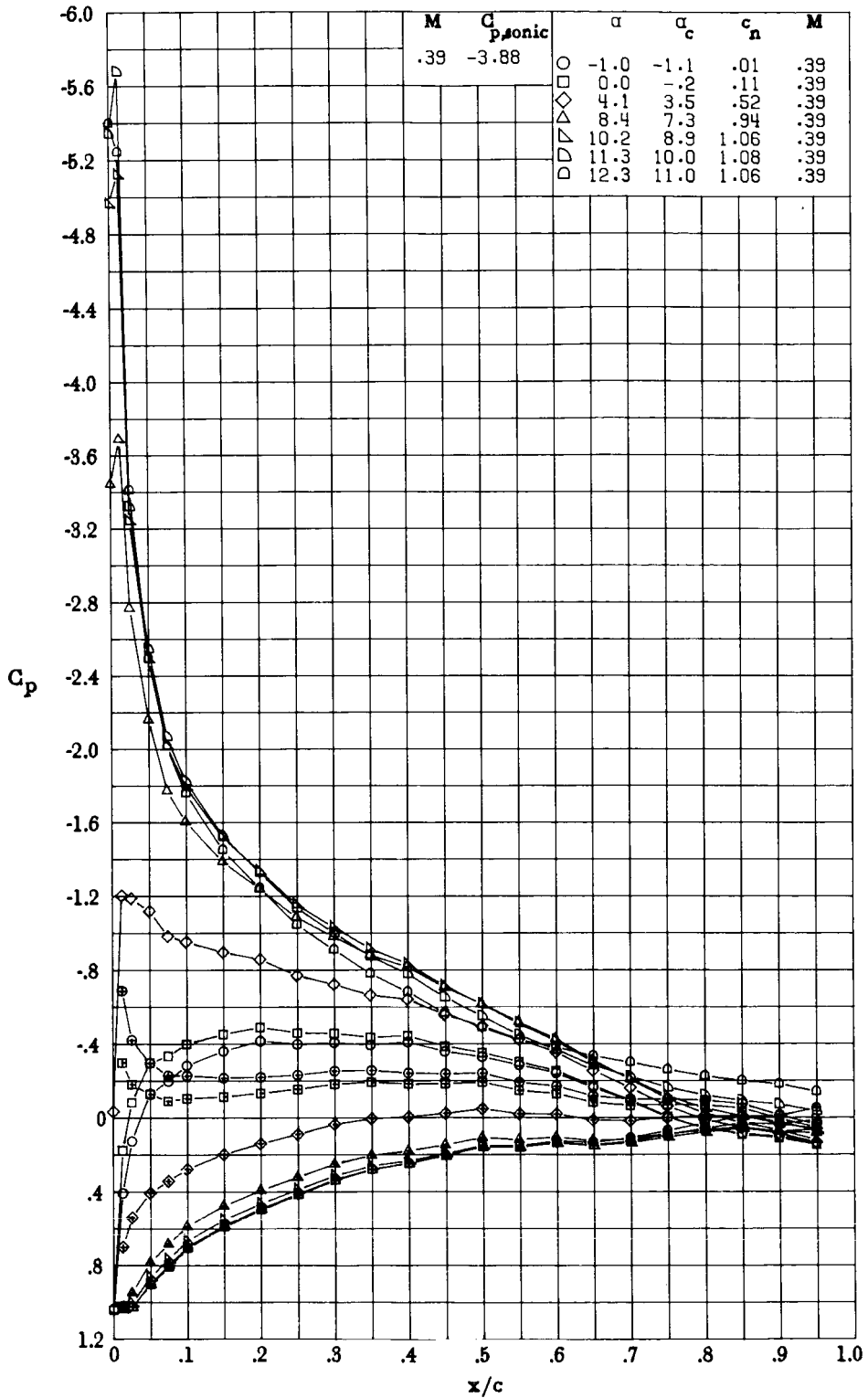


Figure 19.- Drag divergence characteristics of RC-XX(N)-1 airfoil family. Experimental data are for smooth model.



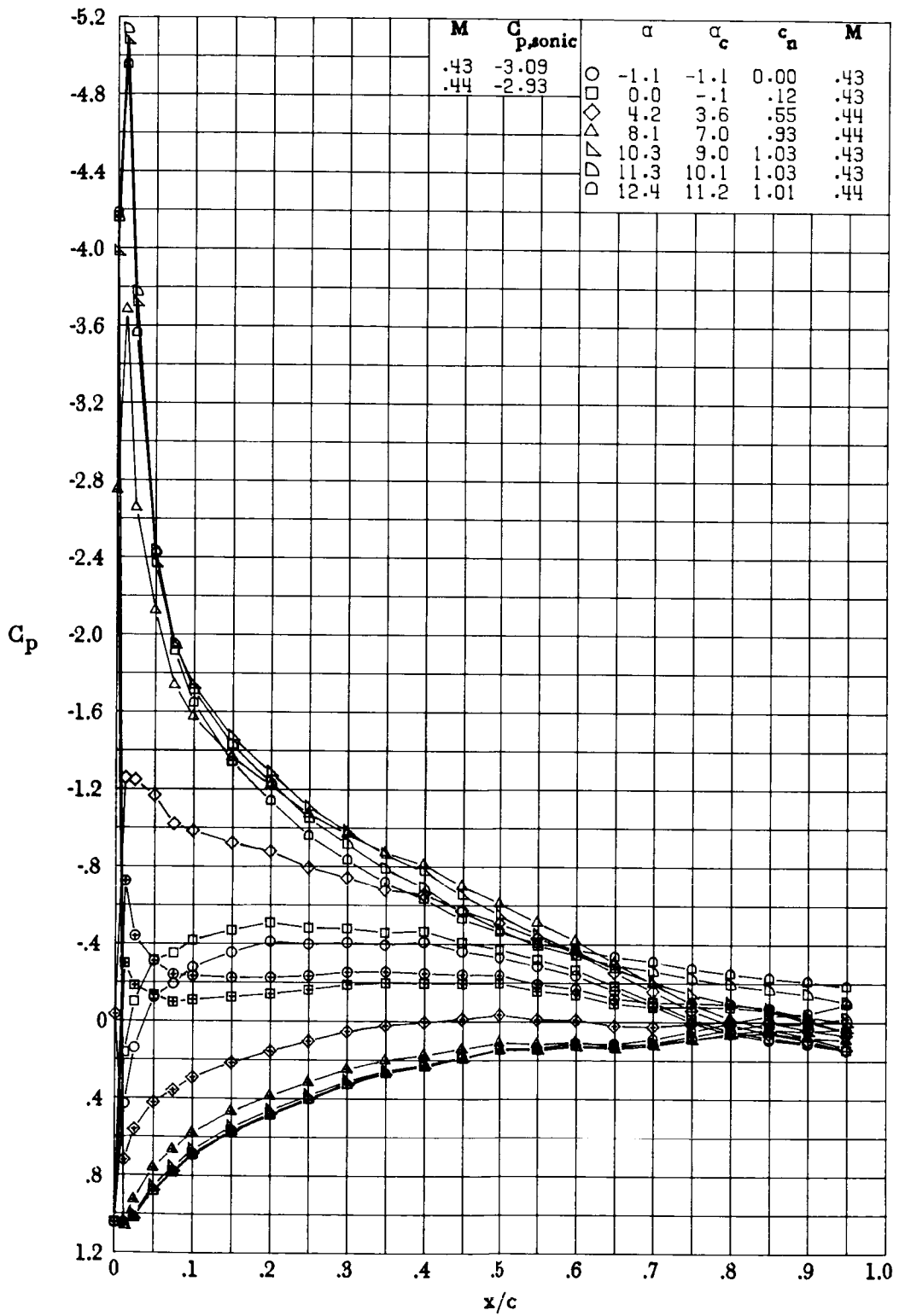
(a) $M \approx 0.33$; $R \approx 4.9 \times 10^6$.

Figure 20.- Effect of angle of attack on chordwise pressure distribution of RC-10(N)-1 airfoil. Centered symbols indicate lower surface.



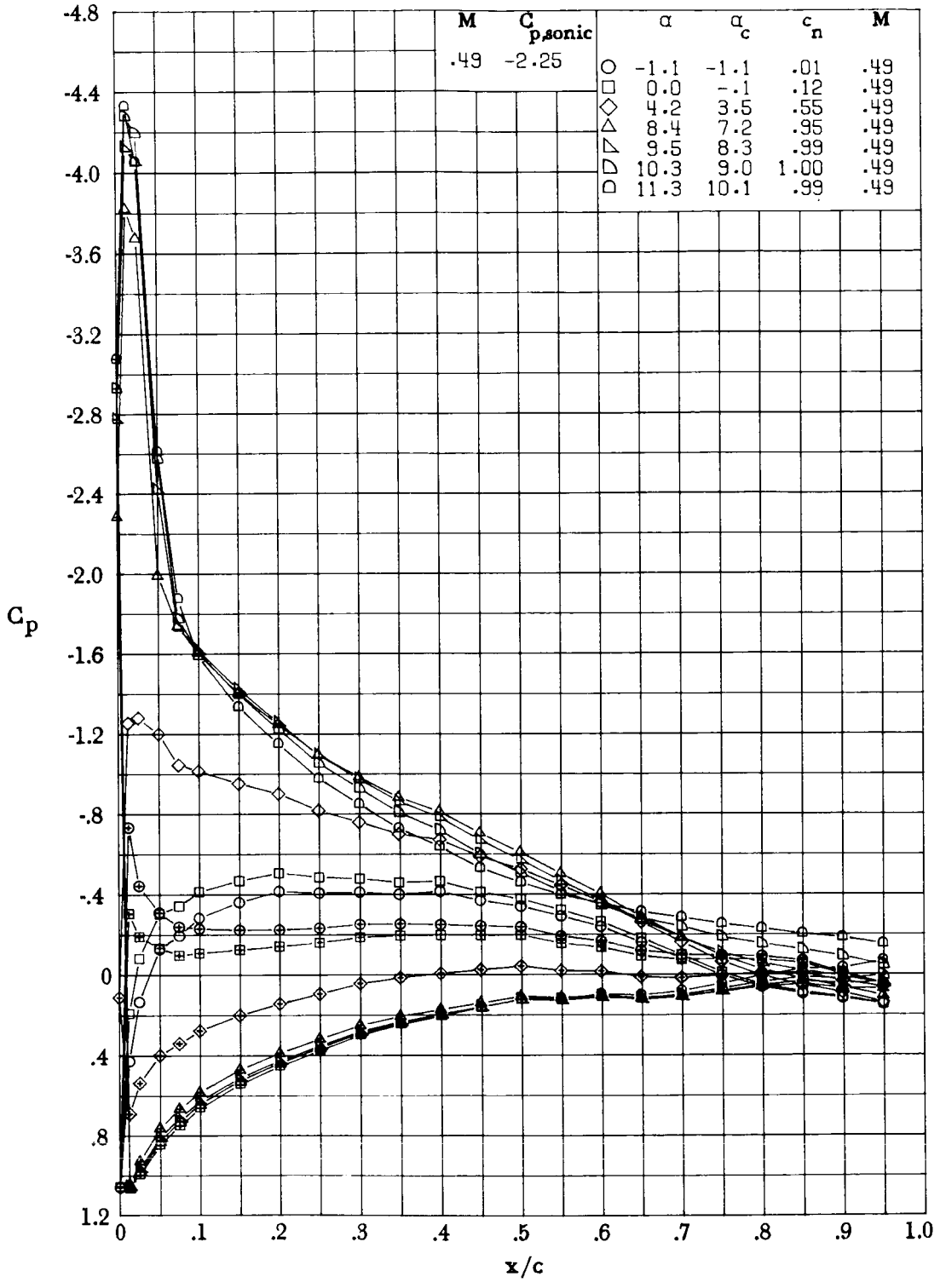
(b) $M = 0.39$; $R \approx 5.5 \times 10^6$.

Figure 20.- Continued.



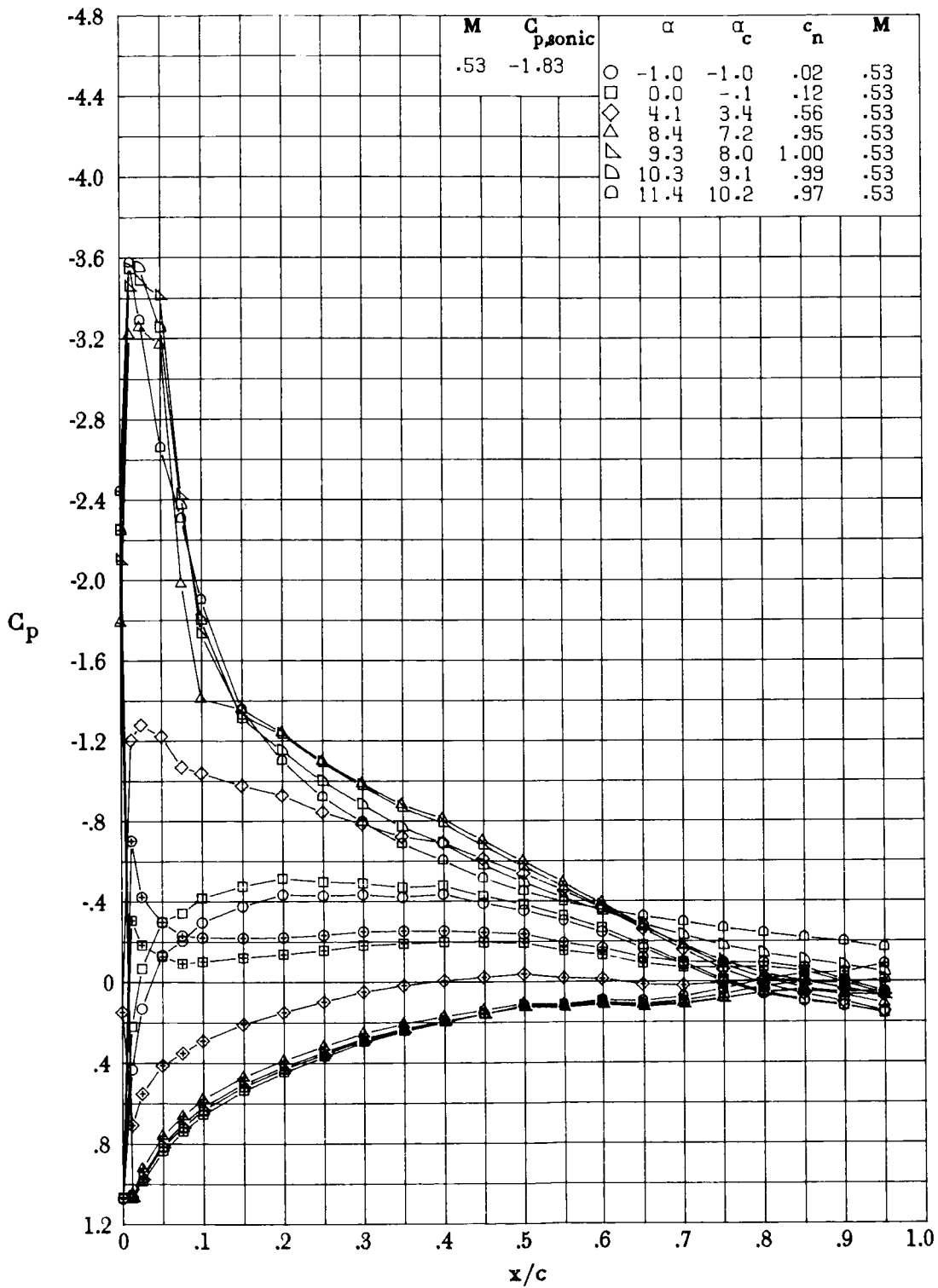
(c) $M \approx 0.43$; $R \approx 6.1 \times 10^6$.

Figure 20.- Continued.



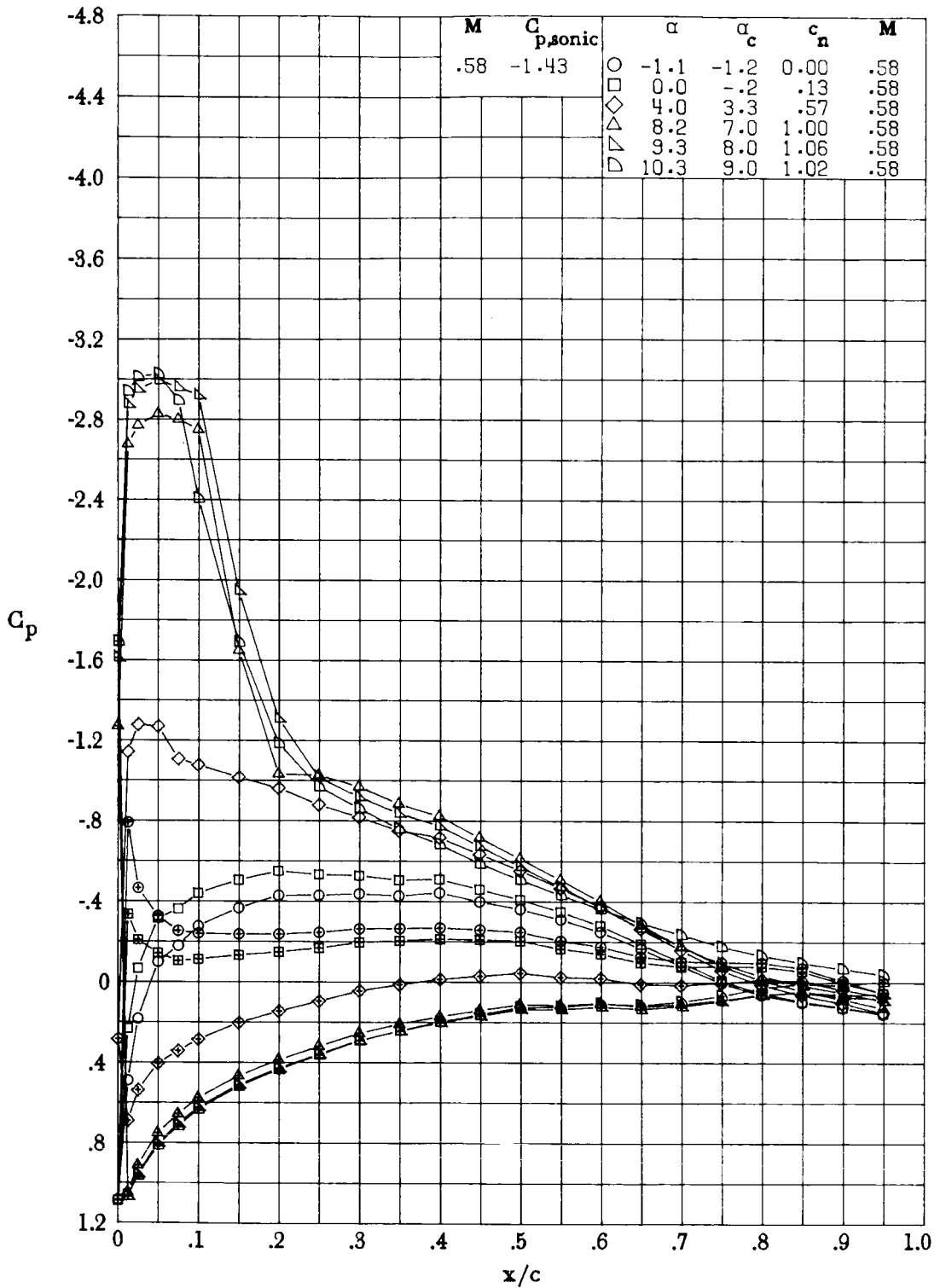
(d) $M = 0.49$; $R \approx 6.8 \times 10^6$.

Figure 20.- Continued.



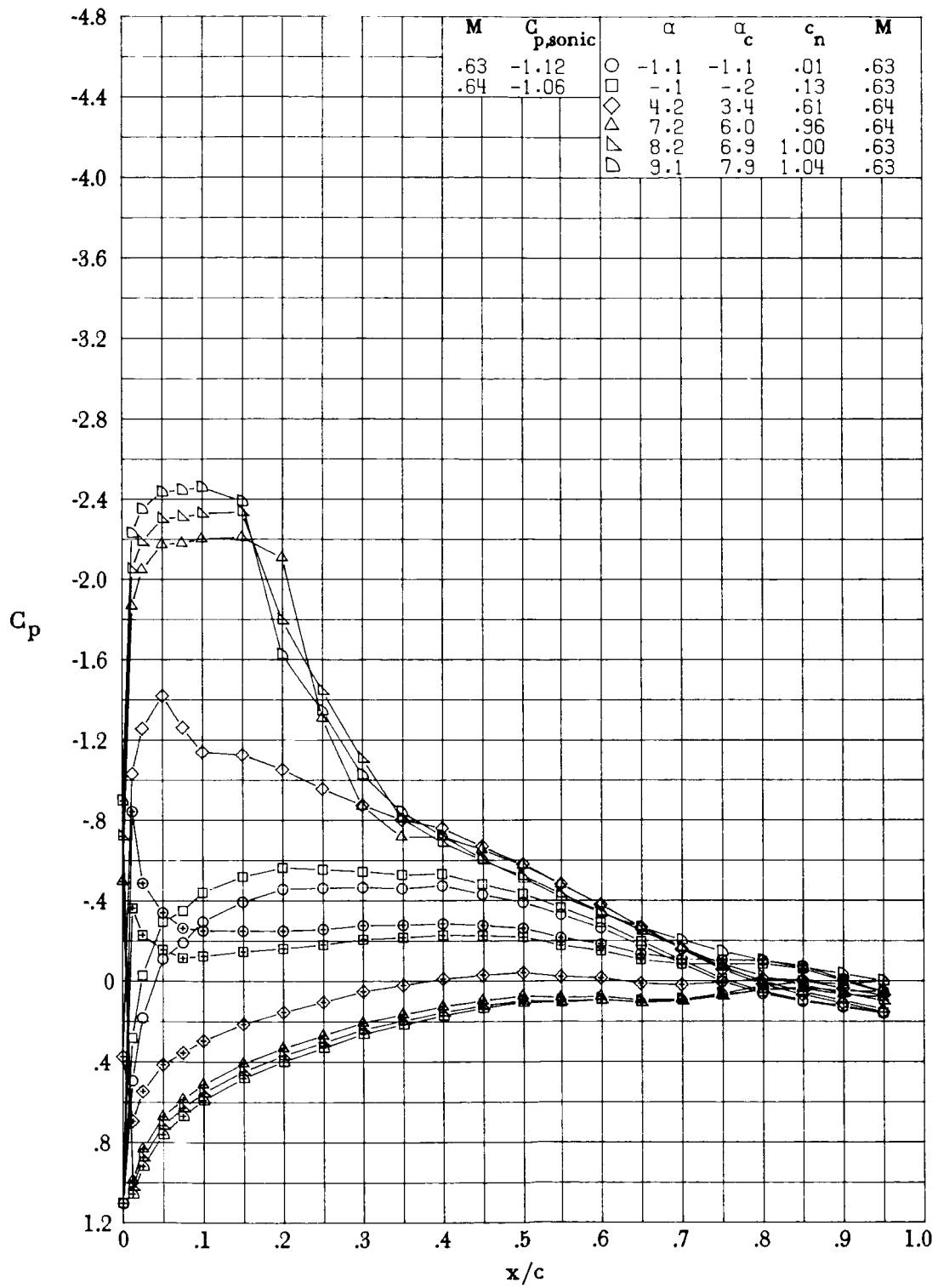
(e) $M = 0.53$; $R \approx 7.2 \times 10^6$.

Figure 20.- Continued.



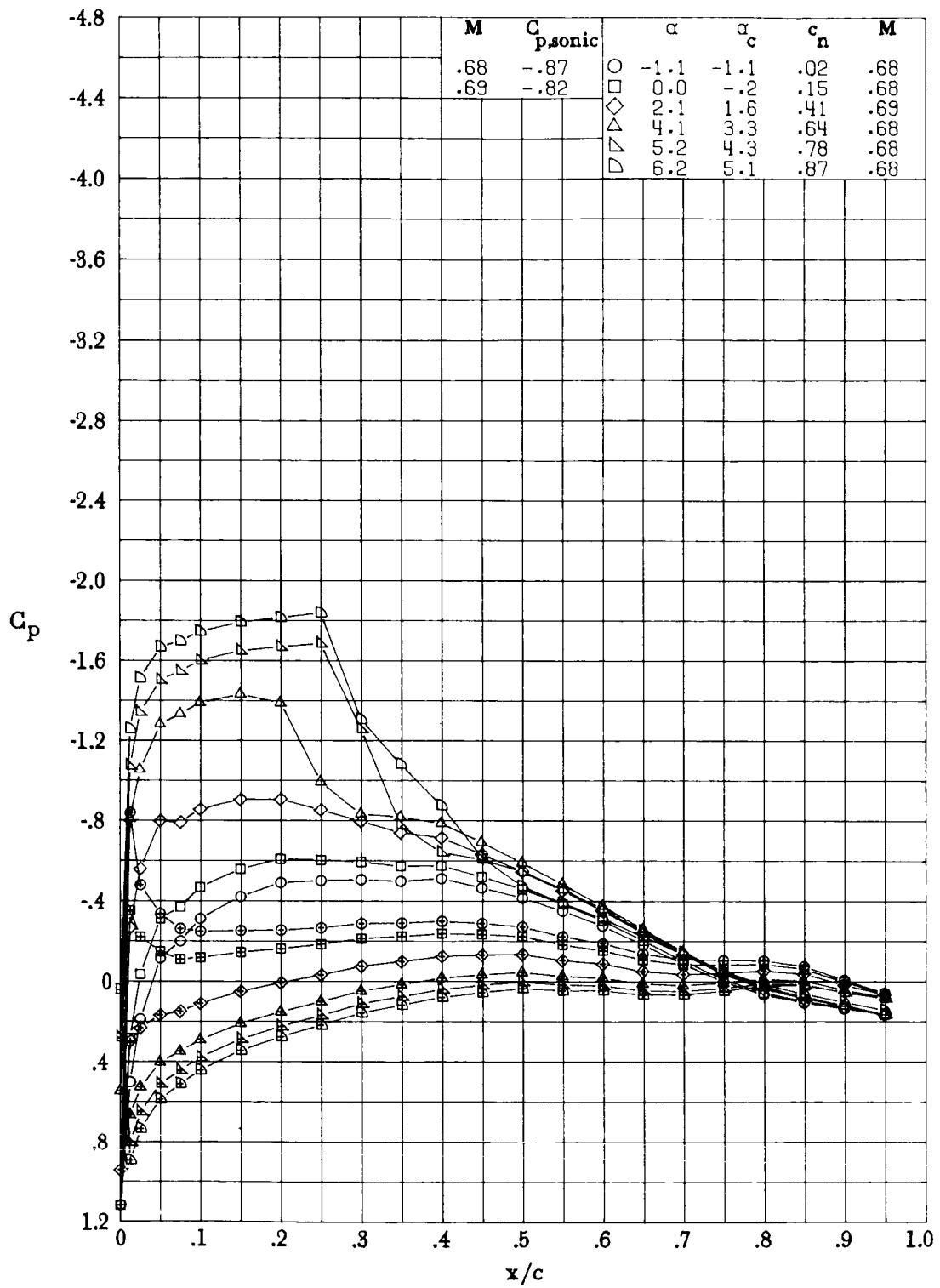
(f) $M = 0.58$; $R \approx 7.6 \times 10^6$.

Figure 20.- Continued.



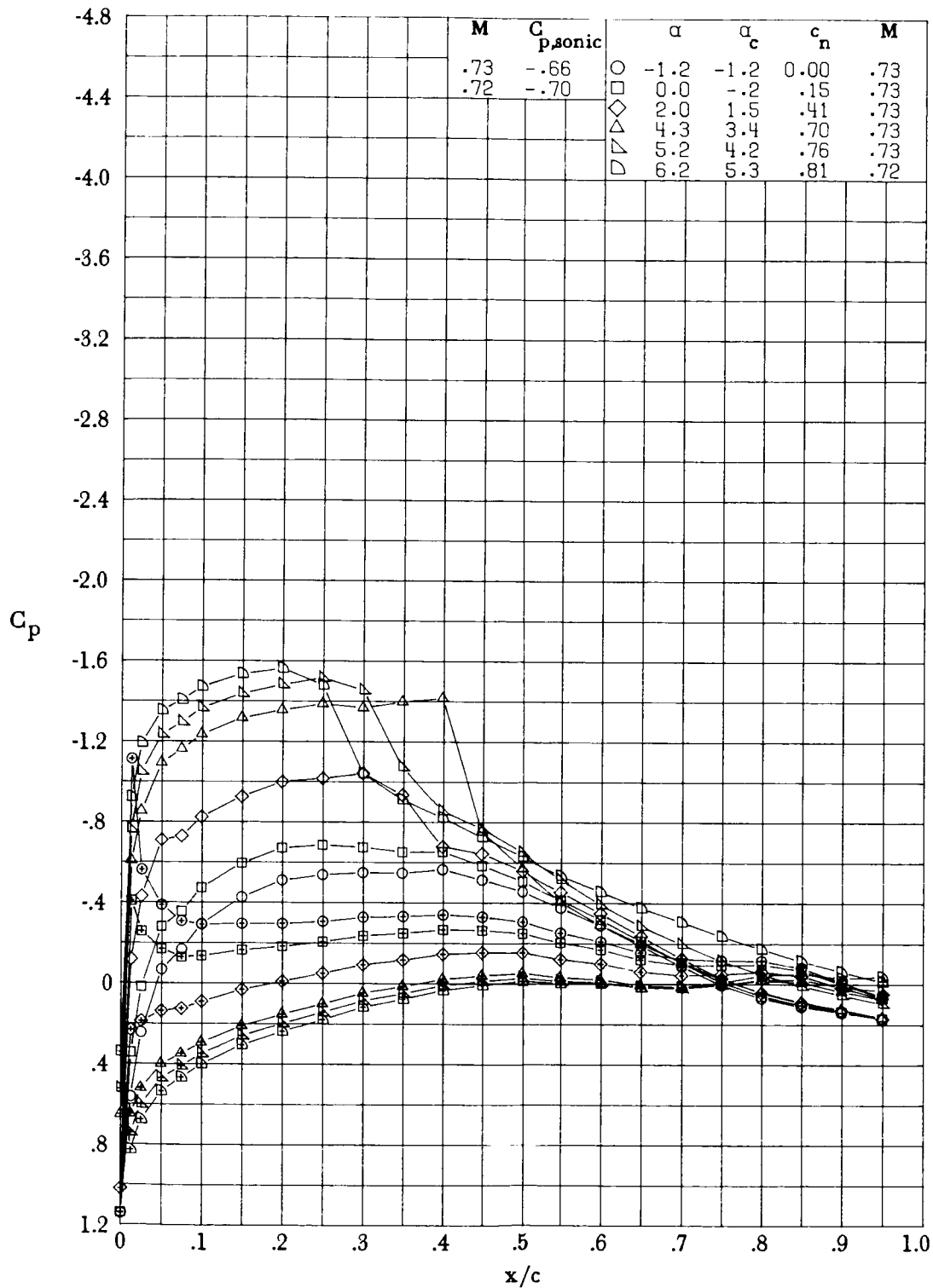
(g) $M \approx 0.63$; $R \approx 8.4 \times 10^6$.

Figure 20.- Continued.



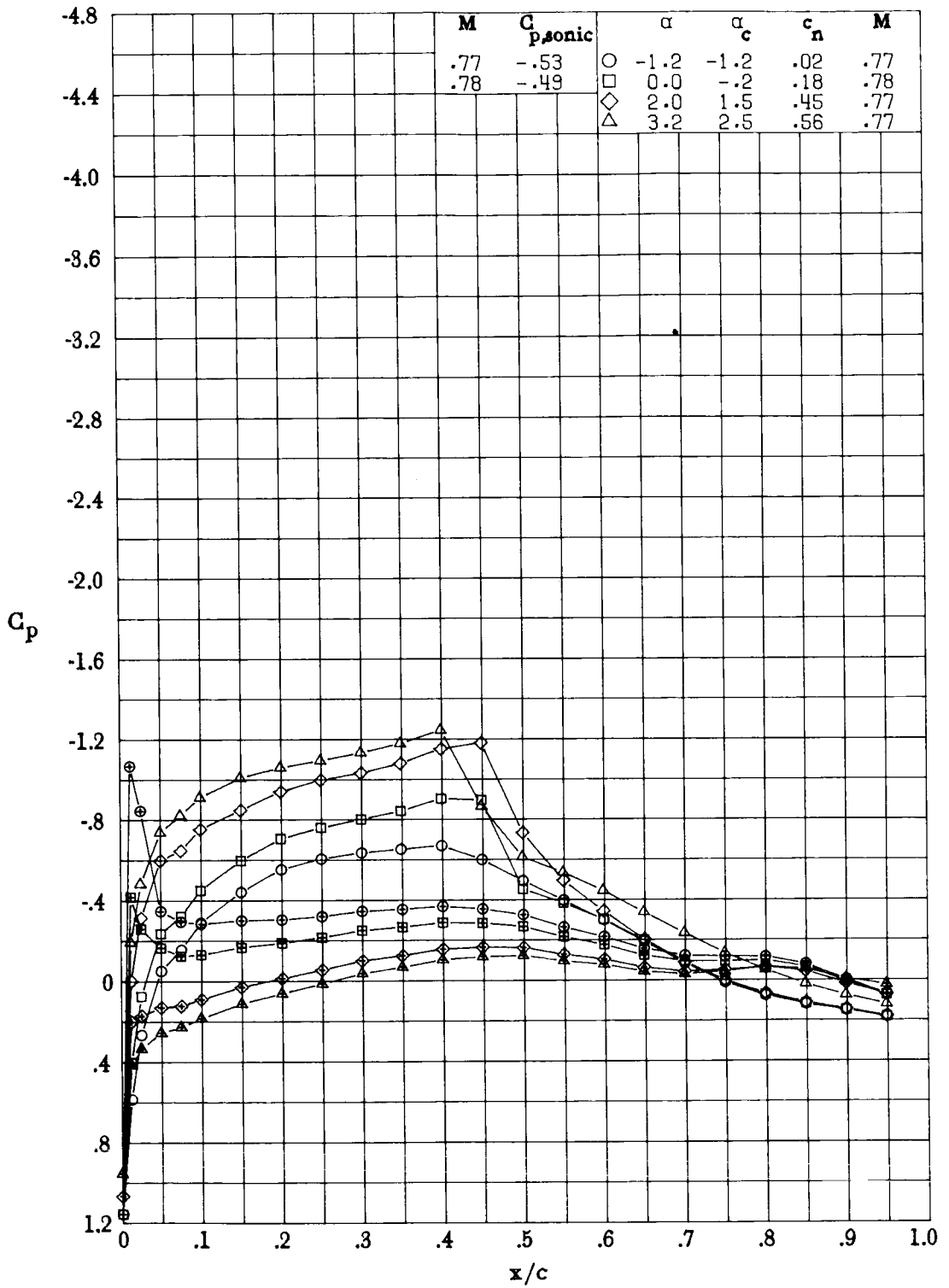
(h) $M \approx 0.68$; $R \approx 8.5 \times 10^6$.

Figure 20.- Continued.



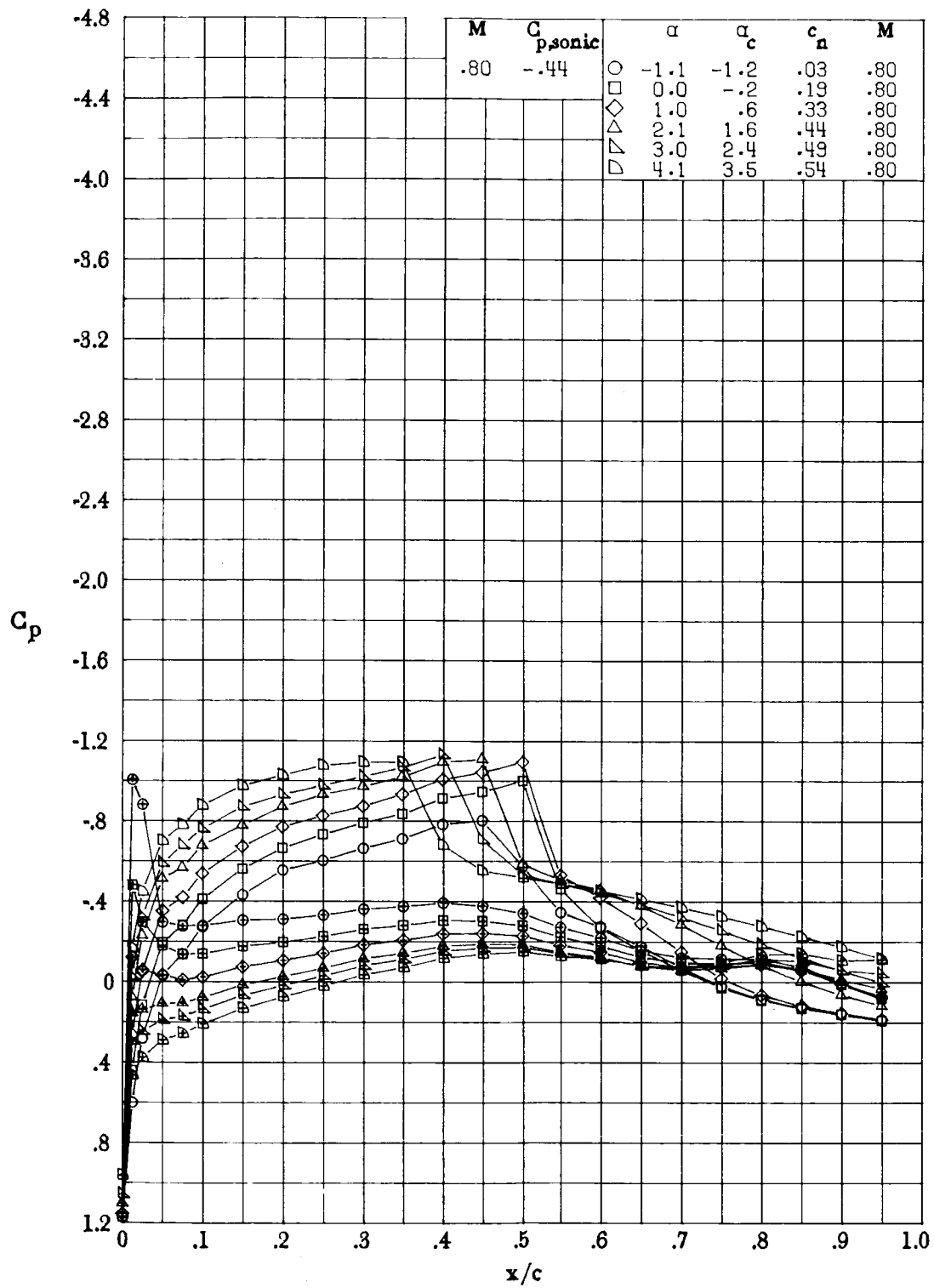
(i) $M \approx 0.73$; $R \approx 9.0 \times 10^6$.

Figure 20.- Continued.



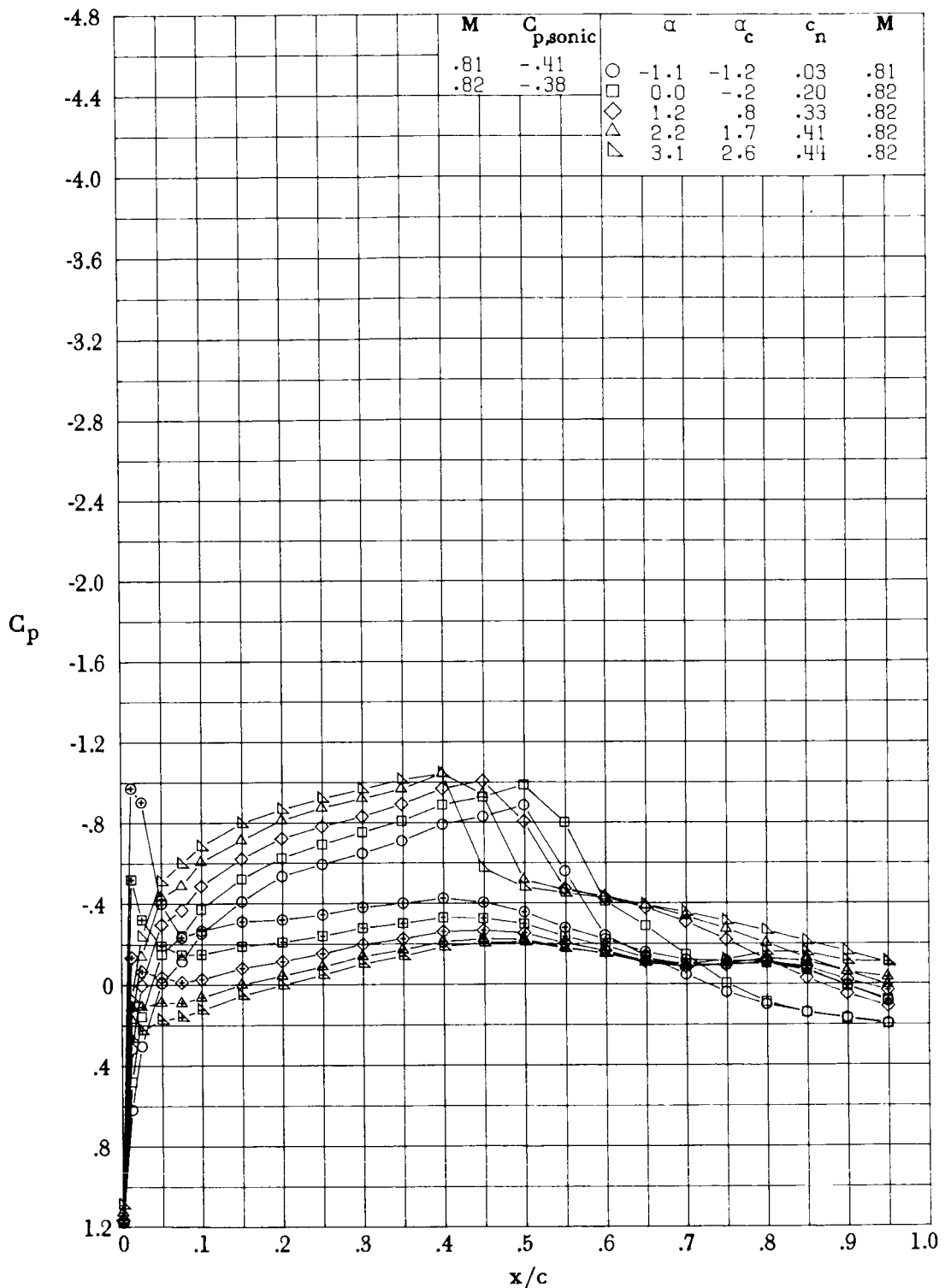
(j) $M \approx 0.77$; $R \approx 9.1 \times 10^6$.

Figure 20.- Continued.



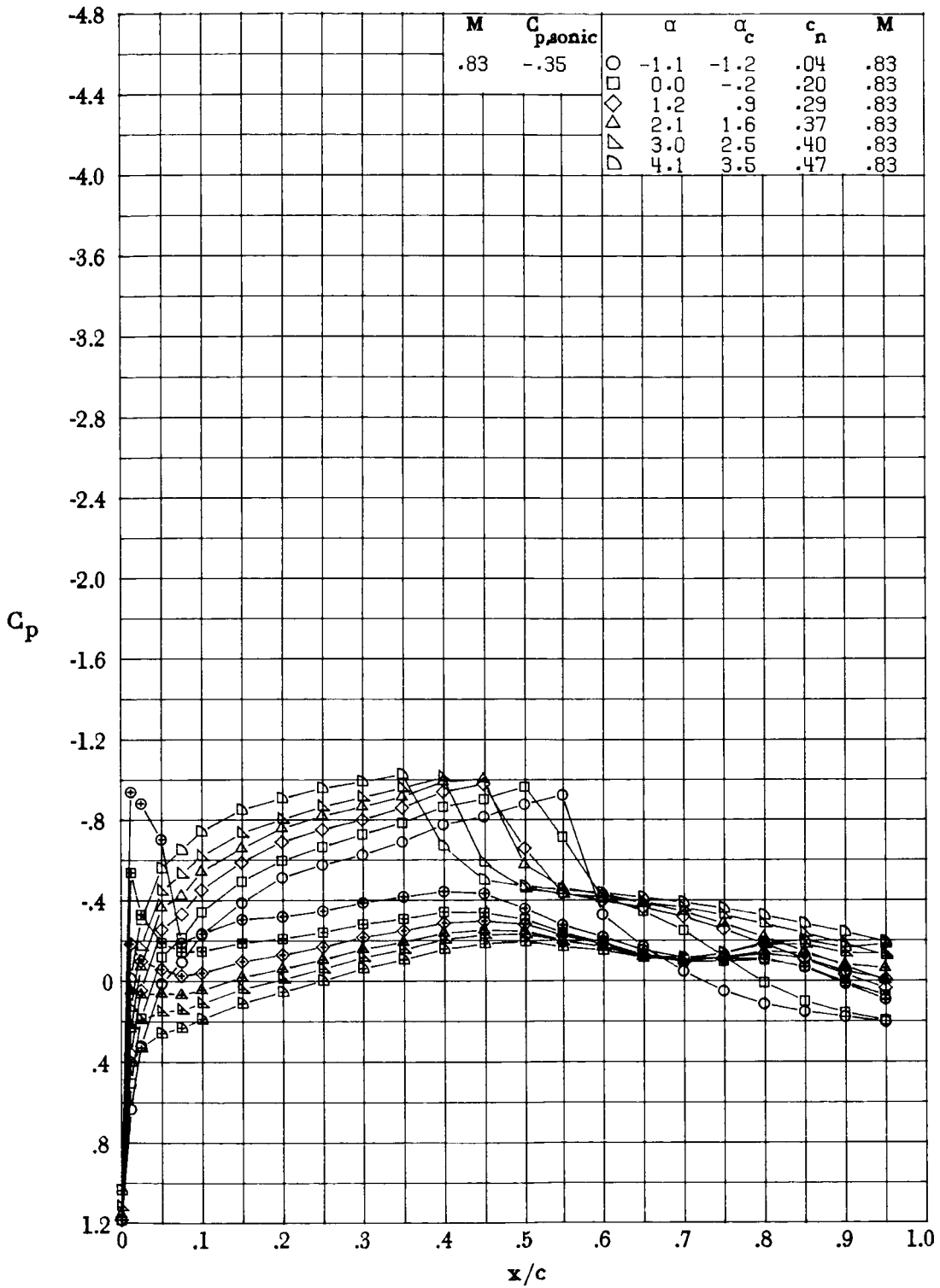
(k) $M = 0.80$; $R \approx 9.4 \times 10^6$.

Figure 20.- Continued.



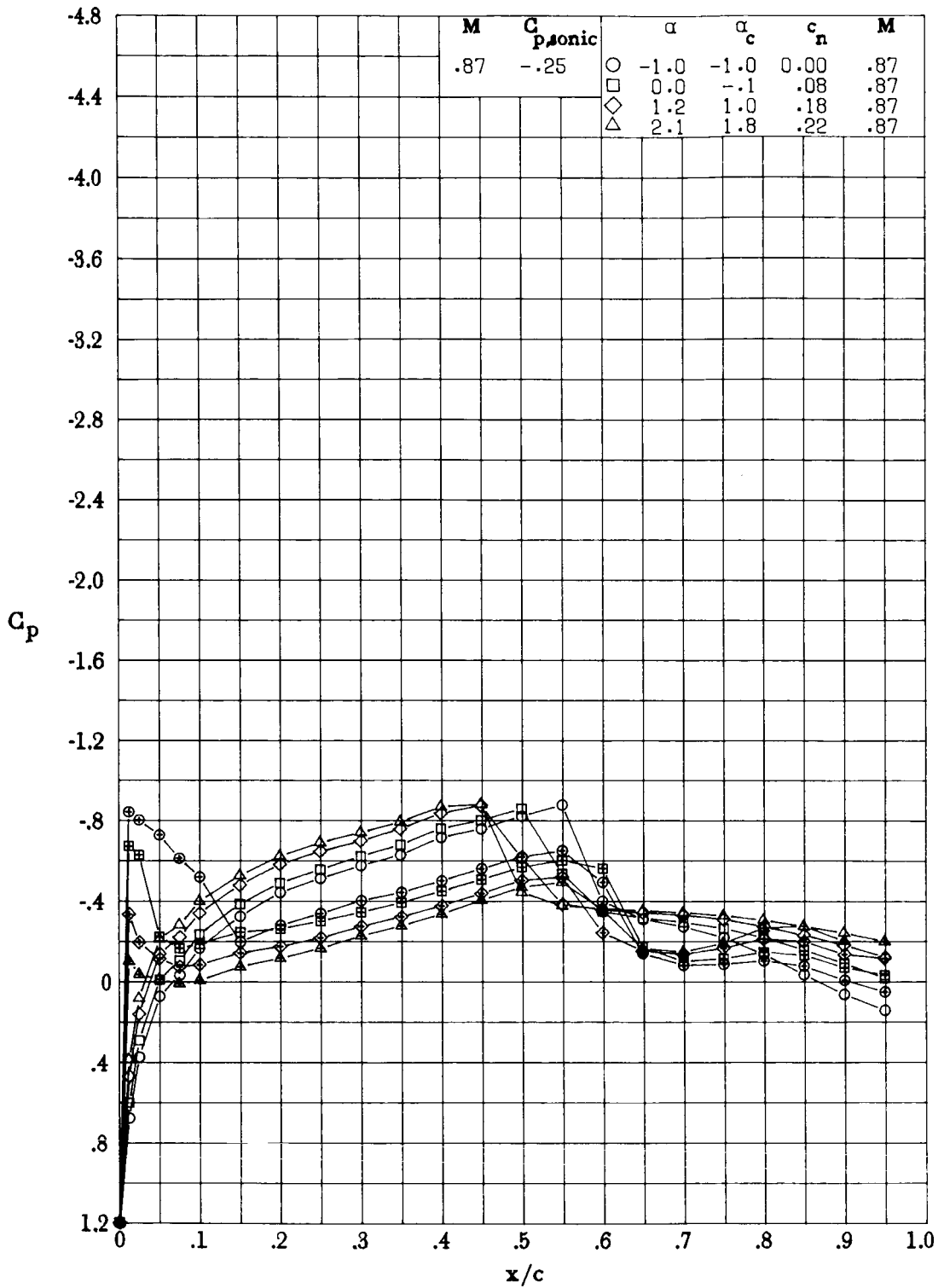
(1) $M \approx 0.82$; $R \approx 9.4 \times 10^6$.

Figure 20.- Continued.



(m) $M = 0.83$; $R \approx 9.5 \times 10^6$.

Figure 20.- Continued.



(n) $M = 0.87$; $R \approx 9.8 \times 10^6$.

Figure 20.- Concluded.

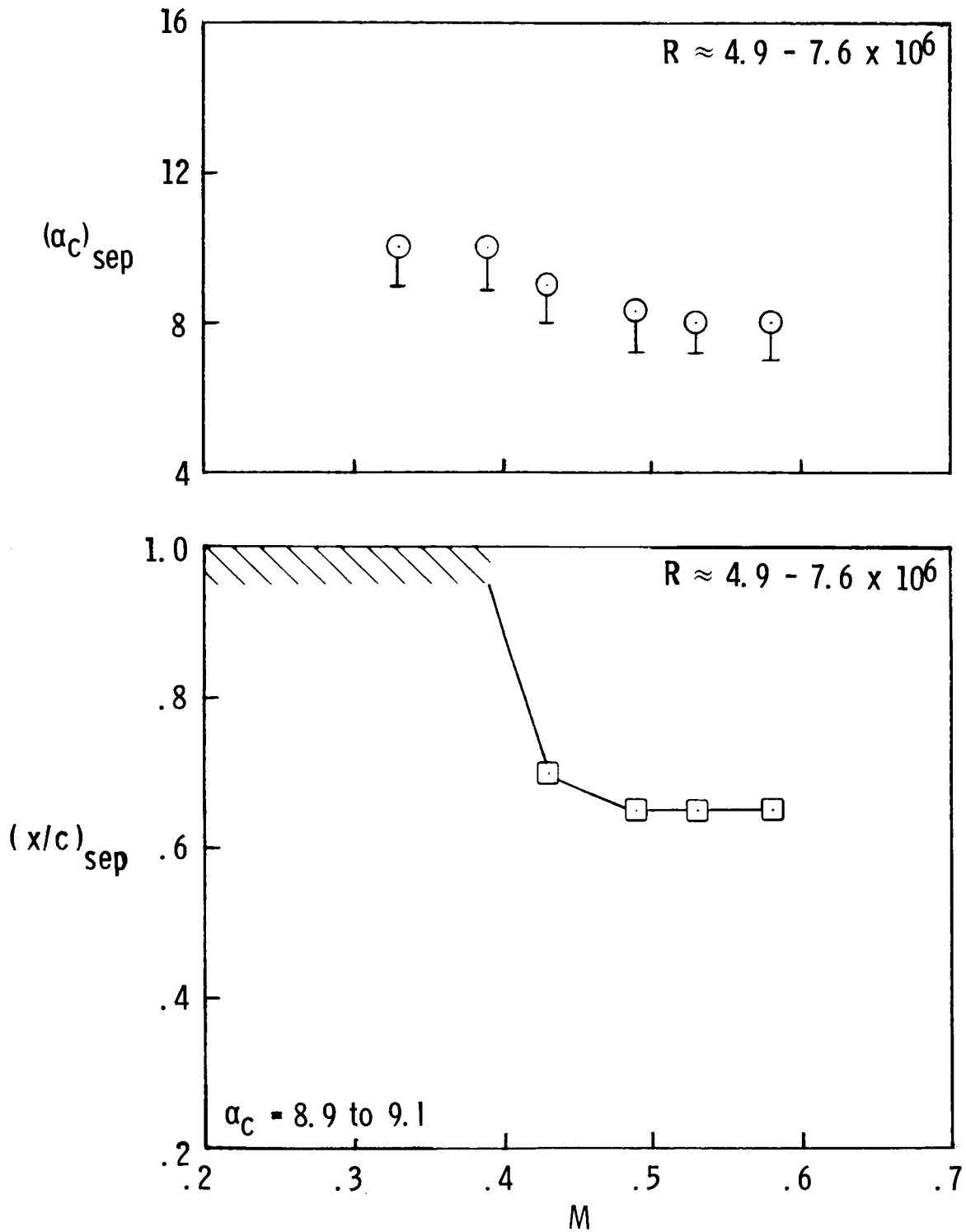
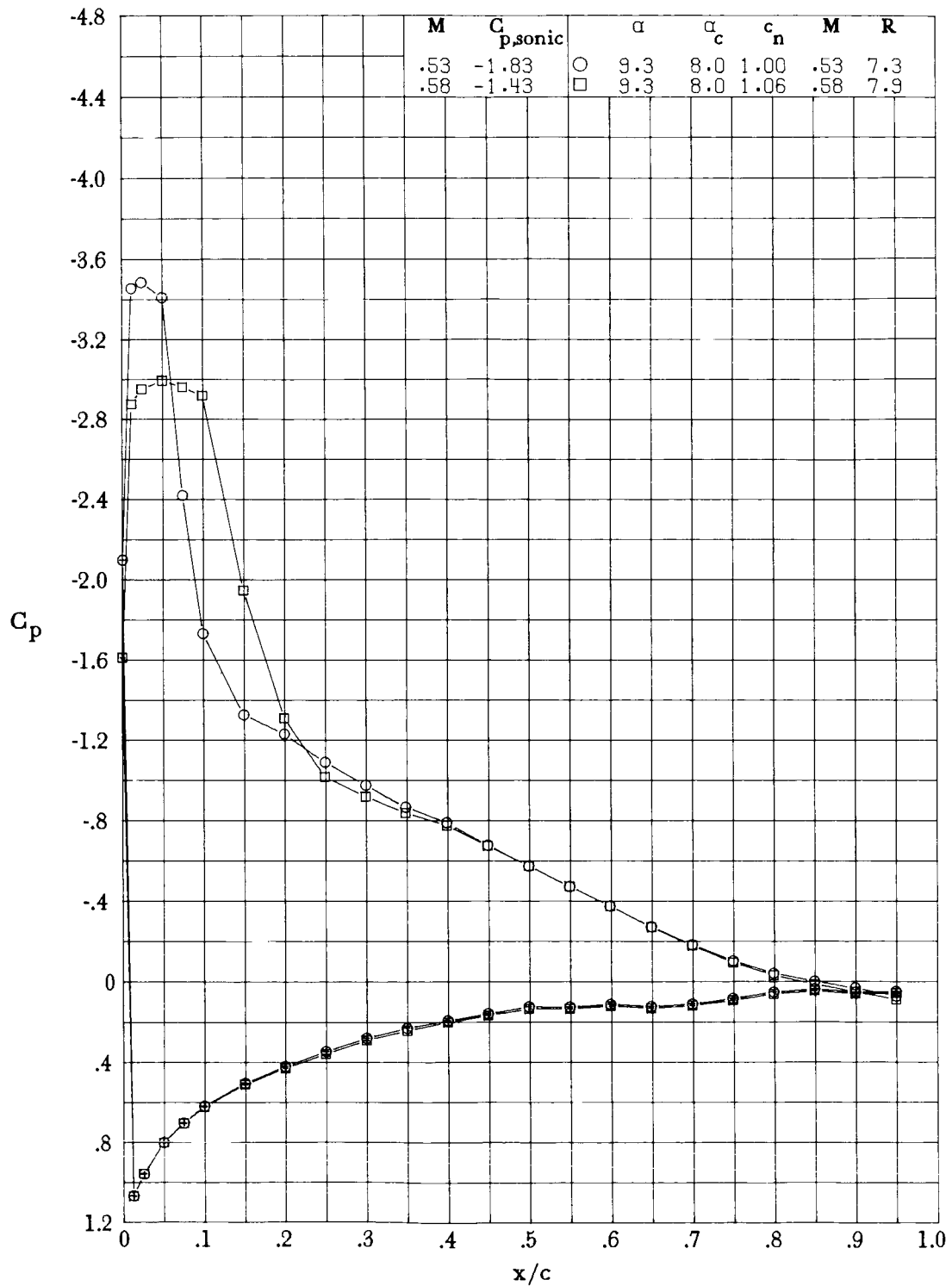
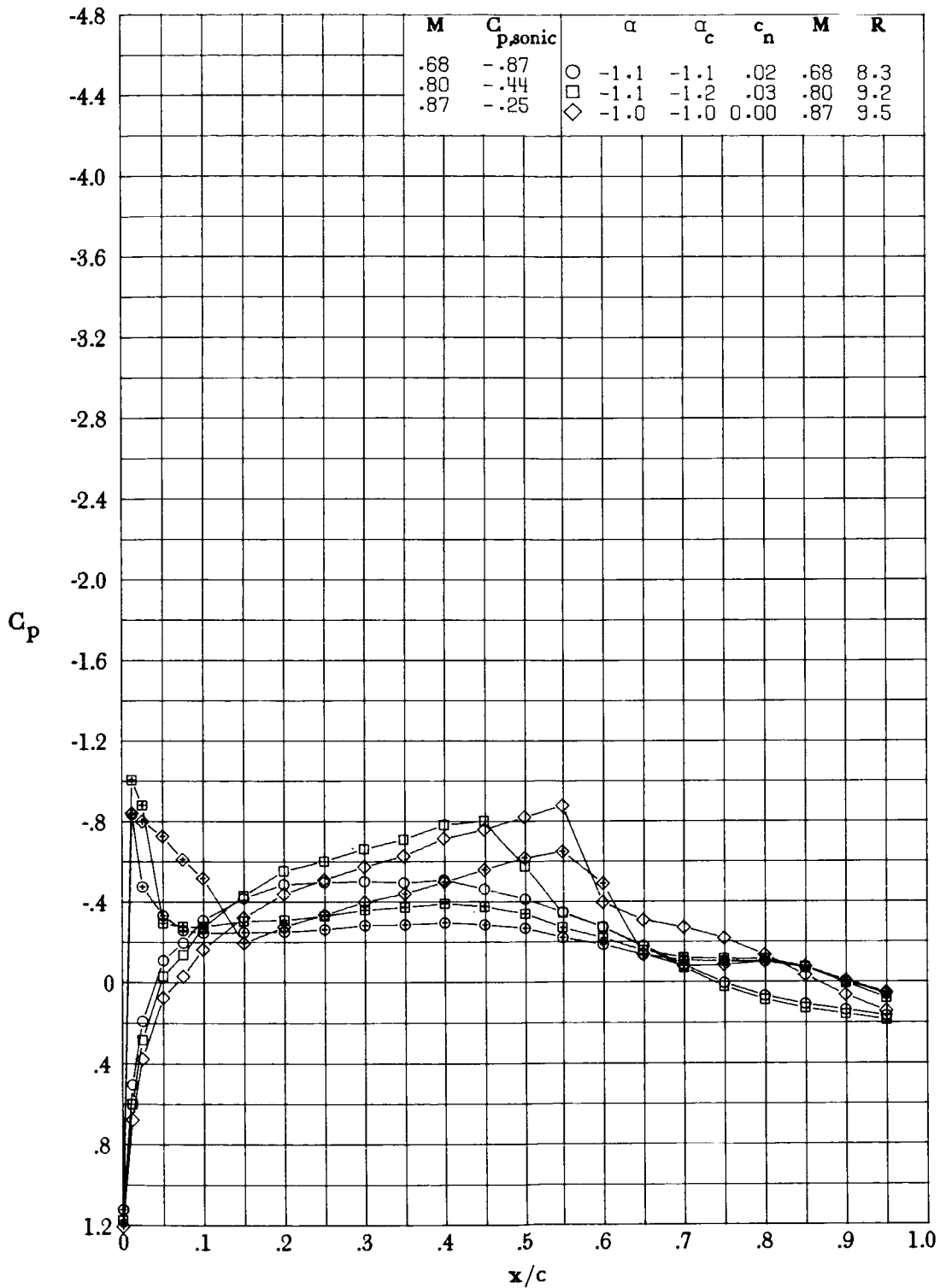


Figure 21.- Effect of Mach number on angle of attack at which boundary-layer separation first occurs and on separation point of RC-10(N)-1 airfoil.



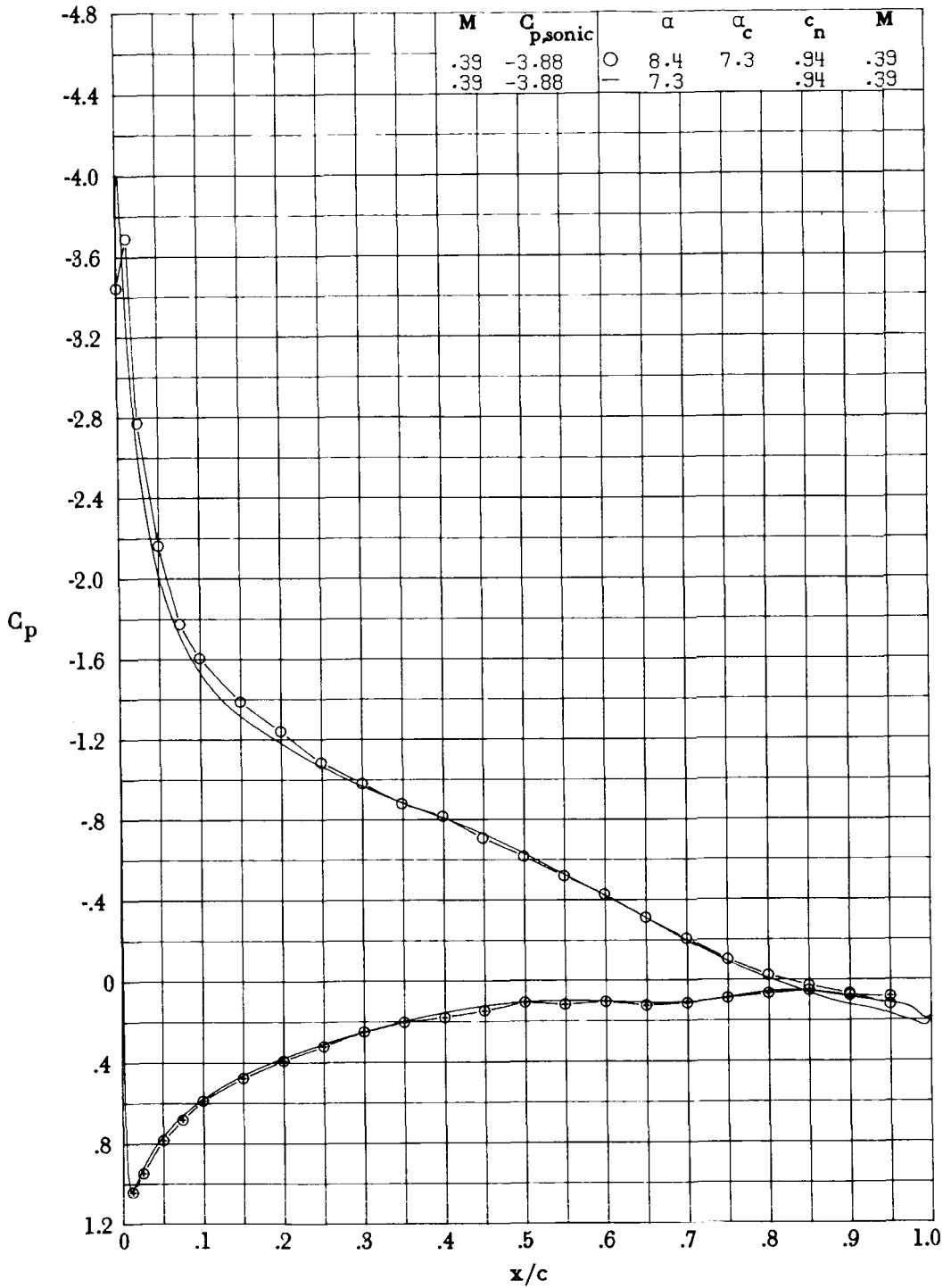
(a) $\alpha_c = 8.0$

Figure 22.- Effect of Mach number on chordwise pressure distribution of RC-10(N)-1 airfoil. Centered symbols indicate lower surface.



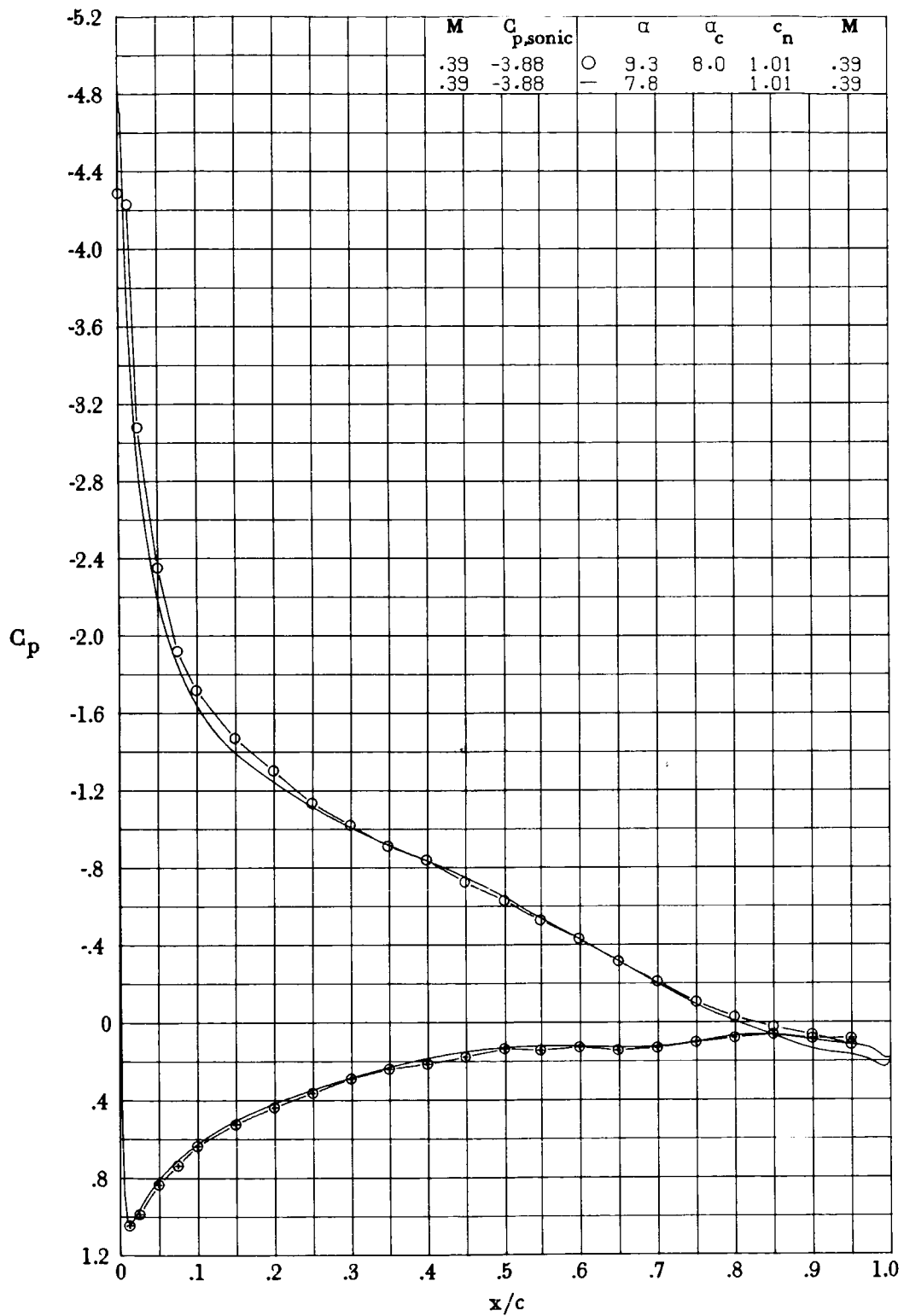
(b) $\alpha_c \approx -1.1$.

Figure 22.- Concluded.



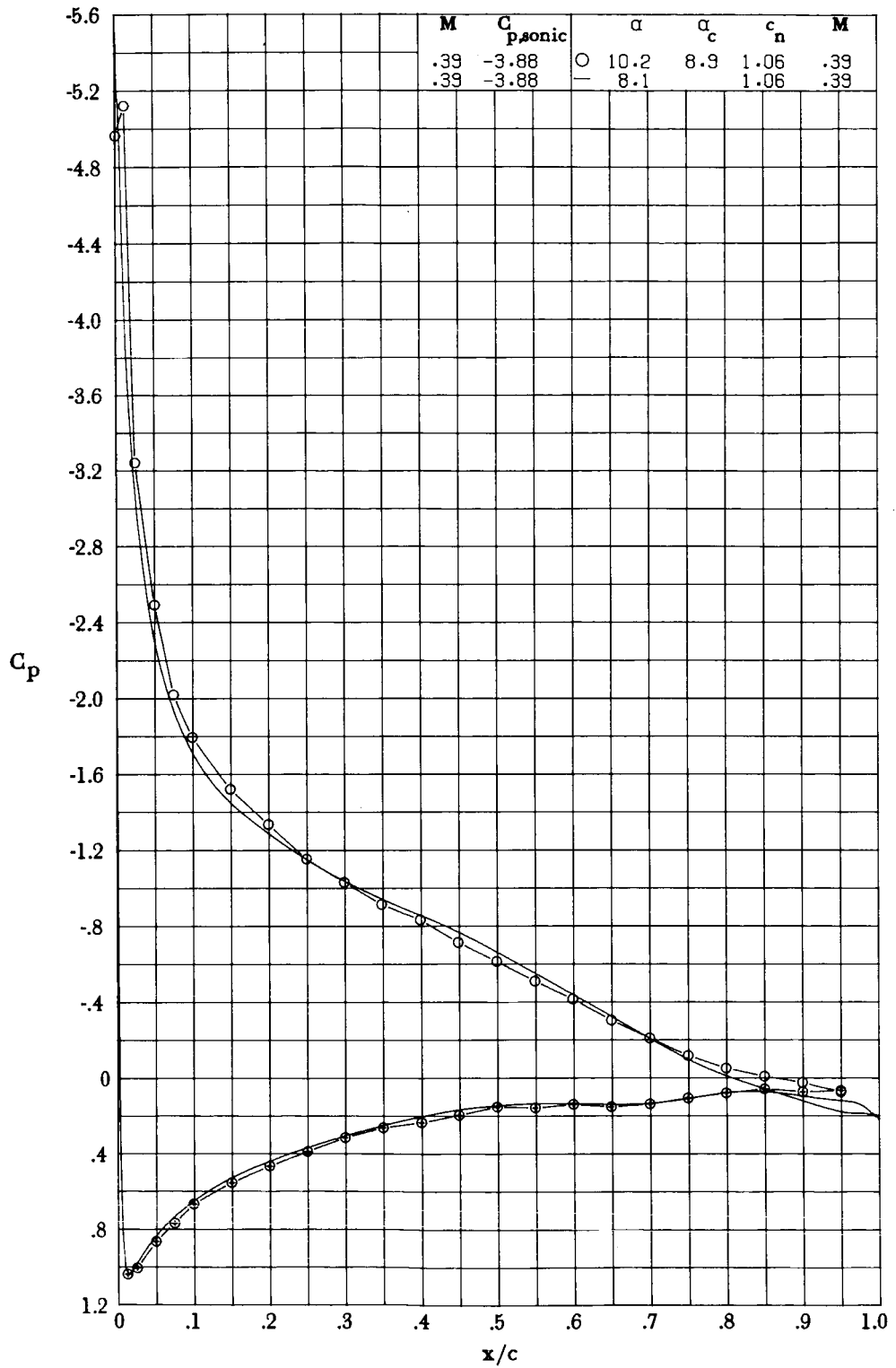
(a) $M = 0.39$; $R = 5.4 \times 10^6$; $c_n = 0.94$.

Figure 23.- Comparison of experimental and theoretical chordwise pressure distributions of RC-10(N)-1 airfoil. Symbols indicate experimental data; centered symbols indicate lower surface. Experimental data are for smooth model.



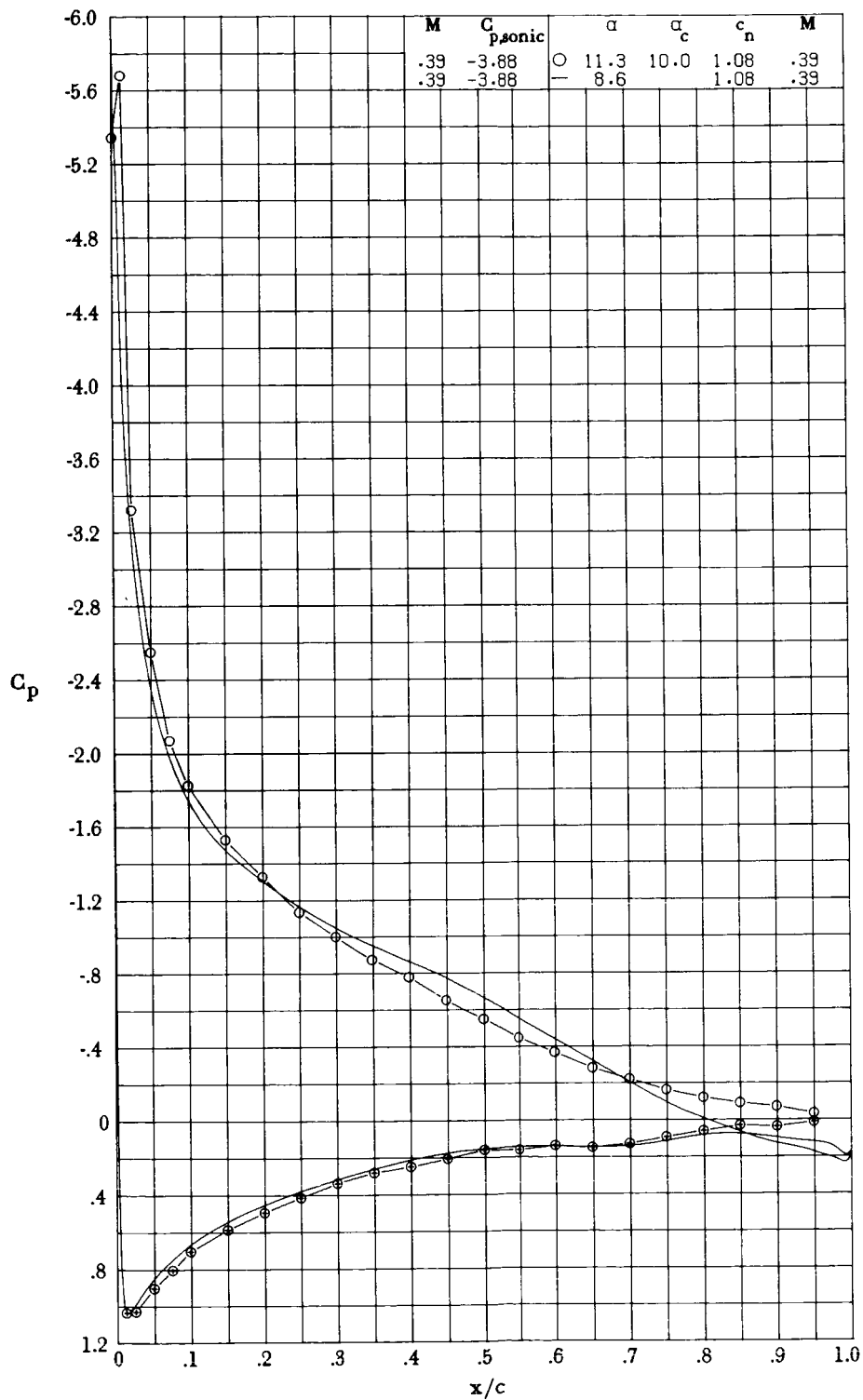
(b) $M = 0.39$; $R = 5.4 \times 10^6$; $c_n = 1.01$.

Figure 23.- Continued.



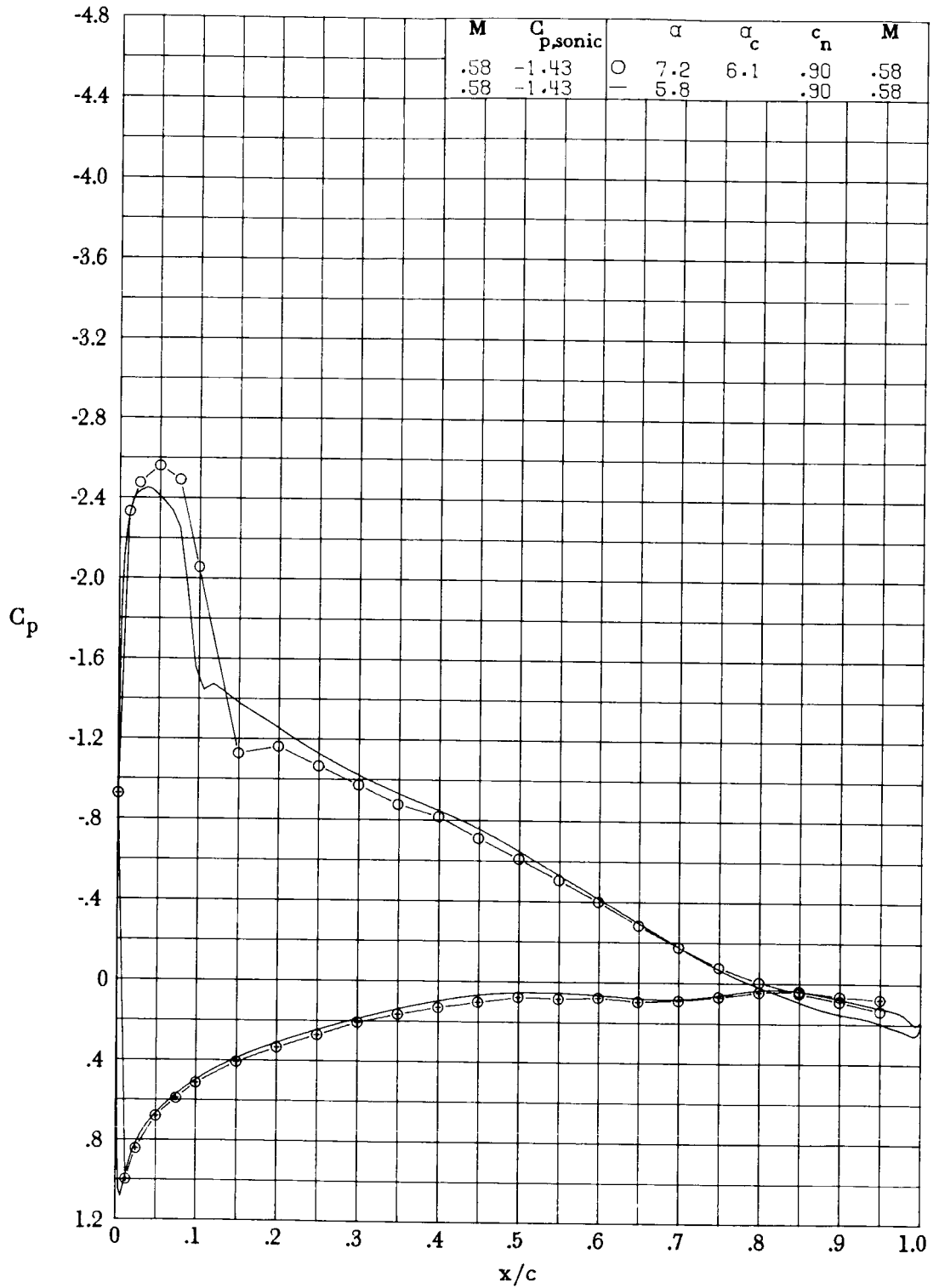
(c) $M = 0.39$; $R = 5.5 \times 10^6$; $c_n = 1.06$.

Figure 23.- Continued.



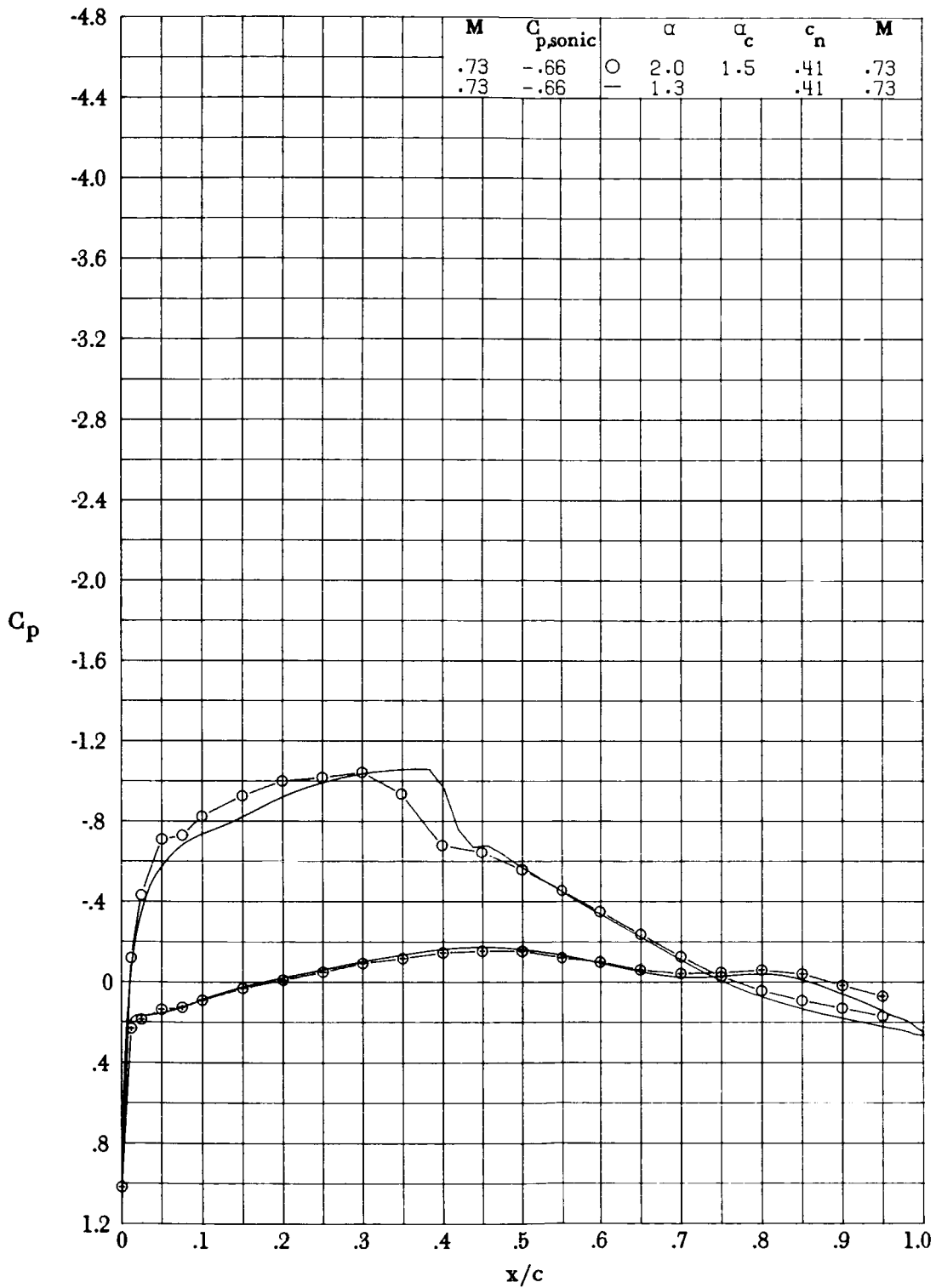
(d) $M = 0.39$; $R = 5.5 \times 10^6$; $c_n = 1.08$.

Figure 23.- Continued.



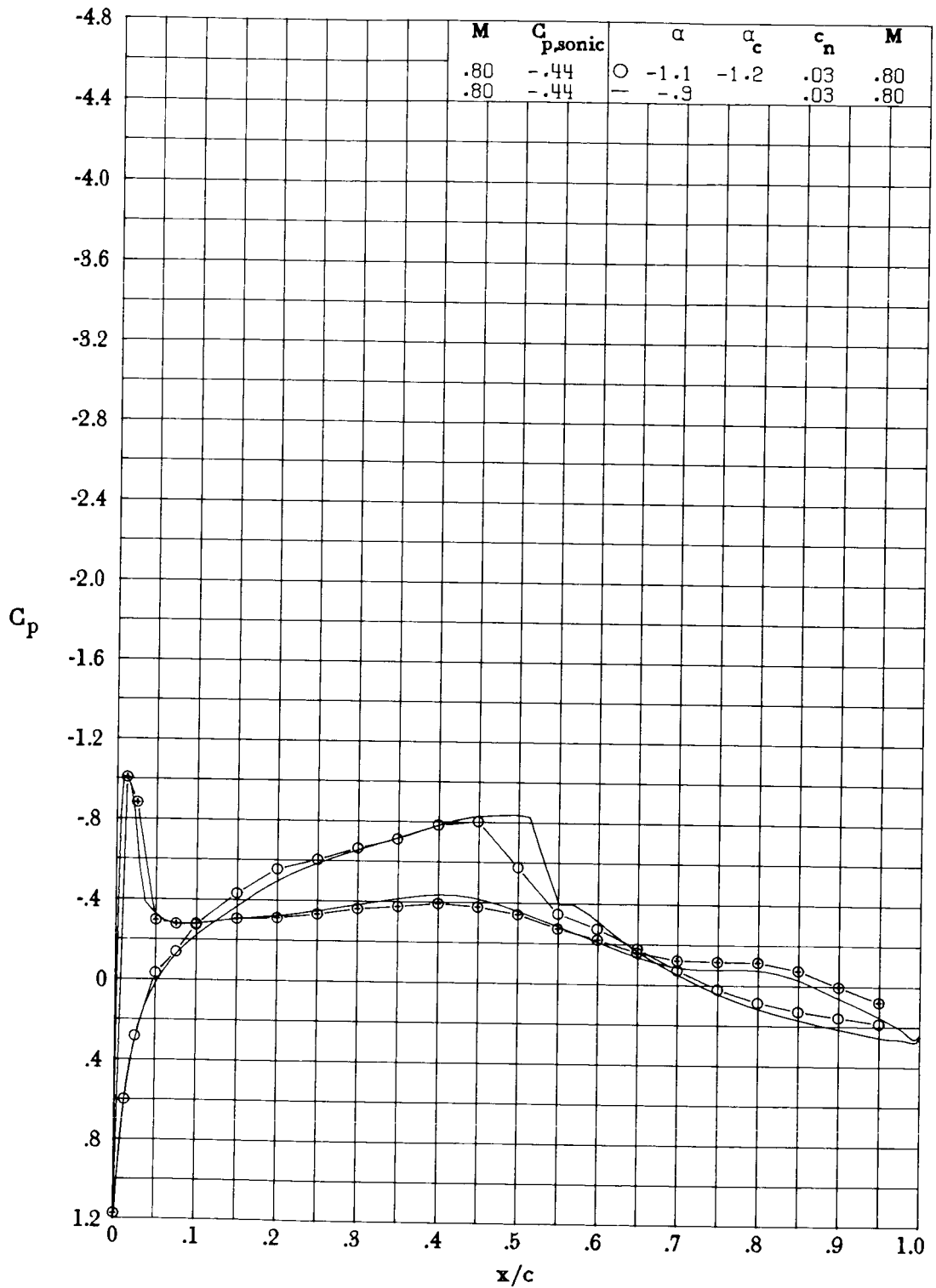
(e) $M = 0.58$; $R = 7.8 \times 10^6$; $c_n = 0.90$.

Figure 23.- Continued.



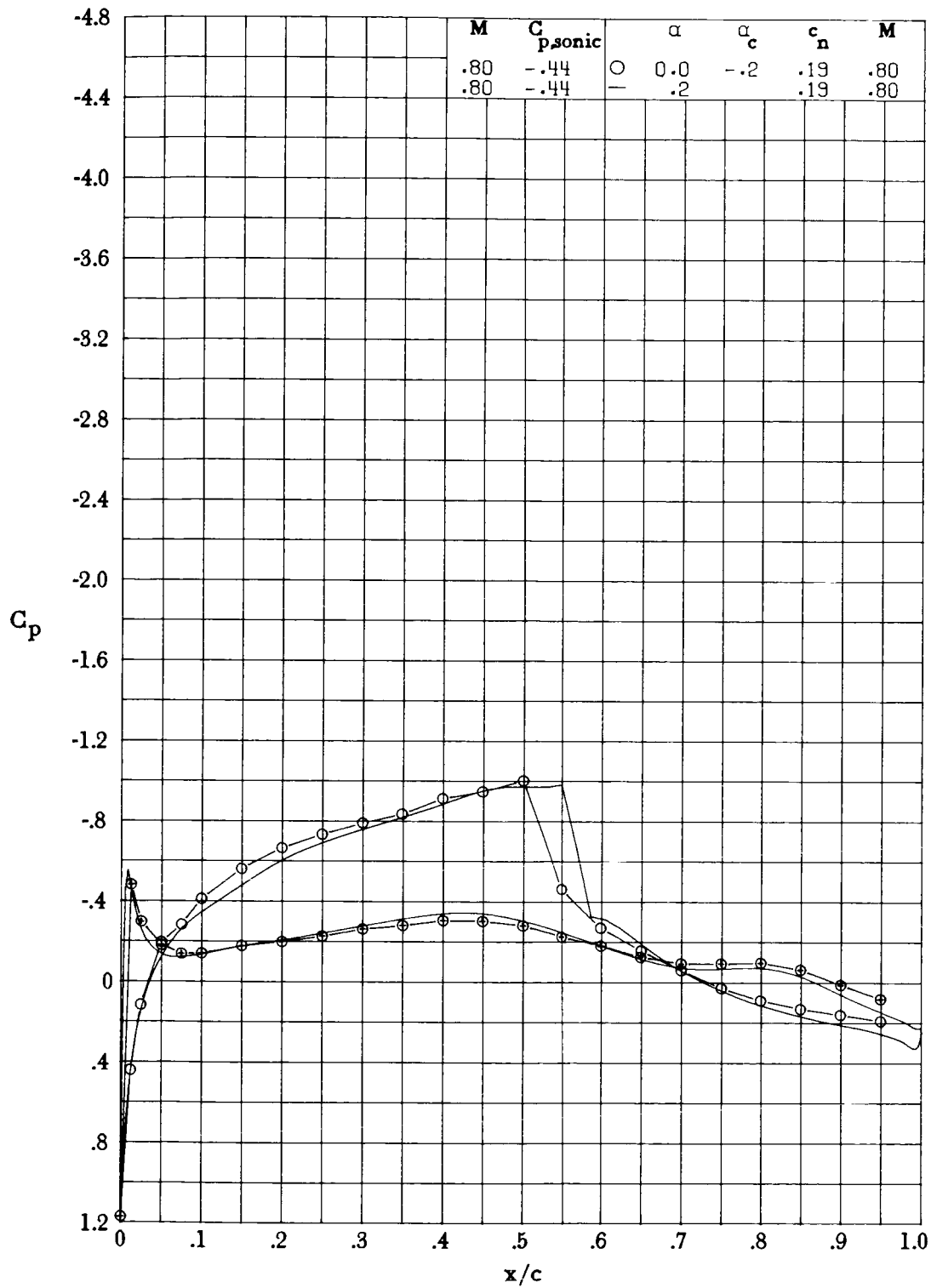
(f) $M = 0.73$; $R = 9.1 \times 10^6$; $c_n = 0.41$.

Figure 23.- Continued.




(g) $M = 0.80$; $R = 9.2 \times 10^6$; $c_n = 0.03$.

Figure 23.- Continued.



(h) $M = 0.80$; $R = 9.1 \times 10^6$; $c_n = 0.19$.

Figure 23.- Concluded.

1. Report No. NASA TP-1864 AVRADCOM TR 81-B-3		2. Government Accession No.		3. Recipient's Catalog No.	
4. Title and Subtitle EXPERIMENTAL INVESTIGATION OF A 10-PERCENT-THICK HELICOPTER ROTOR AIRFOIL SECTION DESIGNED WITH A VISCOUS TRANSONIC ANALYSIS CODE				5. Report Date July 1981	
				6. Performing Organization Code 505-31-33-05	
7. Author(s) Kevin W. Noonan				8. Performing Organization Report No. L-14182	
				10. Work Unit No.	
9. Performing Organization Name and Address Structures Laboratory AVRADCOM Research and Technology Laboratories NASA Langley Research Center Hampton, VA 23665				11. Contract or Grant No.	
				13. Type of Report and Period Covered Technical Paper	
12. Sponsoring Agency Name and Address National Aeronautics and Space Administration Washington, DC 20546 and U.S. Army Aviation Research and Development Command St. Louis, MO 63166				14. Army Project No. 1L161102AH45	
				15. Supplementary Notes Kevin W. Noonan: Structures Laboratory, AVRADCOM Research and Technology Laboratories.	
16. Abstract An investigation has been conducted in the Langley 6- by 28-Inch Transonic Tunnel to determine the two-dimensional aerodynamic characteristics of a 10-percent-thick helicopter rotor airfoil at Mach numbers from 0.33 to 0.87 and respective Reynolds numbers from 4.9×10^6 to 9.8×10^6 . This airfoil, designated the RC-10(N)-1, was also investigated at Reynolds numbers from 3.0×10^6 to 7.3×10^6 at respective Mach numbers of 0.33 to 0.83 for comparison with the SC 1095 (with tab) airfoil. The RC-10(N)-1 airfoil was designed by the use of a viscous transonic analysis code. The results of the investigation indicate that the RC-10(N)-1 airfoil met all the design goals. At a Reynolds number of about 9.4×10^6 , the drag divergence Mach number at zero normal-force coefficient was 0.815 with a corresponding pitching-moment coefficient of zero. The drag divergence Mach number at a normal-force coefficient of 0.9 and a Reynolds number of about 8.0×10^6 was 0.61. The drag divergence Mach number of this new airfoil was higher than that of the SC 1095 airfoil at normal-force coefficients above 0.3. Measurements in the same wind tunnel at comparable Reynolds numbers indicated that the maximum normal-force coefficient of the RC-10(N)-1 airfoil was higher than that of the NACA 0012 airfoil for Mach numbers above about 0.35 and was about the same as that of the SC 1095 airfoil for Mach numbers up to 0.5.					
17. Key Words (Suggested by Author(s)) Airfoils Helicopters Rotor airfoils RC-10(N)-1 airfoil			18. Distribution Statement  Subject Category 02		
19. Security Classif. (of this report) Unclassified		20. Security Classif. (of this page) Unclassified		21. No. of Pages 76	22. Price